UC Riverside

UC Riverside Electronic Theses and Dissertations

Title

Arterial LDL Transport Incorporating Fluid Solid Interactions, Hyperthermia, and Atherosclerosis

Permalink

https://escholarship.org/uc/item/0391w20x

Author

Chung, Stephen

Publication Date

2013

Peer reviewed|Thesis/dissertation

eScholarship.org Powered by the California Digital Library
University of California

UNIVERSITY OF CALIFORNIA
RIVERSIDE

Arterial LDL Transport Incorporating Fluid Solid Interactions, Hyperthermia, and Atherosclerosis

A Dissertation submitted in partial satisfaction
of the requirements for the degree of

Doctor of Philosophy

in

Mechanical Engineering

by

Stephen Chung

August 2013

Dissertation Committee:
Dr. Kambiz Vafai, Chairperson
Dr. Cengiz Ozkan
Dr. Marko Princevac

Copyright by
Stephen Chung
2013

The Dissertation of Stephen Chung is approved

_____

_____

_____

Committee Chairperson

University of California, Riverside

Acknowledgments

I have gratitude for Dr. Kambiz Vafai's strong support in not only academic but also development in personality with his knowledge and zeal through my research project. I also thank Dr. Cengiz Ozkan and Dr. Marko Princevac for being here as my committee members and give advice to my research. Thank to Maryam Shafahi, Shadi Mahjoob, Yong Zeng and Parisa Hakim Javadi for their generous help through the time we worked together in the laboratory and outside. I thank all of my friends especially to Sean Cheng, Bo Liu, Clara Zhang and Jie-bin Zhong for their any of friendship that gave me a substantial time when in UCR. Because of these persons and also lots of others, I can stand here to present for my research and myself.

To my family, with my strongest wish, I am grateful especially to my parents, because I owe them so much that I can not count. Also I need put my reverence to my late grand father and my grand mother who stand as the paragon by their striving through the last century, a hard time. It is my family that gives me the meaning to stand here.

Dedicated to my family

ABSTRACT OF THE DISSERTATION

Arterial LDL Transport Incorporating Fluid Solid Interactions, Hyperthermia, and Atherosclerosis

by

Stephen Chung

Doctor of Philosophy, Graduate Program in Mechanical Engineering
University of California, Riverside, August 2013
Dr. Kambiz Vafai, Chairperson

A comprehensive investigation and analysis of low-density lipoprotein (LDL) transport in an artery is presented to demonstrate the molecular accumulation that can lead to atherosclerosis. This study paves the way for a better treatment and diagnosis of the cardiovascular disease. The impact of LDL accumulation and other pertinent characteristics within an artery due to pulsation, hypertension, plaque formation, lumen stenosis and hyperthermia are systematically examined.

A comprehensive multi-layered model is introduced to incorporate convection-diffusion-reaction and Staverman filtration effects. Endothelium and intima transport properties are obtained using both the micro-structure information as well as the experimental data. The

results are analyzed and validated and an excellent agreement is observed when compared with the earlier works. Additional effects such as the heat and mass transfer, and elastic structure, are also considered and analyzed for LDL transport.

The effects of a deformable wall while incorporating the fluid-structure interaction (FSI) along with, plasma filtration and thermal expansion are accounted for. The fiber matrix model is utilized to link the cholesterol lipid accumulation and tissue proliferation to variable properties of intima. Pore theorem is applied to calculate the endothelium properties using the structural parameters for the endothelial junctions, which affect the elastic wall deformation. The hyperthermia along with the thermo-induced effects due to the thermal expansion and variable LDL diffusivity and consumption rate are analyzed. The coupling effects of Osmotic pressure, Sorret and Dufour diffusion are discussed and their domain of influence on LDL transport is established. A comprehensive investigation of plaque development and wall thickening, lumen stenosis and dysfunctional endothelium due to atherosclerosis is presented.

Contents

Introduction 1
Formulation 10
2.1 Multi-layered model 10
2.2 Governing equations 15
2.3 Governing equations – FSI and hyperthermia 18
2.4 Governing equations – coupling effect 20
2.5 Boundary conditions 21
Methodology and Validation 33
Results Comparison 35
4.1 LDL transport Model 35
4.2 Elastic model and Stenosis 43
4.3 Transport properties obtained by different methods 47
Result and Discussion 50
5.1 FSI effect 50
5.2 Pulsation effect 60
5.3 Impact by Osmotic effect – Osmosis pressure 64

5.4 Heat transfer model and thermal impact 67
5.5 Effect of Sorret effect – Thermo-diffusion 69
5.6 The impact by thermal expansion 71
5.7 Impact by effective LDL consumption rate 76
5.8 Impact of atherosclerotic plaque formation – thickening of the wall and the stenosis location 78
5.9 Sensitivity study on plaque geometry and model simplification 81
5.10 Dysfunctional endothelium and fibrous cap 87
5.11 Calculation of intima properties through fiber matrix model 90
5.12 Impact of variations in intima properties by lipid accumulation 95
Conclusion 100
6.1 FSI and Hyperthermia – Elastic and Thermo induced coupling phenomena .. 101
6.2 Atherosclerosis – Plaque/stenosis formation and endothelium dysfunction.... 102
References 103

List of Tables

1. Transport properties for each of the layers/domains (Chung and Vafai, 2012).... 14
2. Hydraulic and LDL transport properties for each of the layers/domains utilized by a) Yang and Vafai (2006); b) Ai and Vafai (2006)..... 17
3. Properties obtained in previous works for dysfunctional endothelium and fibrous cap. 88
4. Intima properties a) obtained using fiber matrix method with protein fiber radius r_f of 2.31 nm (Eq. 14) and variation of intima porosity, δ or (δ_{PG}, δ_{CG}) given in previous work (Yang and Vafai, 2006; Dabagh et al., 2009); b) obtained using fiber matrix method variations in both intima porosity ε (Dabagh et al., 2009, $\delta = \delta_{PG}\delta_{CG}$) and protein fiber radius r_f; c) obtained in the prior works (Ai and Vafai, 2006; Liu et al., 2011). 93
5. List of intima property variations with porosity ε and protein fiber radius r_f based on fiber matrix model (Eq. 15 and 16)..... 97

List of Figures

1. Configuration for a) Endothelial junctions; b) Multi-layered structure of an arterial wall including glycocalyx, endothelium, intima, IEL, media, and adventitia; c) Endothelium, intima, IEL, and intima fiber matrix; (Chung and Vafai, 2012, 2013). 12
2. Configuration for analyzed domain and boundary conditions of a) flow and mass transfer; b) elastic and heat transfer models. (*: Hydraulic impact on elastic model under 70mmHg transmural pressure is already embedded into a pre-described leaky junction expansion (Chung and Vafai, 2012)). 13
3. Configuration for a) Analyzed domain in the presence of stenosis (Ai and Vafai, 2006) ; b) Proteoglycan fibers within intima (Huang et al. 1994) c) Fiber matrix filled with cholesterol lipid; d) Analyzed region for the stenosis/plaque case. 29
4. Comparison of a) filtration velocity; b) LDL concentration at lumen-endothelium interface with those of Yang and Vafai (2006)..... 37
5. Comparison of normalized LDL concentration across intima, IEL, and media at different gage pressures and effective diffusivities with a) numerical and b) analytical results of Yang and Vafai (2006, 2008) 38
6. Comparison of normalized LDL concentration across intima, IEL, and media with numerical and analytical results of Yang and Vafai (2006, 2008) 39

7. Comparison of filtration velocity at different interface and axial locations with those by Ai and Vafai (2008). 40
8. Comparison of normalized LDL concentration at different interface and axial locations with those by Ai and Vafai (2008). 41
9. Comparison of normalized LDL concentration c/c_0 across each of the arterial layers with those by Ai and Vafai (2006) [presented in Chung and Vafai (2012)]. 42
10. Comparison of Von Mises Stress across arterial wall at different steps in pulsation cycle with those by Khanafer and Ramon (2009) 44
11. Comparison of Von Mises Stress across media at different steps in pulsation cycle and different modulus of elasticity with those by Khanafer and Ramon (2009) .. 45
12. Normalized LDL concentration c/c_0 across diseased artery layers in the presence of stenosis with $\delta = 0.5$, $x_{st} = 5.58cm$ and $x_0 = 2R_0$:a) for comparison with Ai and Vafai (2006) work; b) for two different boundary conditions at the media-adventitia interface ($r = 3.314mm$) $c = 0$ & $c = 0.012c_0$ 46
13. Effect of different sets of properties and the Osmotic pressure on a) Filtration velocity, b) LDL concentration distribution at the lumen-endothelium interface. 48
14. LDL concentration profile across a) endothelium, b) intima, c) IEL, and d) media, for different set of properties from works by Yang and Vafai (2006), Ai and Vafai (2006), and Chung and Vafai (2012). 49
15. Half width of leaky junction (w) variations with the angular strain ε 54
16. Endothelium a) Permeability K_{end} , b) Effective Diffusivity D_{eff} , c) Reflection coefficient σ_{end} , and d) Sieving coefficient γ_{end} (=$1-\sigma_{end}$), variations with angular strain ε at different ϕ and β_{lj} 55
17. Von Misses stress variations at the lumen-endothelium interface for different pressure drops across the arterial wall and different FSI models 56
18. Angular strain ε variations at the lumen-endothelium interface for different pressure drops across the arterial wall and different FSI models 57
19. a) Filtration velocity variations at the lumen-endothelium interface, and Normalized LDL concentration across b) endothelium, c) intima and IEL, and d) media, for different β and Δp 58
20. a) Filtration velocity variations at the lumen-endothelium interface, and Normalized LDL concentration across b) endothelium, c) intima and IEL, and d) media, for different ϕ and Δp 59

21. a) Filtration velocity; and b) Normalized LDL concentration; at different pulsation periods..... 61

22. Effect of FSI on filtration velocity incorporating the pulsation at the mid axial position of the endothelium layer 62

23. Effect of FSI on normalized LDL concentration incorporating the pulsation at the a) mid axial position of the lumen-endothelium interface; b) mid axial position of the endothelium-intima interface 63

24. Effects of different sets of properties on the Osmotic effect ratio in a) endothelium, b) IEL where highest concentration gradient appears..... 66

25. Dufour effect on a) temperature distribution within the arterial wall, b) comparison with ordinary diffusion..... 68

26. Soret and hyperthermia effects on the LDL concentration distribution across endothelium, intima, IEL, and media..... 70

27. Effect of thermal expansion on a) filtration velocity at the lumen-endothelium interface and b) Thermal strain across endothelium. 73

28. Effect of temperature drop, ΔT , and leaky-bulk expansion rate, β_{lj} on the LDL concentration distributions across a) endothelium, intima, IEL, and b) media ($k_T = 0$)..... 74

29. Comparisons between the full and simplified elastic models and their effects on LDL concentration distribution across a) endothelium, intima, IEL, and b) media, incorporating Sorret effect with the variation of Sorret coefficient k_T 75

30. Effect of LDL consumption rate k on its concentration distribution across a) endothelium, intima, IEL, and b) media. 77

31. Normalized LDL concentration c/c_0 across diseased artery layers in the presence of stenosis at center of the plaque ($x = x_{st}$; $x_0 = 2R_0$) with different wall thickening δ_{st} and location of stenosis x_{st} 79

32. Normalized LDL concentration c/c_0 across IEL and media of a diseased artery at different locations x in the presence of stenosis with $\delta_{st} = 0.5$, $x_{st} = 5.58cm$ and $16.74cm$ for three different boundary conditions at the media-adventitia interface ($r = 3.314\,mm$) as $\partial c/\partial r = 0$, $c = 0$, $c = 0.012c_0$ 80

33. Blood pressure, filtration velocity, and LDL concentration along the lumen-endothelium interface for different wall thickening ratio δ_{st} and stenosis locations x_{st} 83

34. Blood pressure, filtration velocity, and LDL concentration along the lumen-endothelium interface for different values of the plaque half widths x_0 84

35. Blood pressure, filtration velocity, and LDL concentration profile along the intima-IEL interface for different plaque half widths x_0 85

36. Effect of reversed boundary conditions (inlet: pressure, outlet: velocity) on blood pressure, filtration velocity, and LDL concentration along the intima-IEL interface for different plaque half widths x_0 86

37. Filtration velocity and LDL concentration across endothelium, fibrous cap, and intima for different physical attributes of endothelium and fibrous cap given in Table 3. 89

38. Filtration velocity and LDL concentration along the intima-IEL interface. Intima properties were obtained through fiber matrix model with a) protein fiber radius r_f of 2.31 nm and variations of intima porosity, δ or (δ_{PG} , δ_{CG}) based on data given in Table 4a; and b) variations of intima porosity δ and effective protein fiber radius r_f based on data given in Table 4b, and compared with those based on the properties obtained by Ai and Vafai (2006) and Liu et al (2011) given in Table 4c..... 94

39. Effect of variations in the effective porosity δ_{Lip} and protein fiber thickening ratio $r_{f,Lip}/r_f$ on the filtration velocity across a diseased arterial wall..... 98

40. Effect of variations in the effective porosity ε_{Lip} and protein fiber thickening ratio $r_{f,Lip}/r_f$ on the LDL molecule concentration across a diseased arterial wall. 99

Nomenclature

c	LDL concentration	mol/m^3
c_T	thermal capacity	$J/kg \bullet K$
$\ddot{d}_s$	acceleration within the solid region	m/s^2
D	LDL diffusivity	m^2/s
f_s	solid domain body force	N/m^3
G	Kozney constant	1
H	thickness of the layers	μm
k	reaction coefficient	$1/s$
k_T	thermal-diffusion coefficient	1
k_D	diffusivity effective rate	1
K	hydraulic permeability	m^2
L	length of the artery	m
M	molecular weight	kg/mol
N''	solute mass flux per area	$mol/m^2 \bullet s$
p	hydraulic pressure	mmHg
Δp	pressure drop across arterial wall	mmHg

Pe	Peclet number	1
r	radial location from the centerline	m
r_m	molecular radius	nm
r_{CF}	radius of central filament	nm
r_{CP}	radius of proteoglycan core protein	nm
r_f	effective intima fiber radius	nm
r_G	radius of glycosaminoglycan	nm
r_M	effective monomer radius	nm
R	universal gas constant	$J/K \bullet mol$
R_0	radius of lumen domain	m
R_{Cell}	radius of endothelial cell	μm
t	time	s
T	temperature	K
T_H	Hyperthermia temperature applied at the lunmen-wall interface	K
T_{ref}	Reference temperature chosen as core body temperature (310K)	K
ΔT	temperature drop from inner to outer surface of the wall	K
u	axial velocity of blood flow	m/s
$\vec{u}$	velocity vector	m/s
U_0	maximum velocity at entrance	m/s

$\mathbf{v}$	filtration (radial) velocity	m/s
w	half width of the leaky junction	Nm
x	axial location from inlet	M
x_0	half width of atherosclerotic plaque	M
x_{st}	axial location of atherosclerotic plaque / stenosis	Cm
α	thermal diffusivity	m^2/s
α_f	the length ratio of proteoglycan monomers to central filament	1
α_{lj}	ratio of LDL molecule radius to half-width of the leaky junction	1
β_f	the length ratio of glycosaminoglycan (GAG) fiber to protein core	1
β_{lj}	leaky-bulk expansion ratio	1
β_T	thermal expansion coefficient	$1/K$
γ	sieving coefficient $(1-\sigma)$	1
δ	porosity	1
δ_{st}	ratio of maximum thickness of plaque to radius of lumen	1
ε	elastic strain	1
ε_T	thermal strain	1
ϕ	fraction of cells with leaky junction	1
μ	viscosity	$kg/m \bullet s$
ρ	fluid density	kg/m^3

σ	reflection coefficient	1
σ_s	Cauchy stress tensor	Pa
Γ	time period for pulsation	S
Subscripts		
0	refers to entrance condition	
70 mmHg	refers to property under 70 mmHg pressure drop across the wall without hyperthermia	
eff	refers to effective property	
end	refers to endothelium property	
int	refers to intima property	
f	refers to plasma property	
nj	refers to normal junction	
lj	refers to leaky junction property	
PG	refers to proteoglycan	
CG	refers to collagen	
Lip	refers to property affected by LDL lipid accumulation	

Chapter 1

Introduction

Cardiovascular disease is a critical issue with respect to human health due to the high rate of death that it causes. Almost 80 million adults in America have one or two types of cardiovascular diseases (American Heart Association, 2007; Khakpour and Vafai, 2008). Atherosclerosis is a type of cardiovascular disease that usually occurs in a larger artery like aorta and leads to other types of cardiovascular diseases. In most of the cases, the first symptom of atherosclerosis is a heart attack, and half of these lead to death, with the subsequent mortality rate increasing by 1-2% per hour after it is discovered (Wang

and Dake, 2006; Khanafer and Berguer 2009). On an annual basis, this aortic disease is not only associated with 1/5 of deaths in the United States by its complications (American Heart Association, 2005, 2006; Hossain et al., 2011) but also the 14th cause of death in America by itself (Gillum, 1995; Khanafer et al., 2009).

In fact, cardiovascular diseases are associated with almost half a trillion dollars expense in the United States of 2008 (American Heart Association, 2008; Hossain et al., 2011), and apparently, its impact to human society is still increasing now. Therefore, better understanding of the formation of atherosclerosis can lead to a better diagnosis and treatment of this disease. Although the main cause of atherosclerosis is still not fully established, many researchers consider the accumulation of macromolecules such as Low-density lipoproteins (LDL) initiates atherosclerosis. LDL oxidized with free radicals inside the arterial wall damages the cells and compromises the immune response, thus resulting in a wall dysfunction, plaque formation and lumen stenosis. As such, low-density lipoprotein (LDL) is considered to be one of the main factors in causing atherosclerosis.

A comprehensive model of LDL accumulation within the arterial wall is crucial in better demonstration of the involved processes leading to atherosclerosis. Prosi et al. (2005) introduced the wall-free and lumen wall models for representing an artery, which have been widely used to study mass transfer within arteries (Rappitsch and Perktold, 1996; Wada and Karino, 2000; Moore and Ethier, 1997; Stangeby and Ethier, 2002a, b).

However, the arterial wall posses a complex structure, and as such it is far more appropriate to consider several layers with different properties, referred to as the multi-layered model. Layers often encountered from lumen-side to the outer surface are glycocalyx, endothelium, intima, internal elastic lamina (IEL), media, and adventitia. Adventitia, which stabilizes the arterial attachment to organs, has a gel-like structure with connective tissues. Surrounded by adventitia, media is made up of smooth muscle cells and elastic tissues with capillaries. A very thin fenestrated membrane, referred as internal elastic lamina (IEL) separates the next laryer, intima, which is made up of collagen and proteoglycan fibers. Finally endothelium which is composed of a layer of cells is sandwiched between intima and a gel-like layer named glycoalyx which reduces the turbulence in blood flow.

Transport phenomena through porous media has been studied for numerous different fields of research (Hadim and Vafai, 2000; Vafai and Hadim, 2000; Razi et al.). Darcy and extended Darcy models were usually applied in earlier works (Chung and Vafai, 2010; Shi and Vafai, 2010). After Darcy model was presented by Henry Darcy, a number of works were tried to build the model comprehensively describing the flow and heat behavior inside porous medium. Brinkman (1947) counted the effect of solid boundary to develop a modification of Darcy model. The calculation for viscous force exerted by fluid on particle was given, and the relation between the particle geometry and the permeability was obtained. Vafai and Tien (1981) further analyzed the effects of solid boundary and inertial forces on transport through porous media. Volume-averaging

technique and matched asymptotic expansions were app lied in developing the governing equations. The generalized Darcy-Brinkman model collaborating with convection-diffusion-reaction equation is invoked in the present study, as well as the early works (Yang and Vafai, 2006, 2008; Ai and Vafai, 2006; Chung and Vafai, 2012, 2013).

The hydraulic and mass transport properties are different in each of these layers. Transport within these layers have been investigated, both from macro-scale view point (Huang et al., 1994; Tada and Tarbell, 2004; Prosi et al., 2005; Ai and Vafai, 2006) as well as a micro-scale point of view (Curry, 1984a, b; Fry, 1985; Wen et al., 1988; Huang et al., 1992; Huang et al., 1997; Huang and Tarbell, 1997; Yuan et al., 1991; Weinbaum et al., 1992; Karner et al., 2001; Liu et al., 2011; Chung and Vafai, 2012). For example, Ai and Vafai (2006) utilized a reverse procedure to solve for hydraulic permeability, effective diffusivity, and reflection coefficient of arterial porous layers using a circuit analogy. On the other hand, Huang et al. (1994), Karner et al. (2001), Liu et al. (2011) and Chung and Vafai (2012, 2013) obtained the properties with the methods using the micro-structure information, such as pore theorem and fiber matrix model.

Yang and Vafai (2006, 2008) and Ai and Vafai (2006) developed a comprehensive new four-layer model to describe the hydraulic and molecular transport inside an arterial wall. This model considers the arterial wall as four layers with different homogeneous properties. These layers are endothelium, intima, IEL, and media, while glycocalyx is neglected and adventitia is embedded into outer boundary condition. The Staverman-

Kedem-Katchalsky membrane equation (Kedem and Katchalsky, 1958) is invoked to describe the mass convection inside a low permeability porous medium. Also, osmotic pressure is brought into play inside thin layers of endothelium and IEL due to their high concentration gradient. Based on this model, the impact of macro-structure such as stenosis (Ai and Vafai, 2006; Kanafer et al., 2009) or bifurcation (Khakpour and Vafai, 2008) has also been studied. Furthermore, Chung and Vafai (2012, 2013) coupled the model with extended physics to represent the effect of fluid-structure interactions and atherosclerotic plaque.

The impact of stenosis on LDL transport has been discussed in Ai and Vafai's (2006) work. Starting with lipid accumulation, atherosclerosis results a lipid filled plaque that can block blood flow through an artery. Three stages can be cited during development of atherosclerosis: 1) cholesterol lipid accumulation inside arterial wall, especially within the intima layer; 2) thickening of the wall due to component deposits that cause stenosis; and 3) dysfunction of endothelium and fibrous cap formed on the inner wall surface within endothelium and intima (Hossain et al., 2011). Likewise, stenosis can be classified into three grades (Buchanan and Kleinstreuer, 1997): 1) no Stenosis (almost 0% blockage in the cross-sectional area); 2) moderate stenosis (less than 75% plaque blockage in the cross-sectional area); severe stenosis (more than 75% blockage in the cross-sectional area) (Ai and Vafai, 2006).

Ai and Vafai (2006) had discussed the LDL transport and its deposition inside the arterial wall along with variations in the thickness of the wall due to plaque formation. Their results show limited impact on LDL transport by stenosis due to the relatively higher permeability of intima. Hossain et al. (2011) obtained the hydraulic and molecular transport properties for the fibrous cap, as well as lipid filled intima, based on Stoke-Einstein equation assuming that the lipid viscosity is similar to that of the olive oil. Their results were applied to the simulation of drug delivery into a diseased artery, represented by a transient concentration distribution.

Most of the earlier works treat the arterial wall as a solid non-elastic medium, which does not represent the real physiological condition. The arterial wall is an elastic bio-material which will deform due to the pressure difference across the arterial wall. Furthermore, this deformation changes in time since the pressure applied from lumen side is affected by the pulsation of cardiovascular system. Gao et al. (2006a, b) performed a numerical simulation on the stress distribution across the aorta wall. Based on the work of Gao et al. (2006a, b), which considers zero pressure at the outlet of aorta, Khanafer and Berguer (2009) introduced a more realistic model by applying time-dependent pressure in a wave-form. Utilizing the fluid-structure interaction (FSI) model, Khanafer et al (2009) further analyzed the turbulent flow effect and the wall stress on aortic aneurysm.

Osmotic effect, accounting for flow driven by the gradient of solute density, typically is considerable across a thin porous membrane with significantly higher flow permeability and molecular concentration gradient than its solute permeability and hydraulic pressure. Osmotic pressure term was invoked for LDL transport through endothelium and IEL in some of the earlier works (Yang and Vafai, 2006, 2008; Ai and Vafai, 2006) due to a relatively high LDL concentration gradient across the two layers. However, although high gradient of LDL concentration does appears, there also is a high pressure drop (70mmHg or higher) across the wall dominating the plasma filtration. One of the missions in current study is to identify the impact of the Osmotic pressure, based on the earlier works (Yang and Vafai, 2006, 2008; Ai and Vafai, 2006, Chung and Vafai, 2012, 2013).

Hyperthermia is involved as an important factor or solution in several health issues, such as cancer treatment (Denekamp, 1984; Jain, 1987) or vascular stent delivery (Stoeckel et al., 2004; Baer et al., 2007), and the application can possibly be extended to treatment on atherosclerosis or other cardiovascular diseases. Therefore, for transport with an artery, since thermal impact is an important issue, the consideration of heat-induced effect may also be critical. It is known that the movement of molecules can also be driven by temperature gradient, the so called Sorret effect, and its counter part Dufour effect need to be analyzed particular for hyperthermia application. Furthermore, based on Einstein- Stoke model, the molecular diffusivity is dominated by temperature. The thermal expansion behavior of an artery has been studied by numbers of researchers

(Rabin and Plitz, 2005; Jimenez Rios and Rabin, 2006; Xu et al., 2007), and as such hyperthermia can cause change of transport properties, based on Chung and Vafai's FSI model (2012). Another aspect which can suspected to be affected by temperature is the reaction rate of LDL in the media layer.

In summary, the current work presents a model that couples the multi-layer model for LDL transport while fully incorporating plasma flow, deformable wall, elastic structure, effective properties, and heat transfer. FSI is invoked by considering a elastic wall with the endothelium properties affected by pore deformation. The change of hydraulic and mass transfer properties due to the wall deformation is analyzed, and its effect on flow and LDL transport through the arterial wall is investigated. Furthermore, the impact of pulsatile flow is studied along with its effect on the LDL transport within an arterial wall.

Then, the impact of atherosclerotic plaque on LDL transport is considered and analyzed, following Ai and Vafai's (2006) work which examined the stenosis rate and location. This work discusses the sensitivity to the plaque geometry, such as wall thickening, axial width etc. The impact of a simplified computational domain, as well as consideration of endothelium for a diseased artery and the role of the fibrous cap, is examined in this work. Furthermore, the intima properties affected by cholesterol accumulation are developed through fiber matrix method (Huang et al., 1992, 1994), and its effect on the variation of LDL transport is illustrated and discussed.

Moreover, coupling between hydraulic, mass, and heat transport, the influences of Osmotic, Sorret, and Dufour effects are examined. Further, to study the impact of the hyperthermia effect on molecular transport in an artery, thermal expansion, as well as temperature-dependent effective diffusivity and reaction rate of LDL, are analyzed. This study will provide a detailed understanding of the physics know to be involved in cause, result, or treatment of atherosclarosis.

Chapter 2

Formulation

2.1 Multi-layered model

The layered structure of the wall for an artery is shown in Fig. 1, from inner to the outer side, we have lumen, glycocalyx, endothelium, intima, IEL, media, and adventitia. In the present work, glycocalyx is neglected for the entire study due to its negligible thickness (Michel and Curry, 1999; Tarbell, 2003), and adventitia is embedded into the boundary condition on the outer wall surface for the models of plasma flow and heat and

mass transfer due to its low resistance (Yang and Vafai, 2006, 2008; Ai and Vafai, 2006). The lumen domain is considered as a cylindrical geometry with radius of R_0 $(310\mu m)$ and axial length L (0.2232 m), surrounded by the porous layers of endothelium, intima, IEL, and media. As such, the corresponding computational domain is given as Fig. 2 for each of the layers with their detailed information given in Table 1 (Karner et al., 2001; Yang and Vafai, 2006, 2008; Khanafer and Berguer, 2009; Chung and Vafai, 2012, 2013).

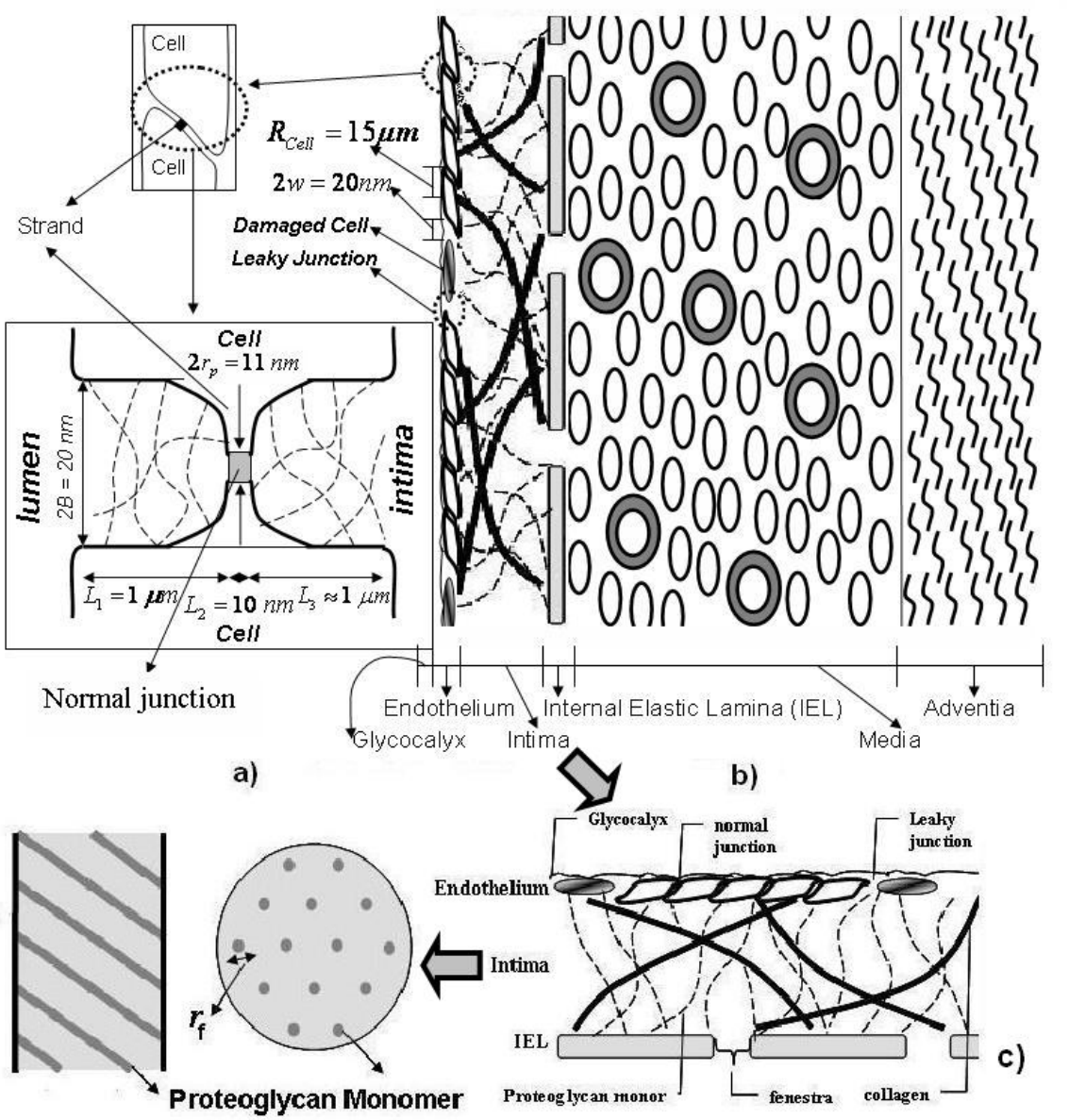

Figure 1 Configuration for a) Endothelial junctions; b) Multi-layered structure of an arterial wall including glycocalyx, endothelium, intima, IEL, media, and adventitia; c) Endothelium, intima, IEL, and intima fiber matrix; (Chung and Vafai, 2012, 2013).

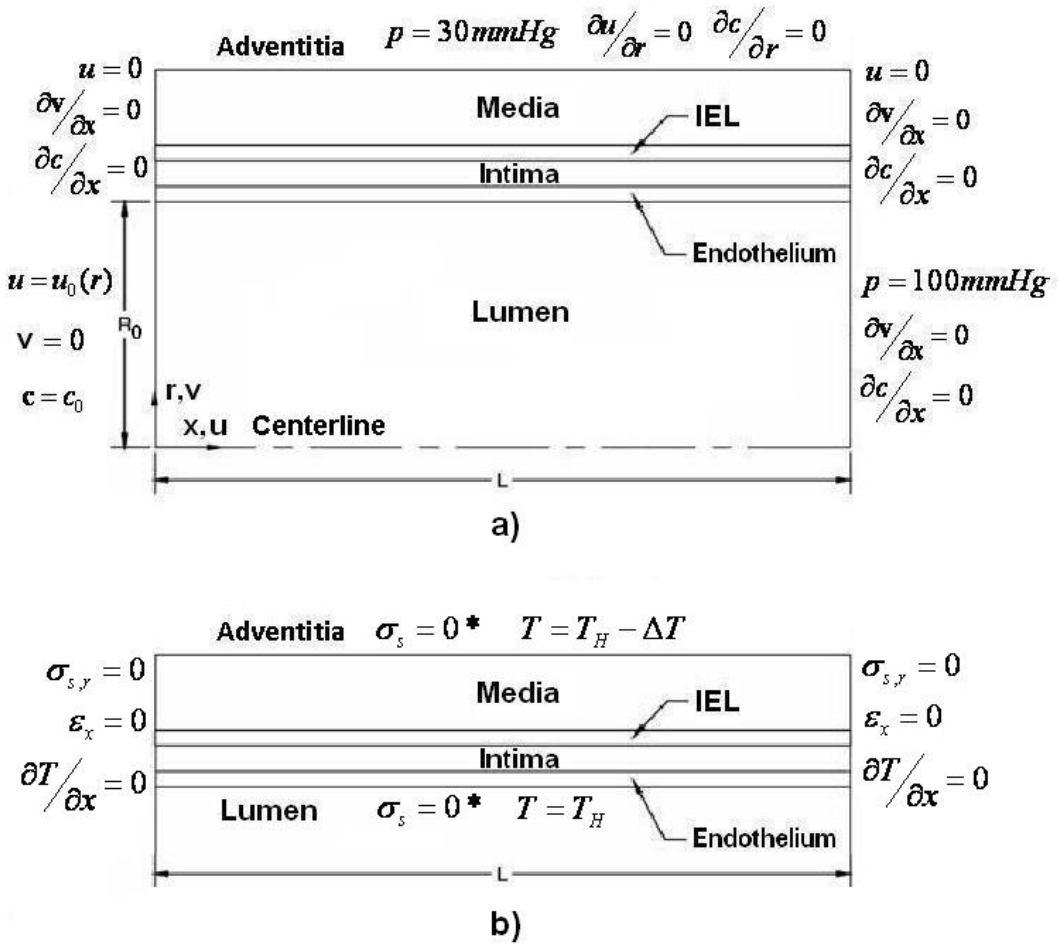

Figure 2 Configuration for analyzed domain and boundary conditions of a) flow and mass transfer; b) elastic and heat transfer models. (*: Hydraulic impact on elastic model under 70mmHg transmural pressure is already embedded into a pre-described leaky junction expansion (Chung and Vafai, 2012)).

	Lumen	Endothelium	Intima	IEL	Media	Adventitia
Thickness $[\mu m]$	3100	2	10	2	200	100
Density $\rho\ [kg/m^3]$	1.07×10^3	1.057×10^3	1.057×10^3	1.057×10^3	1.057×10^3	-
Viscosity $\mu_{eff}\ [kg/m\bullet s]$	3.7×10^{-3}	0.72×10^{-3}	0.72×10^{-3}	0.72×10^{-3}	0.72×10^{-3}	-
Hydraulic permeability K $[m^2]$	-	3.22×10^{-21}*	2×10^{-16}	4.392×10^{-19}	2×10^{-18}	-
LDL effective diffusivity $D_{eff}\ [m^2/s]$	2.87×10^{-11}	5.7×10^{-18}*	5.4×10^{-12}	3.18×10^{-15}	5×10^{-14}	-
refection coefficient σ	-	0.9888*	0.8272	0.9827	0.8836	-
reaction coefficient $k\ [s^{-1}]$	0	0	0	0	3.197×10^{-4}	-
elasticity $[MPa]$	-	2	2	2	6	4
Thermal diffusivity $\alpha\ [m^2/s]$	-	1.42×10^{-7}	1.42×10^{-7}	1.42×10^{-7}	1.42×10^{-7}	-

*** indicate the parameters with gage pressure of** $70 mmHg$

Table 1 Transport properties for each of the layers/domains (Chung and Vafai, 2012)

2.2 Governing equations

The hydraulic and molecular transport in the lumen region is described by continuity, Navier-Stokes and convection-diffusion equations, and thus the governing equations for conservation of mass, momentum and species are given as:

$$\nabla \bullet \vec{u} = 0 \tag{1a}$$

$$\rho \frac{D\vec{u}}{Dt} = -\nabla p + \mu_f \nabla^2 \vec{u} \tag{1b}$$

$$\frac{\partial c}{\partial t} + \vec{u} \bullet \nabla c = D_f \nabla^2 c \tag{1c}$$

where $\vec{u}$ is the velocity vector, c LDL concentration, p hydraulic pressure and μ_f and D_f are the plasma viscosity and diffusivity coefficient respectively.

The flow and mass transfer behaviors within the four layers, endothelium, intima, IEL, and media, are represented by Darcy-Brinkman and diffusion-convection-reaction equations while incorporating the Staverman-Kedem-Katchalsky membrane equation (Kedem and Katchalsky, 1958), and thus the governing equations are given (Yang and Vafai, 2006; Ai and Vafai, 2006, Chung and Vafai, 2012, 2013) as:

$$\nabla \bullet \vec{u} = 0 \tag{2a}$$

$$\frac{\rho}{\delta} \frac{\partial \vec{u}}{\partial t} + \frac{\mu_{eff}}{K} \vec{u} = -\nabla p + \mu_{eff} \nabla^2 \vec{u} \tag{2b}$$

$$\frac{\partial c}{\partial t} + (1-\sigma)\vec{u} \bullet \nabla c = D_{eff} \nabla^2 c - kc \qquad (2c)$$

where μ_{eff} is effective fluid viscosity, K hydraulic permeability; σ reflection coefficient; D_{eff} effective LDL diffusivity. reaction coefficient k which represents the LDL consumption is $3.197 \times 10^{-4}\ [s^{-1}]$ inside the media layer and zero in the other layers (Prosi et al., 2005; Yang and Vafai, 2006, 2008). The properties utilized in the early works by Yang and Vafai (2006) and Ai and Vafai (2006) are given in Table 2, used for methodology validation and results comparison in the later section. The property values for each of the layers are listed in Table 1 (Chung and Vafai, 2012), while the variable endothelium properties due to FSI or hyperthermia and the variable intima properties due to the lipid accumulation are considered later in this work.

Ref	Parameter	Lumen	Endothelium	Intima	IEL	Media
(a) Yang and Vafai (2006)	Diffusivity $D_{eff}\ [m^2/s]$	2.87×10^{-11}	6×10^{-17}	5.4×10^{-12}	3.18×10^{-15}	5×10^{-14}
	Permeability K $[m^2]$		4.32×10^{-21}	2×10^{-16}	4.392×10^{-19}	2×10^{-18}
	Refection coefficient σ		0.9979	0.8272	0.9827	0.8836
	Porosity δ		5×10^{-4}	0.983	0.002	0.258
	Viscosity $\mu_{eff}\ [kg/m\bullet s]$	3.7×10^{-3}	0.72×10^{-3}	0.72×10^{-3}	0.72×10^{-3}	0.72×10^{-3}
(b) Ai and Vafai (2006)	Diffusivity $D_{eff}\ [m^2/s]$	2.87×10^{-11}	8.154×10^{-17}	5×10^{-12}	3.18×10^{-15}	5×10^{-14}
	Permeability K $[m^2]$		3.2172×10^{-21}	2.2×10^{-16}	3.2188×10^{-19}	2×10^{-18}
	Refection coefficient σ		0.9886	0.8292	0.8295	0.8660
	Porosity δ		5×10^{-4}	0.96	0.004	0.15
	Viscosity $\mu_{eff}\ [kg/m\bullet s]$	3.5×10^{-3}	0.72×10^{-3}	0.72×10^{-3}	0.72×10^{-3}	0.72×10^{-3}

Table 2 Hydraulic and LDL transport properties for each of the layers/domains utilized by a) Yang and Vafai (2006); b) Ai and Vafai (2006)

2.3 Governing equations – FSI and hyperthermia

When deformable wall is considered within the wall, a hyper-elastic model is used to describe the elastic structure of the artery, and thus the elastodynamic equation can be written as:

$$\rho_s \ddot{d}_s = \nabla \sigma_s + f_s \tag{3}$$

where ρ_s is the density, $\ddot{d}_s$ acceleration within the solid region, f_s solid domain body force and σ_s is the Cauchy stress tensor, where Mooney-Rivlin material model is invoked to describe the strain-energy relationship (Khanafer and Berguer, 2009). Strain due to hydraulic effect is embedded into the properties by assuming that pressure difference through the wall stays constant at 70mmHg.

When heat transfer is considered within the wall, a uniform temperature ($T = T_H$) and no solid (free structure) are assumed for the lumen region. The heat transfer within an arterial wall is described by the equation of energy conservation, expressed as:

$$\vec{u} \bullet \nabla T = \alpha \nabla^2 c \tag{4}$$

where T is temperature and α is the thermal diffusivity. Since the thermal permeability is much higher than the molecular permeability, which is mostly assumed negligible, through cells and fibers of an arterial wall, the porosity and structure does not affect

much on as Therefore, the thermal diffusivity is assume to be the same as $1.42\times10^{-7}[m^2/s]$ (Kolios et al., 1995; Kotte et al., 1996) for all the arterial layers.

2.4 Governing equations – coupling effect

Osmotic pressure expression is represented by $RT\sigma\nabla c$ where R is the universal gas constant. Similar to Osmotic effect, the temperature gradient can also cause energy potential to drive molecular movment from higher to lower temperature The Soret diffusion is given by $D_{eff}\frac{k_T\rho_f}{TM_f}\nabla^2 T$ (Chapman and Cowling, 1952; Wakeham et al., 1991; Kays and Crawford, 1993), where k_T is the thermal-diffusion coefficient, M_f the molecular weight of solvent (plasma), and ρ_f is the density of plasma. The counter part of the Sorret effect is the Dufour effect, which indicates that the molecular transport will enhance heat transfer by the energy carried by the solute. Dufour effect is represented by $D_{eff}\frac{RTk_T}{c_T M_f c}\nabla^2 c$, where c_T is the plasma's thermal capacity. Incorporating these three physical effects, the coupled equations for flow, heat and mass transfer can be presented as:

$$-\nabla p+\mu_{eff}\nabla^2\vec{u}-\frac{\mu_{eff}}{K}\vec{u}+RT\sigma\nabla c=0 \tag{5a}$$

$$(1-\sigma)\vec{u}\bullet\nabla c=D_{eff}(\nabla^2 c+\frac{k_T\rho_f}{TM_f}\nabla^2 T)-kc \tag{5b}$$

$$\vec{u}\bullet\nabla T=\alpha\nabla^2 T+D_{eff}\frac{RTk_T}{c_T M_f c}\nabla^2 c \tag{5c}$$

2.5 Boundary conditions

The boundary conditions are illustrated in Fig. 2, where the axial velocity u at the entrance is considered to have a fully developed profile $u_0(r)$ expressed by:

$$u_0 = U_0(1-(r/R_0)^2) \qquad at\ x = 0, 0 \le r \le R_0 \tag{6}$$

where the maximum entrance velocity U_0 is taken as $0.338\, m/s$ (Yang and Vafai, 2006; Karner et al., 2001) and LDL concentration at the entrance c_0 is taken as $28.6\times10^{-3}\, mol/m^3$ (Katz, 1985; Tarbell, 1993; Yang and Vafai, 2006). Hydraulic pressure p is set to be fixed with the values of $30 mm\,Hg$ and a total pressure drop of $\Delta p = 70 mm\,Hg$ through the arterial wall (Meyer et al., 1996; Yang and Vafai, 2006) is given at the outer surface (media-adventitia interface) resulting the highest pressure within lumen as $100 mm\,Hg$. For a pulsatile flow with a time period of $\Gamma = 1s$, U_0 and Δp become time-dependent by added $U_0 \sin(2\pi t/\Gamma)\,[m/s]$ and $25\sin(2\pi t/\Gamma)\,[mm\,Hg]$ respectively (Chung and Vafai. 2012)

Continuity conditions for the flow and mass transfer are invoked at the interface between each of the layers while incorporating the Staverman filtration condition (Yang and Vafai, 2006; Chung and Vafai, 2012) as:

$$[(1-\sigma)\mathbf{v}c - D_{eff}\frac{\partial c}{\partial r}]\Big|_{+} = [(1-\sigma)\mathbf{v}c - D_{eff}\frac{\partial c}{\partial r}]\Big|_{-} \quad (7)$$

where $\mathbf{v}$ is the filtration velocity of the blood flow penetrating through the arterial wall in the radial direction. Also, the lumen-wall interface is experiences the hyperthermia effect with a temperature of T_H, while the media-adventitia interface has a temperature drop through the wall given by ΔT. Both inner and outer surfaces of arterial wall are set as a free surface since the hydraulic impact is embedded within the transport properties (Chung and Vafai, 2012).

2.6 Calculation of Endothelium Properties from the Micro-structure attributes

Endothelium causes the most hydraulic and mass transfer resistance across the wall compared to other arterial layers due to its low porosity and small pore size. Therefore, the endothelium pore expansion due to elastic deformation on the arterial wall will have much higher impact on the flow and mass transfer characteristics within an artery. Based on the work of Chung and Vafai (2012), the Pore theorem, which is well accepted for calculating transport properties of endothelium (Curry, 1984a, b; Huang et al., 1992; Karner et al., 2001), is utilized here to couple the thermal expansion with the property variations within the endothelium. The pores of endothelium can be characterized as normal or leaky junction as shown in Fig. 1a. Normal junction is the space between strands which connects the endothelial cells, while its area is barely affected by the electric deformation due to a stronger support by strands than the leaky junction. Leaky junction is formed due to the dysfunctional strands around the damaged cells with a substantially larger cross-sectional area than that of a normal junction.

Pore theorem is well accepted for calculating permeability, effective diffusivity, and reflection coefficient in the literature (Curry, 1984; Huang et al., 1992; Karner et al., 2001). Applying pore theorem, the endothelium permeability K_{end} can be expressed as:

$$K_{end} = K_{lj} + K_{nj} \tag{8a}$$

$$K_{lj} = \frac{w^2}{3}\frac{4w\phi}{R_{Cell}} \tag{8b}$$

where w is the half-width of the leaky junction, R_{Cell} is radius of the endothelial cell taken as $15\mu m$, and ϕ is the fraction of the leaky junction taken as 5×10^{-4} (Huang et al., 1992).

In this study, the normal junction is assumed to be impermeable for the LDL molecule ($D_{nj}=0;\sigma_{nj}=1$), since the average radius of the normal junction is $5.5nm$, which is smaller the radius of LDL molecule ($r_m=11nm$). Therefore using the pore theorem and incorporating the effect of the tissue matrix, the effective diffusivity and reflection coefficients can be calculated as:

$$D_{end} = D_{lj} = D_{free}(1-\alpha_{lj})(1-1.004\alpha_{lj}+0.418\alpha_{lj}^3-0.169\alpha_{lj}^5)\frac{4w}{R_{Cell}}\phi \tag{9}$$

$$\sigma_{end} = \frac{\sigma_{nj}K_{nj}+\sigma_{lj}K_{lj}}{K_{nj}+K_{lj}} = 1-\frac{(1-\sigma_{lj})K_{lj}}{K_{nj}+K_{lj}} \tag{10a}$$

$$\sigma_{lj} = 1-(1-\frac{3}{2}\alpha_{lj}^2+\frac{1}{2}\alpha_{lj}^3)(1-\frac{1}{3}\alpha_{lj}^2) \tag{10b}$$

where α_{lj} is the ratio of r_m to w.

Huang et al. (1992) and (Karner et al., 2001) specified the half width of the leaky junction as $w=10nm$, which is the same as the cleft opening for a normal junction. This

value of width is smaller than the radius of LDL particle, so leaky junction, by pore theorem, becomes impermeable to LDL molecule. However, when deformation occurs, realistically, without the connection of strands between cells, leaky junction should have a larger gap. As such, a more reasonable representation should be calculated based on the approach given in Ai and Vafai (2006).

To obtain more realistic values of w, Ai and Vafai (2006) presented a logical approach through the application of circuit analogy to obtain

$$N''/_C = \frac{D_{end} Pe_{end} \exp(Pe_{end})}{H_{end}(\exp(Pe_{end})-1)} \tag{11}$$

where N'' is solute mass flux per area, H_{end} thickness of endothelium, and the Peclet number for endothelium Pe_{end} can be expressed as:

$$Pe_{end} = \frac{(1-\sigma_{end})H_{end}}{D_{end}} u \tag{12}$$

Further, in Ai and Vafai's (2008) work, the normal case corresponded to a lumen pressure of $100 mmHg$, $N''/_C = 2\times10^{-10}\,[m/_s]$, $u = 1.78\times10^{-8}\, m/s$, and $K_{end} = 3.22\times10^{-21}\,[m^2]$ (Truskey et al., 1992; Meyer et al., 1996; Huang and Tarbell's, 1997). Solving equations 8 to 12, results in the half width of the leaky junction as $14.343\, nm$, when the gage pressure is $70 mmHg$. The corresponding properties of endothelium with gage pressure of $70 mmHg$ can be seen in Table 1, which is used as a reference value when calculating properties due to deformation.

2.7 Strain-pore size ($\varepsilon - w$) relation

The θ – direction strain ε ,obtained from the elastic equation, is considered to have a substantially more impact on the pore size w due to the pore shape and distribution. To correlate ε with w, a coefficient β_{lj} is introduced as:

$$\beta_{lj} = \frac{\varepsilon_{lj}}{\varepsilon} \tag{13a}$$

where ε_{lj} is the expansion ratio of the leaky junction. Since cross-sectional area of the leaky junction is $2\pi R_{cell} w$, w can be considered as a function of ε:

$$w = w_{70mmHg} \frac{1+\beta_{lj}\varepsilon}{1+\beta_{lj}\varepsilon_{70mmHg}} \tag{13b}$$

Transport properties of endothelium given in Table 1 for endothelium are obtained by Chung and Vafai (2012) based on a 70mmHg pressure drop across the arterial wall, using the pore theorem with corresponding half-width of the leaky junction of 14.34nm. On the other hand, the impact of thermal expansion due to hyperthermia is considered through the thermal strain ε and temperature T relationship given by:

$$\varepsilon_T = \beta_T (T - T_{ref}) \tag{13c}$$

where β_T is the thermal expansion coefficient with a value of $6.376\times10^{-5}\ 1/K$ (Rabin and Plitz, 2005; Jimenez Rios and Rabin, 2006; Xu et al., 2007) and T_{ref} is the reference

temperature given as the regular organ temperature of 310K. Applying pore theorem (Chung and Vafai, 2012), the endothelium permeability K_{end} can be solved using Eqs. 8. Also, the effective diffusivity D_{end} and reflection coefficients σ_{end} can be calculated using Eqs. 9 and 10.

2.8 Atheromatous plaque and stenosis

To study LDL transport inside a diseased artery, a computational domain similar to that used in Ai and Vafai's (2006) work is utilized as shown in Fig. 3a. The atherosclerotic plaque is considered by a partial wall thickening within the intima layer that causes stenosis, characterized by δ_{st}, ratio of maximum thickness to lumen radius, x_{st}, its axial location from inlet, and x_0, its half width. Ai and Vafai's work (2006), considered the transport properties of all arterial layers for a diseased artery with atherosclerotic plaque to be the same as those within a normal artery when cholesterol lipid accumulation is not considered. However, the variable properties of intima due to lipid filling should be considered. In this work, this is done by applying the fiber matrix theory within a computational domain that incorporates the multi-layered structure of the diseased arterial wall as shown in Fig. 3d.

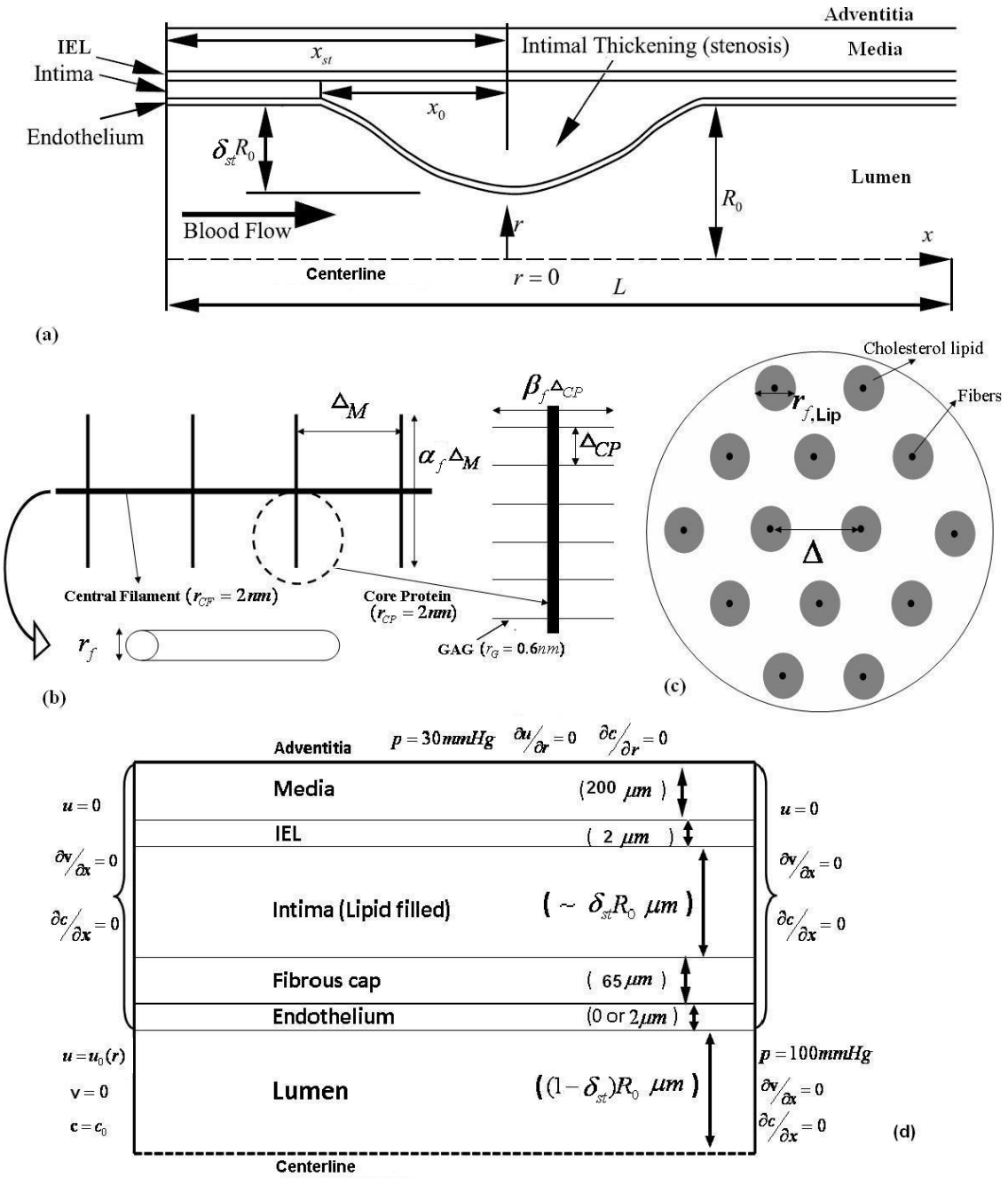

Figure 3 Configuration for a) Analyzed domain in the presence of stenosis (Ai and Vafai, 2006) ; b) Proteoglycan fibers within intima (Huang et al. 1994) c) Fiber matrix filled with cholesterol lipid; d) Analyzed region for the stenosis/plaque case.

2.9 Fiber matrix model and intima properties

The intima is mainly formed by proteoglycan fibers (Fig. 3b), and looser-thicker collagen fibers (Frank and Fogelman, 1989), which can be represented as a homogeneous fiber matrix as shown in Fig. 1c. Intima has less influence on flow and molecular transport than endothelium and IEL have on a normal arterial wall due to its high permeability. Ai and Vafai (2006) pointed out that diffusion in intima layer is not substantial, which was also confirmed in Yang and Vafai's (2006) study. The micro-structure of intima fiber matrix can be characterized by its porosity δ and effective fiber radius r_f. A common way to calculate the effective radius of intima protein, r_f (Huang et al., 1994; Dabagh et al., 2009) is:

$$r_f = [\frac{\alpha_f r_M^{\ 2} + r_{CF}^{\ 2}}{\alpha_f + 1}]^{1/2} \tag{14a}$$

where α_f is the length ratio of proteoglycan monomers to central filament, with a value which is variant between 3 to 10 (Lark et al., 1988), r_{CF} is radius of central filament with a value around 2 nm (Buckwalter and Rosenberg, 1982), and r_M is the effective monomer radius calculated by:

$$r_M = [\beta_f r_G^{\ 2} + r_{CP}^{\ 2}]^{1/2} \tag{14b}$$

where β_f is the length ratio of glycosaminoglycan (GAG) fiber to protein core with a

value which is variant between 5 to 10 (Lark et al., 1988), r_G is radius of GAG with a value of 0.6 nm, r_{CP} is radius of proteoglycan core protein with a value of 2 nm (Buckwalter and Rosenberg, 1982). By taking $\alpha_f = 3$ and $\beta_f = 5$ (Dabagh et al., 2009; Liu et al. 2011), we can obtain the effective fiber radius for proteoglycan as 2.31 nm.

Utilizing the Carman-Kozney equation (Curry and Michel, 1980; Curry, 1984a, b), the intima's permeability K_{int} can calculated as:

$$K_{\text{int}} = \frac{{r_f}^2 \delta^3}{4G(1-\delta)^2} \tag{15a}$$

where ε is the porosity of intima, and G is the Kozney constant which, for randomly oriented fibers, is calculated as (Happel and Brenner, 1965):

$$G = \frac{2}{3}\frac{2\delta^3}{(1-\delta)[2\ln(\frac{1}{1-\delta}) - 3 + 4(1-\delta) - (1-\delta)^2]} + \frac{1}{3}\frac{2\delta^3}{(1-\delta)[\ln(\frac{1}{1-\delta}) - \frac{1-(1-\delta)^2}{1+(1-\delta)^2}]} \tag{15b}$$

The molecular transport properties for LDL particle through intima, such as the effective diffusivity D_{eff} and reflection coefficient σ can be calculated by (Huang et al. 1992, 1994):

$$D_{eff} = D_f \exp[-(1-\delta)^{1/2}(1+\frac{r_m}{r_f})] \tag{16a}$$

$$\sigma = (1-\phi_{\text{int}})^2 \tag{16b}$$

where r_m is LDL molecular radius taken as 11 nm (Huang et al., 1992, 1994), and ϕ_{int} is the partition coefficient obtained by:

$$\phi_{\text{int}} = \exp[-(1-\delta)(\frac{2r_m}{r_f} + \frac{r_m^2}{r_f^2})] \tag{16c}$$

In the work of Dabagh et al. (2009) and Liu et al. (2011), in addition to proteoglycan fibers, the collagen fibers are also considered. As such the transport properties were calculated as:

$$\frac{1}{K_{\text{int}}} = \frac{1}{K_{PG}} + \frac{1}{K_{CG}} \tag{17a}$$

$$D_{eff} = D_f \exp[-(1-\delta_{PG})^{1/2}(1+\frac{r_m}{r_f})](\delta_{PG} + \delta_{CG} - 1)\exp[-(1-\delta_{CG})^{0.5}(1+\frac{r_m}{r_{CG}})] \tag{17b}$$

$$\sigma = (1-\phi_{\text{int}})^2 \tag{17c}$$

$$\phi_{\text{int}} = \exp[-(1-\delta_{PG})(\frac{2r_m}{r_f} + \frac{r_m^2}{r_f^2})](\delta_{PG} + \delta_{CG} - 1)\exp[-(1-\delta_{CG})^{0.5}(1+\frac{r_m}{r_{CG}})] \tag{17d}$$

where δ_{PG} and δ_{CG} are the porosity of proteoglycan and collagen fibers, and r_{CG} is radius of collagen fiber set as 20 nm (Dabagh et al, 2009). Also, K_{PG} and K_{CG} are calculated through equations 15, using δ_{PG} and δ_{CG} as the porosity and r_f and r_{CG} as the fiber radius. However, due to a much coarser distribution of collagen fibers, it is considered to have an insignificant impact. Therefore, an alternative way is to use equations 15 and 16 with porosity defined by $\delta = \delta_{PG}\delta_{CG}$ (Dabagh, 2009).

Chapter3

Methodology and Validation

The results for the velocity field and mass concentration are obtained using, Comsol Multi-physics, with post-processing through the use of a Matlab code. Comsol utilizes a finite element method with adaptive meshing and error control within different numerical solvers for governing partial differential equations. The direct linear system solver UMFPAC is utilized in this work. Rigorous grid independence was established for the results presented in this work with relative and absolute errors less than 10^{-3} and 10^{-6} respectively. Our model and the computational results were validated through

comparison with the available limiting cases in the literature. The LDL component was compared (Figs. 4-9) with the works of Yang and Vafai (2006, 2008) and Ai and Vafai (2008), while validation for FSI model (Figs. 10 &11) was done with the work of Khanafer and Berguer (2009).

Chapter4

Results Comparison

4.1 LDL transport Model

Figures 4 and 5 illustrate the comparisons with Yang and Vafai's (2006) work. As can be seen both the filtration velocity and LDL concentration are in very good agreement with Yang and Vafai's (2006) numerical results which were obtained using an entirely different solution scheme. Comparisons of LDL concentration across intima, IEL and media with both numerical and analytical results of Yang and Vafai (2006, 2008) are

demonstrated in Fig. 6. Once again a very good agreement is observed with only a very small difference near endothelium-intima interface. The present results are very close to those of Yang and Vafai (2006, 2008), especially to Yang and Vafai's analytical work (2008).

For further validation of computational results and LDL transport model within the multi-layers, another set of comparisons with Ai and Vafai's (2008) work are shown in Figures 7-9. Filtration velocity and LDL concentration at endothelium-intima interface obtained in the present work are compared with those in an earlier study, resulting very good agreement as seen in Figs 7 and 8. A perfect agreement can be seen in Fig. 9, for LDL concentration across each of the arterial layers against the results of Ai and Vafai (2008).

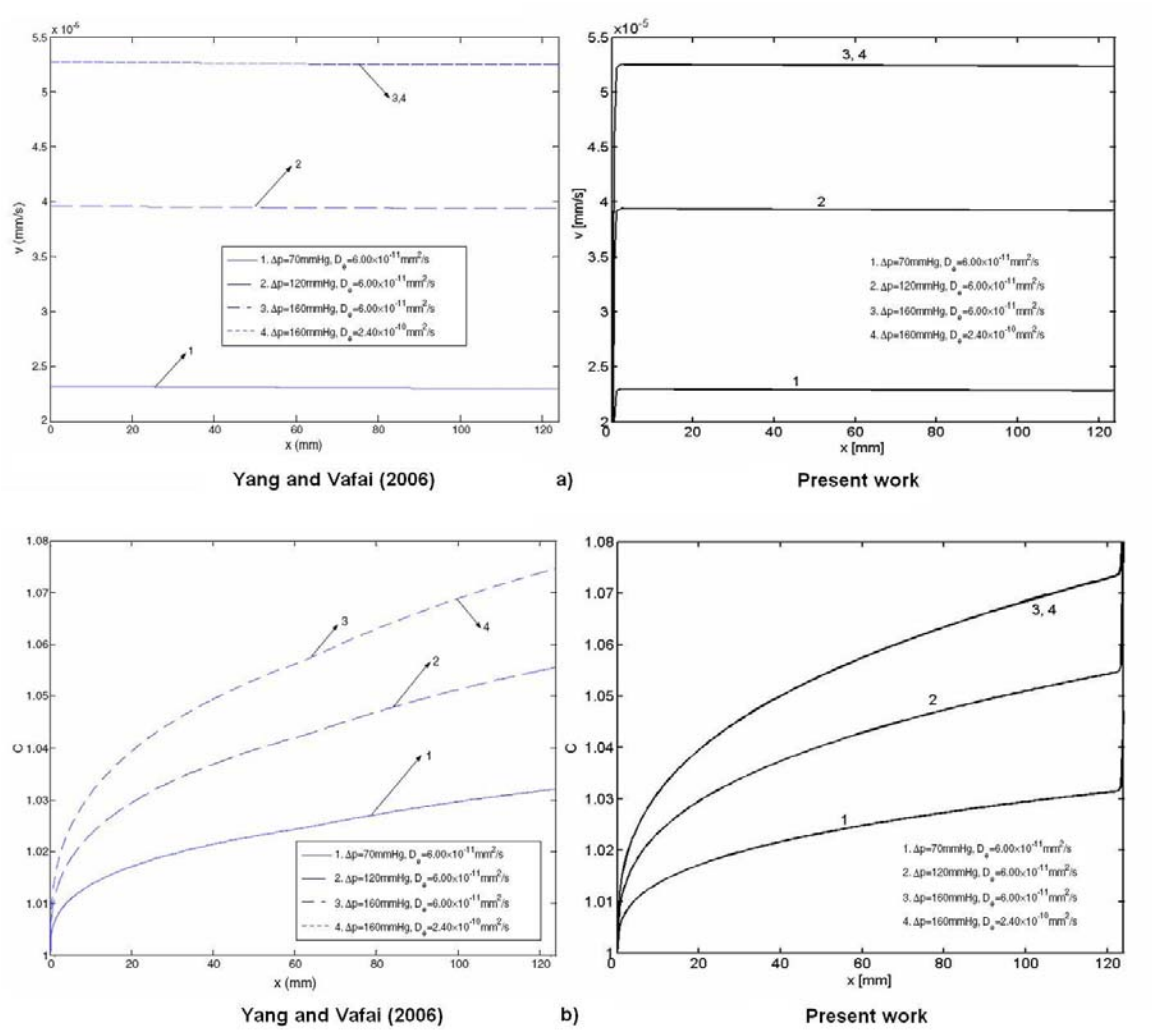

Figure 4 Comparison of a) filtration velocity; b) LDL concentration at lumen-endothelium interface with those of Yang and Vafai (2006)

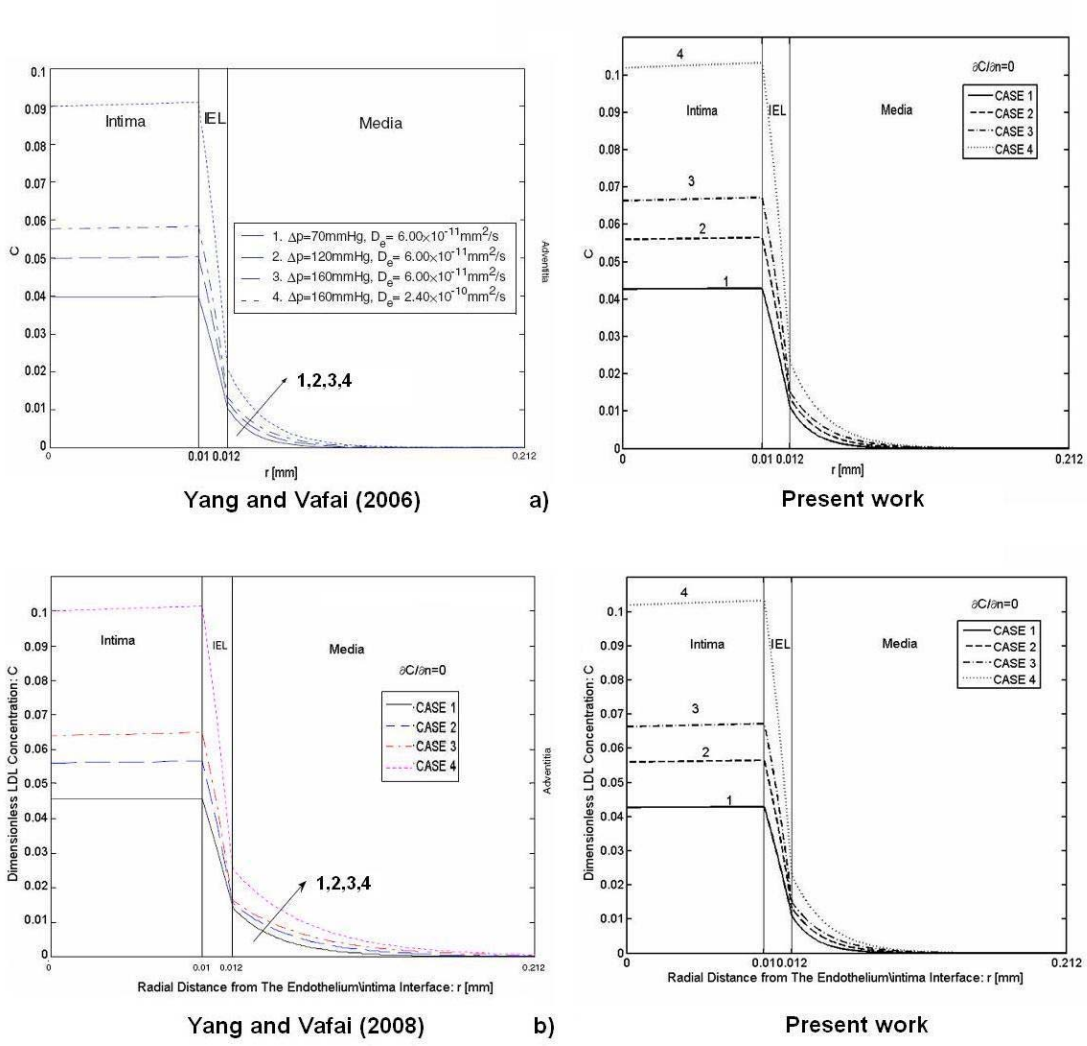

Figure 5 Comparison of normalized LDL concentration across intima, IEL, and media at different gage pressures and effective diffusivities with a) numerical and b) analytical results of Yang and Vafai (2006, 2008)

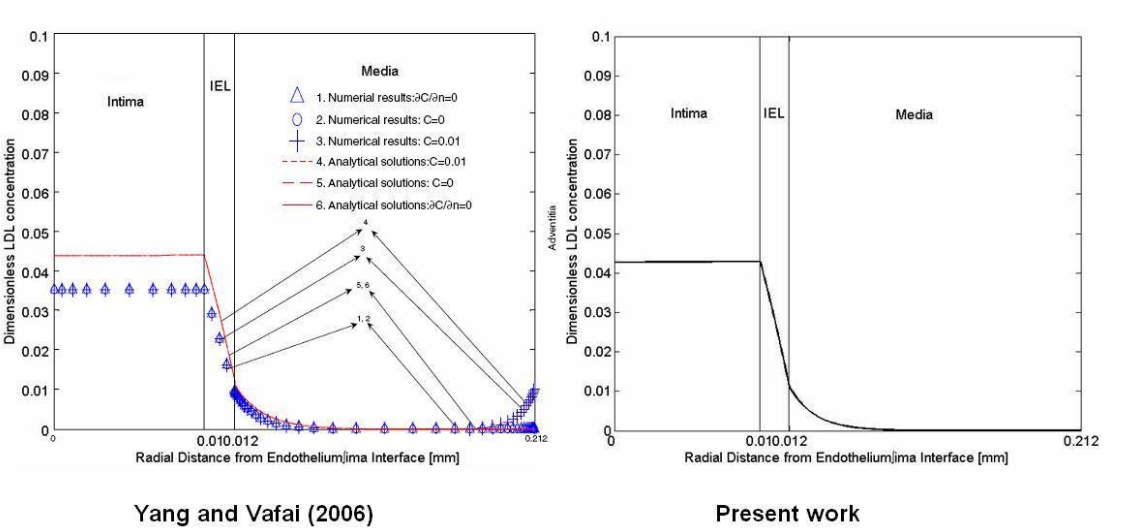

Figure 6 Comparison of normalized LDL concentration across intima, IEL, and media with numerical and analytical results of Yang and Vafai (2006, 2008)

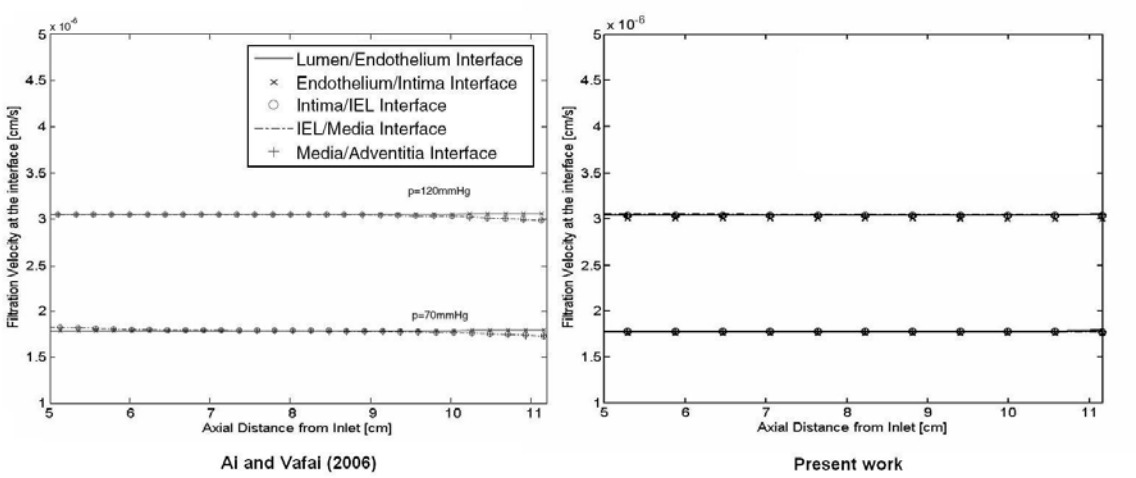

Figure 7 Comparison of filtration velocity at different interface and axial locations with those by Ai and Vafai (2008).

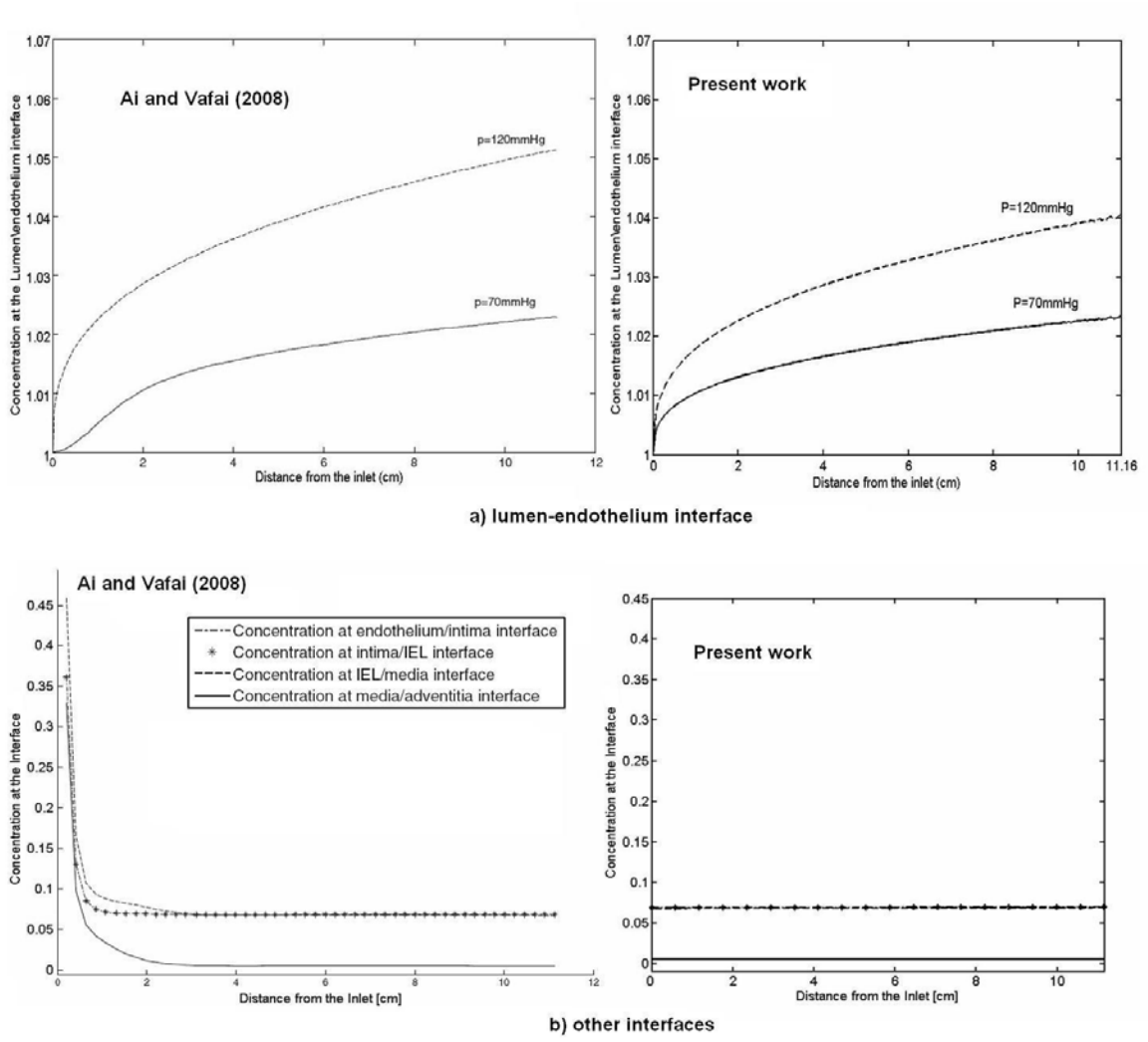

Figure 8 Comparison of normalized LDL concentration at different interface and axial locations with those by Ai and Vafai (2008).

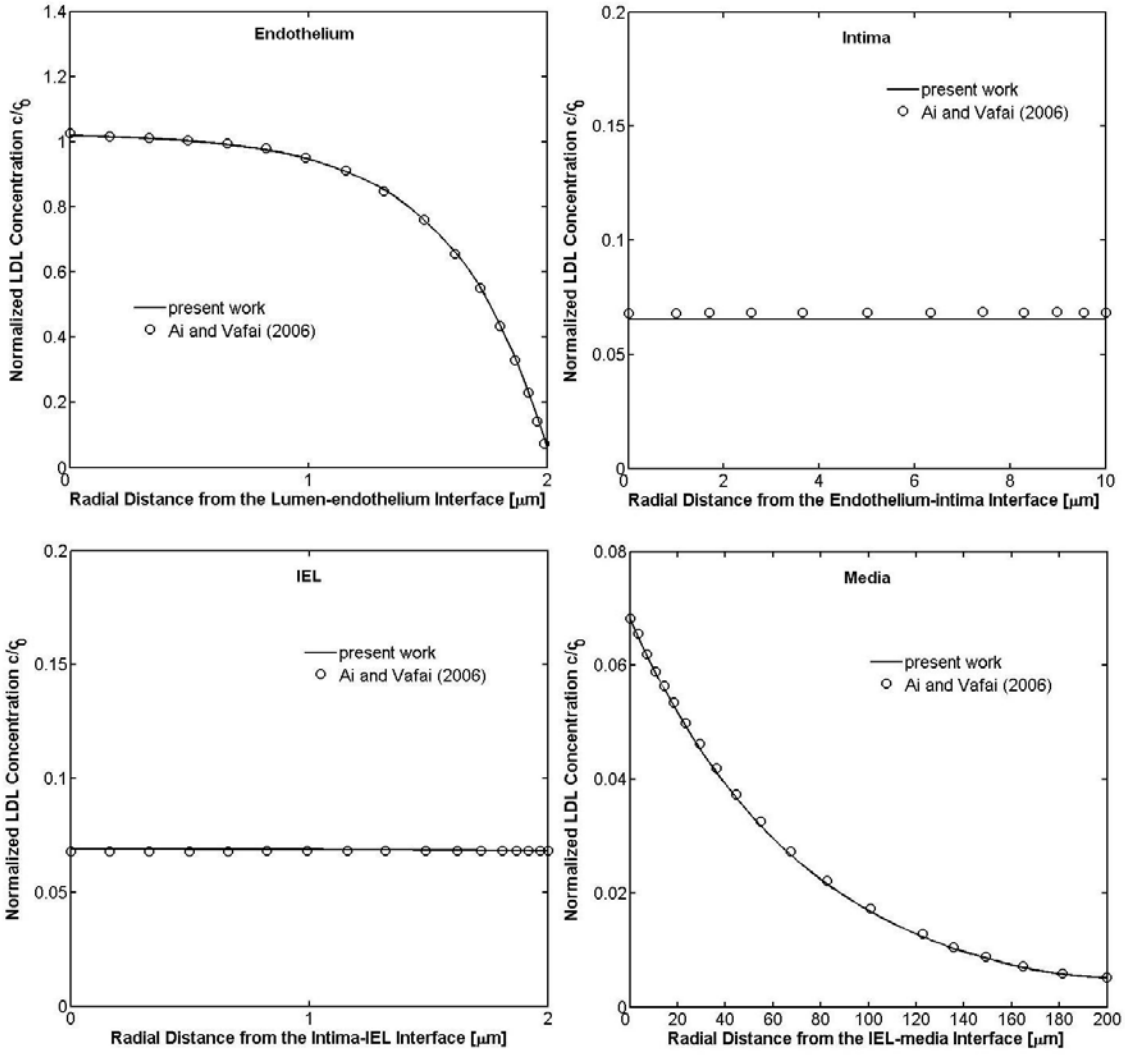

Figure 9 Comparison of normalized LDL concentration c/c_0 across each of the arterial layers with those by Ai and Vafai (2006) [presented in Chung and Vafai (2012)].

4.2 Elastic model and Stenosis

Figure 10 displays Von Misses stress at different parts of the pulsation cycle across the arterial wall. Effects of higher value of elasticity across media are shown in Fig. 9 The present results are compared with those obtained by Khanafer and Berguer (2009), showing excellent agreement for the results presented in Figs. 10 and 11. Figures 2-9 establish and validate different modules of the current models against available limiting cases in the literature covering both multilayer as well as the FSI attributes

.

Besides the normal artery, the model developed in this work is also compared with the work of Ai and Vafai (2006) for a diseased artery with stenosis, using a different solution methodology. In the comparison, the results from both shows an insignificant impact as result of either thickening of the wall or different stenosis locations (Fig. 12a), even with different boundary conditions on the outer surface (adventitia side, $r = 3.314mm$) that is commonly applied (Fig 12b). As can be seen, the results are comparable, with a small discrepancy due to different setting of boundary condition on the adventitia side.

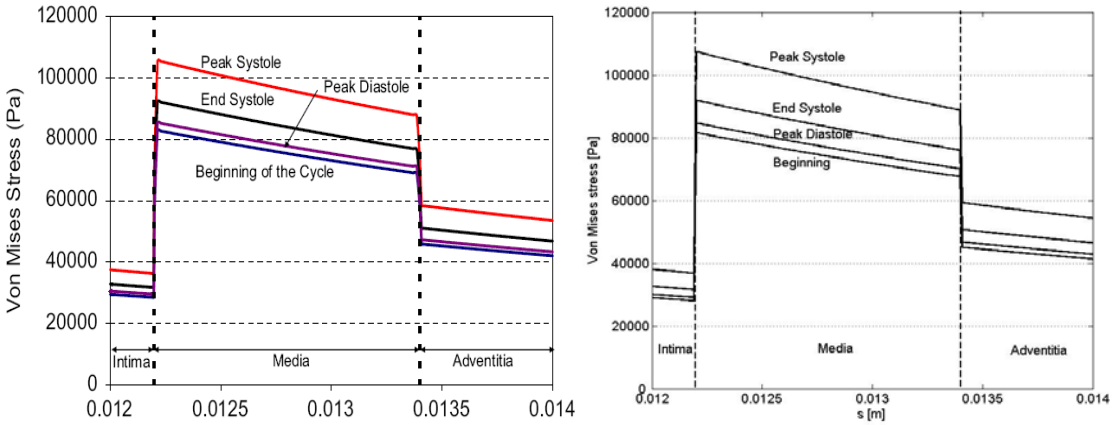

Khanafer and Berguer (2009) **Present work**

Figure 10 Comparison of Von Mises Stress across arterial wall at different steps in pulsation cycle with those by Khanafer and Ramon (2009)

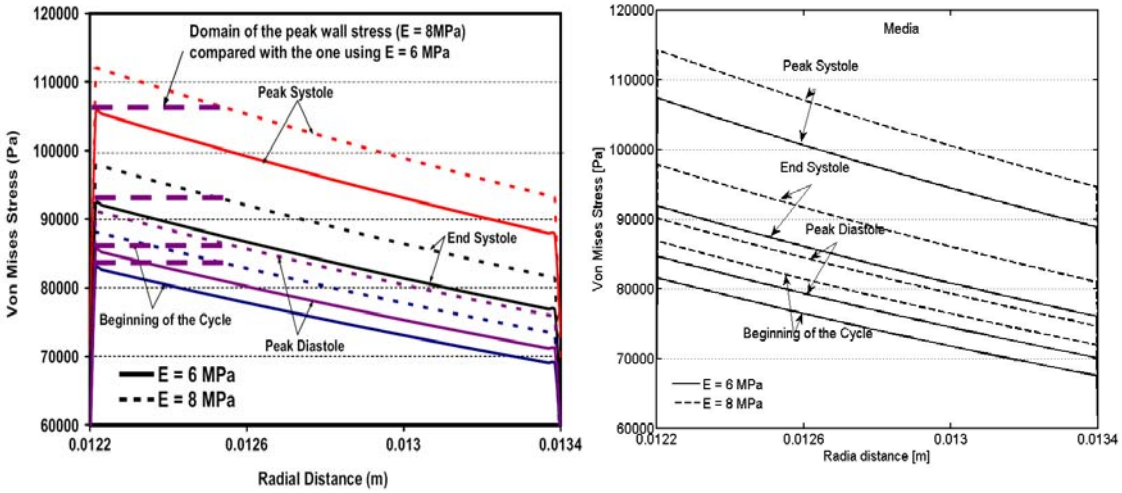

Khanafer and Berguer (2009) **Present work**

Figure 11 Comparison of Von Mises Stress across media at different steps in pulsation cycle and different modulus of elasticity with those by Khanafer and Ramon (2009)

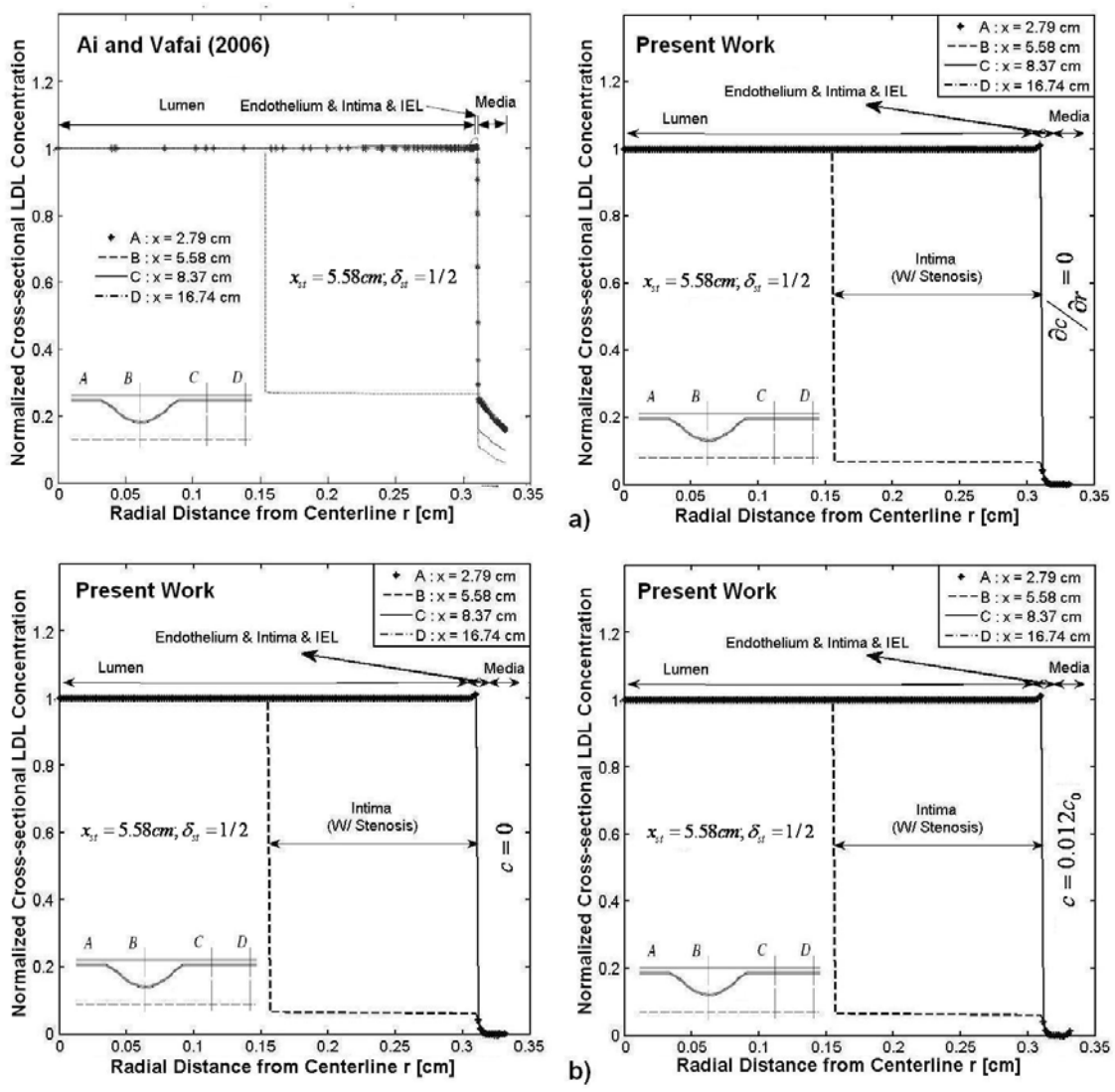

Figure 12 Normalized LDL concentration c/c_0 across diseased artery layers in the presence of stenosis with $\delta = 0.5$, $x_{st} = 5.58cm$ and $x_0 = 2R_0$:a) for comparison with Ai and Vafai (2006) work; b) for two different boundary conditions at the media-adventitia interface ($r = 3.314\,mm$) $c = 0$ & $c = 0.012c_0$.

4.3 Transport properties obtained by different methods

As mentioned, the transport properties in an artery utilized by Yang and Vafai (2006) and Ai and Vafai (2006) are obtained by two different methods, pore theorem and circuit analogy, while Chung and Vafai (2012) combined the two and resulted another set of properties. Comparing the results solved with properties utilized by Yang and Vafai (2006), Ai and Vafai (2006), and Chung and Vafai (2012), figure 13 shows a small difference on filtration velocity and, however, a negligible influence on LDL concentration. Looking into each of the arterial layers in Fig 14, the transport properties are obtained with different methods in the three works. It should be noted that the filtration velocity into the artery is the same, however, when he transport properties are obtained by three different methods, this will result in three different Peclet number for each of these studies even for the same filtration velocity. As such, the main difference in the results between the three methods characterized by Peclet numbers in mass transfer of about 1, 5, and 70 respectively (Yang and Vafai, 2006; Ai and Vafai, 2006; Chung and Vafai, 2012). With different transport properties, the Peclet number which represents the competition between diffusive and convective molecular transport affects the concentration profiles. As a result, the concentration gradient driving the penetration can be smooth (Yang and Vafai, 2006), locally enhanced (Chung and Vafai, 2011), or between (Ai and Vafai, 2006).

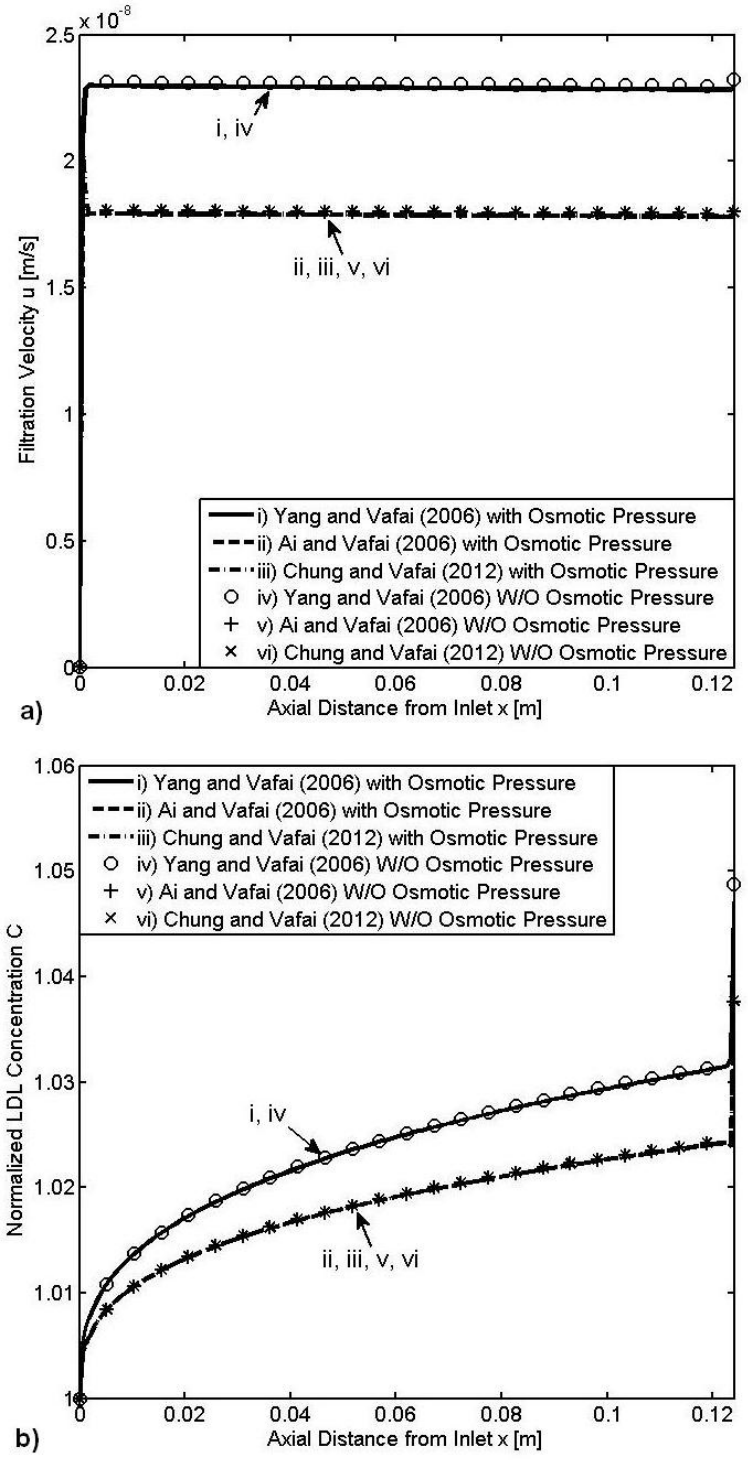

Figure 13 Effect of different sets of properties and the Osmotic pressure on a) Filtration velocity, b) LDL concentration distribution at the lumen-endothelium interface.

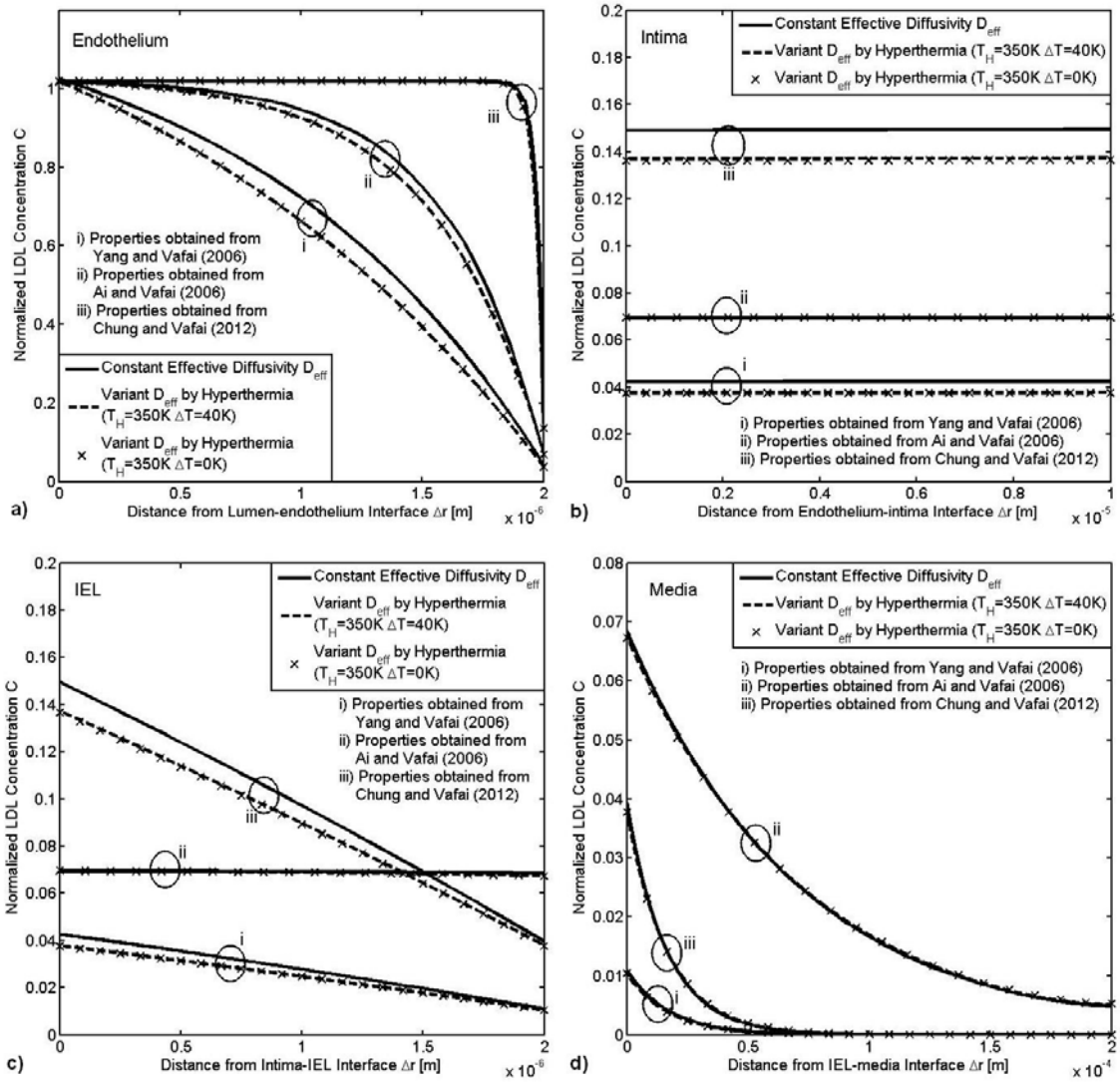

Figure 14 LDL concentration profile across a) endothelium, b) intima, c) IEL, and d) media, for different set of properties from works by Yang and Vafai (2006), Ai and Vafai (2006), and Chung and Vafai (2012).

Chapter 5

Result and Discussion

5.1 FSI effect

Figure 15 displays the variations of the half width of the leaky junction, w versus the angular strain, ε. This representation is based on equation 13, which shows that w increases linearly with an increase in ε. Larger β_{lj} produces a more substantial deformation of the pore size at larger values of ε, while reaching a limiting case at a certain value of ε, beyond which, w decreases as β_{lj} increases. Using equations 8-13,

the variations of pertinent properties such as endothelium's permeability, effective diffusivity, and reflection coefficient with ε are illustrated in Fig. 16. The effective properties for a higher fraction of leaky junction $\phi = 0.10\%$ are also shown in Fig. 16.

With respect to flow penetration, the permeability of a leaky junction is more than that of a normal junction permeability, which experiences a negligible change with deformation. However, the fraction of leaky junctions is much smaller than normal junction. On the other hand, LDL will mainly pass across the endothelium layer through a leaky junction, rather than a normal junction whose cross-section area is too small for LDL transport. Therefore, as can been seen in Fig. 16, variations in ε have a more pronounced impact on the effective diffusivity and reflection coefficient as compared to the permeability. To further illustrate the deformation effect on the reflection coefficient, the variations of the sieving coefficient $\gamma_{end} = (1 - \sigma_{end})$ with the $\theta-$ strain ε are displayed on Fig. 16, showing how convection is affected by deformation. Figure 16, confirms our physical expectations, that endothelium is more permeable for both blood flow and LDL molecule transport for larger deformations. Also, as can be seen in Fig. 16, the endothelium becomes more permeable at a higher fraction of leaky junctions ϕ. This is due to the fact that a single leaky junction has a substantially larger cross-sectional area than a single normal junction has.

Figures 17 and 18 illustrate the angular strain and von Misses stress variations of the endothelium layer for different pressure drops across the lumen and the outer arterial wall.

It can be seen that consideration of porous wall has a significant impact on the FSI results. On the other hand, variable permeability caused by deformed pores has a minor influence on the elastic behavior of the arterial wall due to a small fraction of leaky junctions ($\phi = 0.05\% \& 0.10\%$). The filtration and concentration distributions within different layers, while accounting for FSI effects and variable permeability, diffusivity and reflection coefficient at different pressure levels are shown in Fig. 19. The results of angular strain ε are then incorporated with those in Fig. 16, resulting the flow penetration and LDL concentration distributions shown in Fig. 19. Part a of figure. 19 shows that the hydraulic pressure gradient dominates the flow penetration within different layers of an artery. FSI has a substantially more limited effect in enhancing the flow penetration in terms of creating a variable permeability and deformed leaky junction. This is because the deformation by FSI poses an insignificant effect, due to the limited flow through the leaky junction ($\phi = 0.05\% \& 0.10\%$) as compared to that through the normal junction.

Figure 19 also shows the impact of endothelium deformation on LDL transport for different pressure drops across lumen and the outer arterial wall. Since leaky junction affects the diffusion of LDL macromolecules, FSI has a more pronounced affect on the concentration distribution across different layers as seen in Fig.19. This is in contrast to the relatively insignificant effect of FSI on the filtration velocity. Figure 19 clearly shows that FSI augments the impact of pressure change across the arterial wall. As can be seen in Fig. 19 the pressure and FSI effects are most significant within the intima layer. The

impact of FSI becomes more pronounced as β_{lj} increases, due a larger cross-sectional area of a leaky junction.

As seen in Fig. 20, when ϕ increases from 0.05% to 0.10%, the permeability for blood flow as well as LDL transport increases, resulting in a higher value of filtration velocity and LDL concentration. Again this is due to the fact that a leaky junction has a much larger cross-sectional area than a normal junction, which allows more blood flow and LDL molecules through the endothelium layer. As ϕ increases, the impact of FSI becomes more pronounced, because the deformation of a leaky junction is significantly more than that of a normal junction.

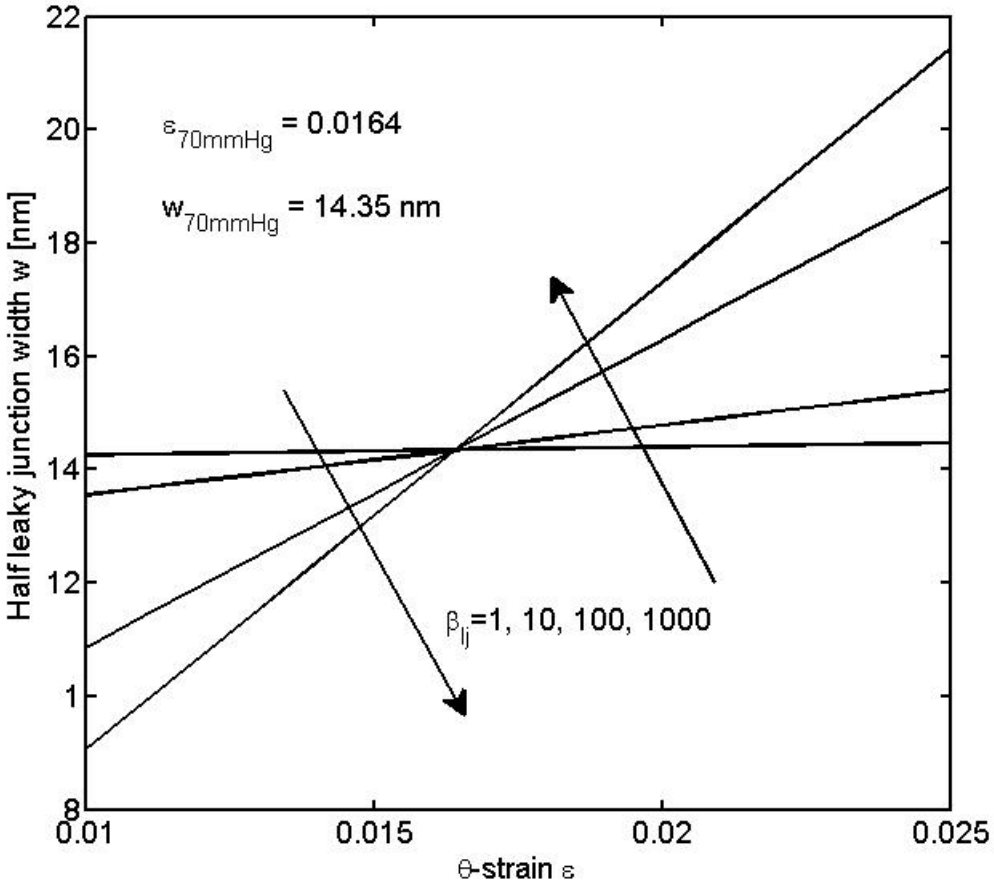

Figure 15 Half width of leaky junction (w) variations with the angular strain ε

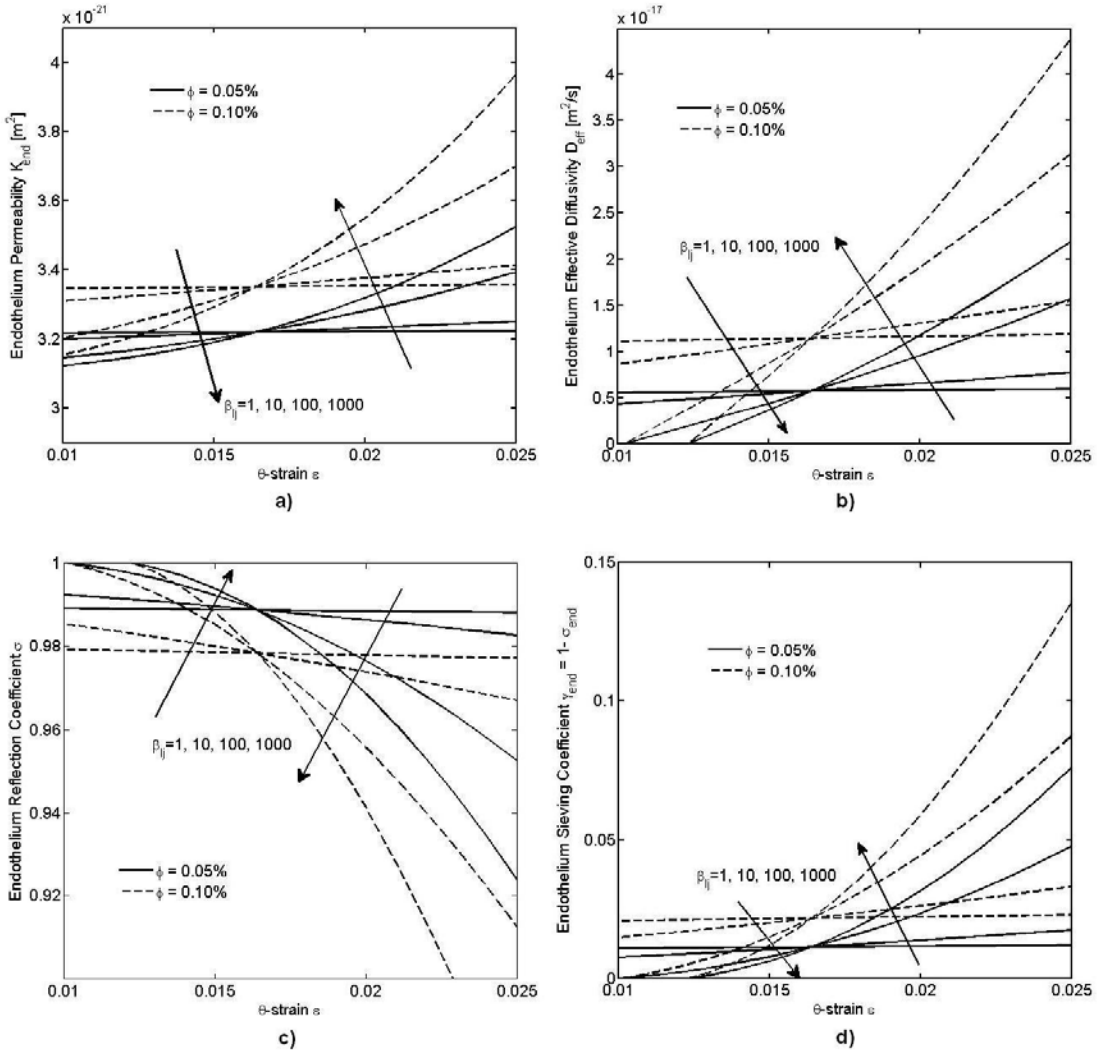

Figure 16 Endothelium a) Permeability K_{end}, b) Effective Diffusivity D_{eff}, c) Reflection coefficient σ_{end}, and d) Sieving coefficient γ_{end} ($=1-\sigma_{end}$), variations with angular strain ε at different ϕ and β_{lj}

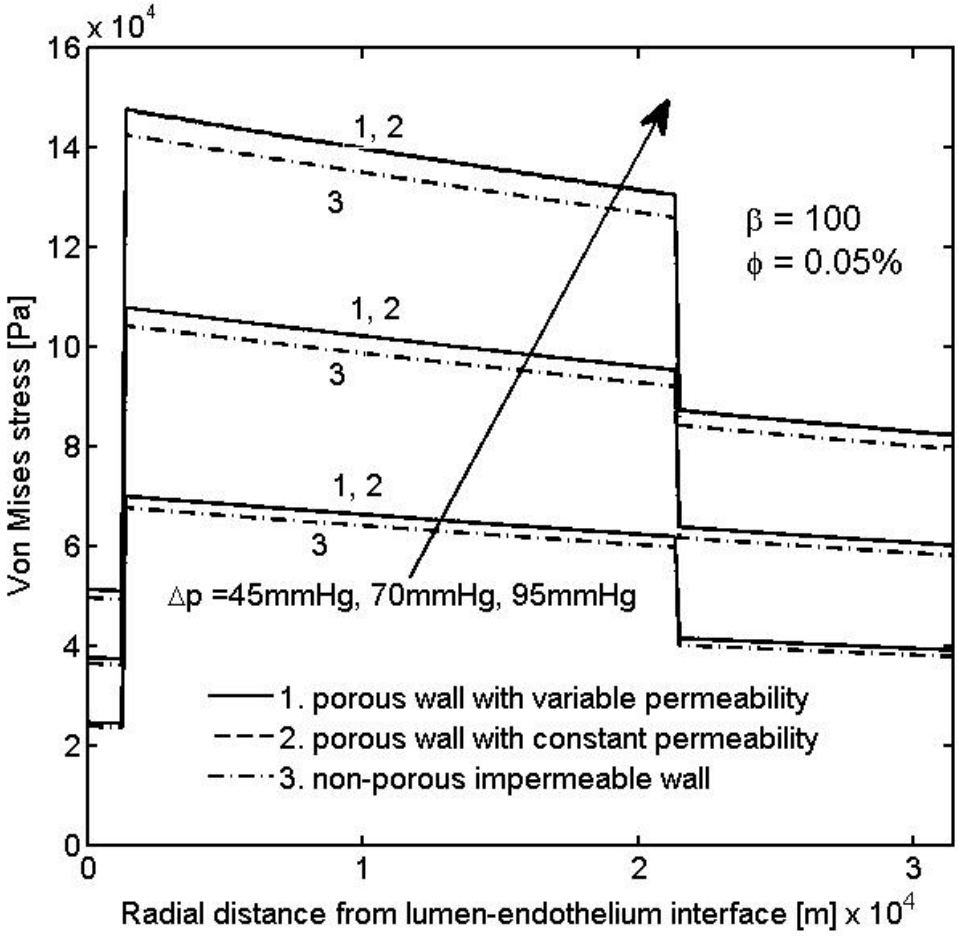

Figure 17 Von Misses stress variations at the lumen-endothelium interface for different pressure drops across the arterial wall and different FSI models

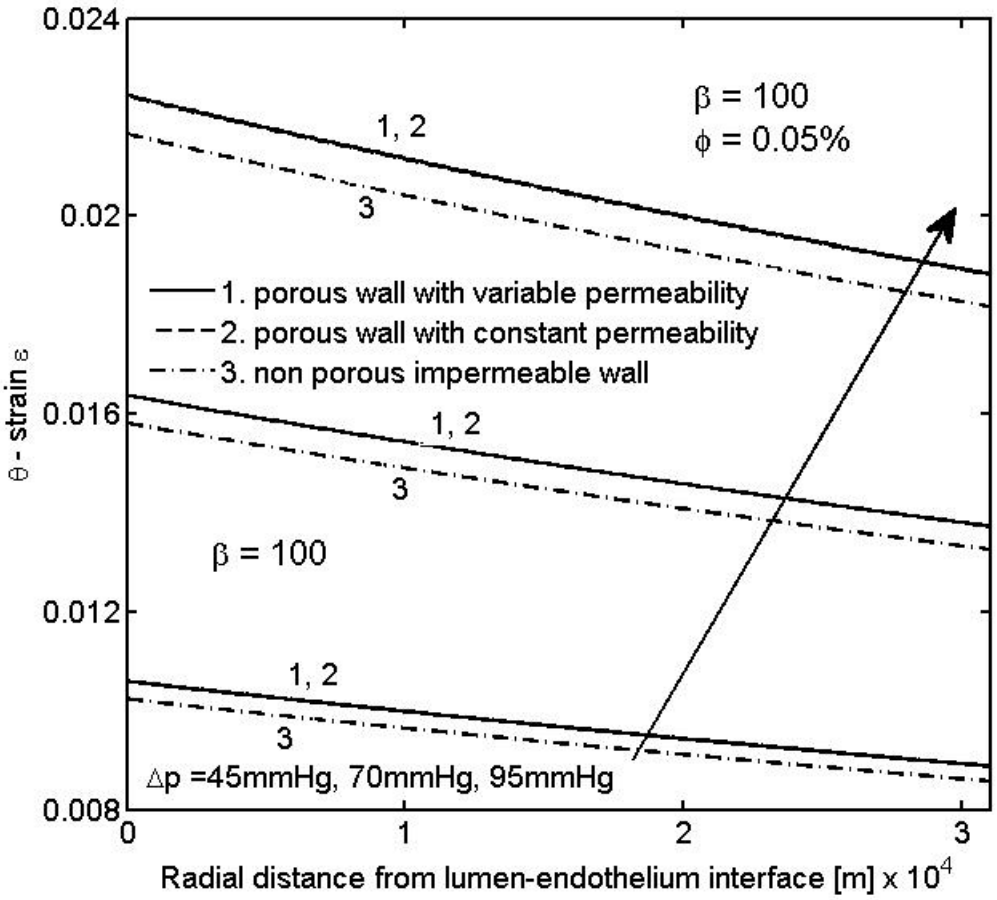

Figure 18 Angular strain ε variations at the lumen-endothelium interface for different pressure drops across the arterial wall and different FSI models

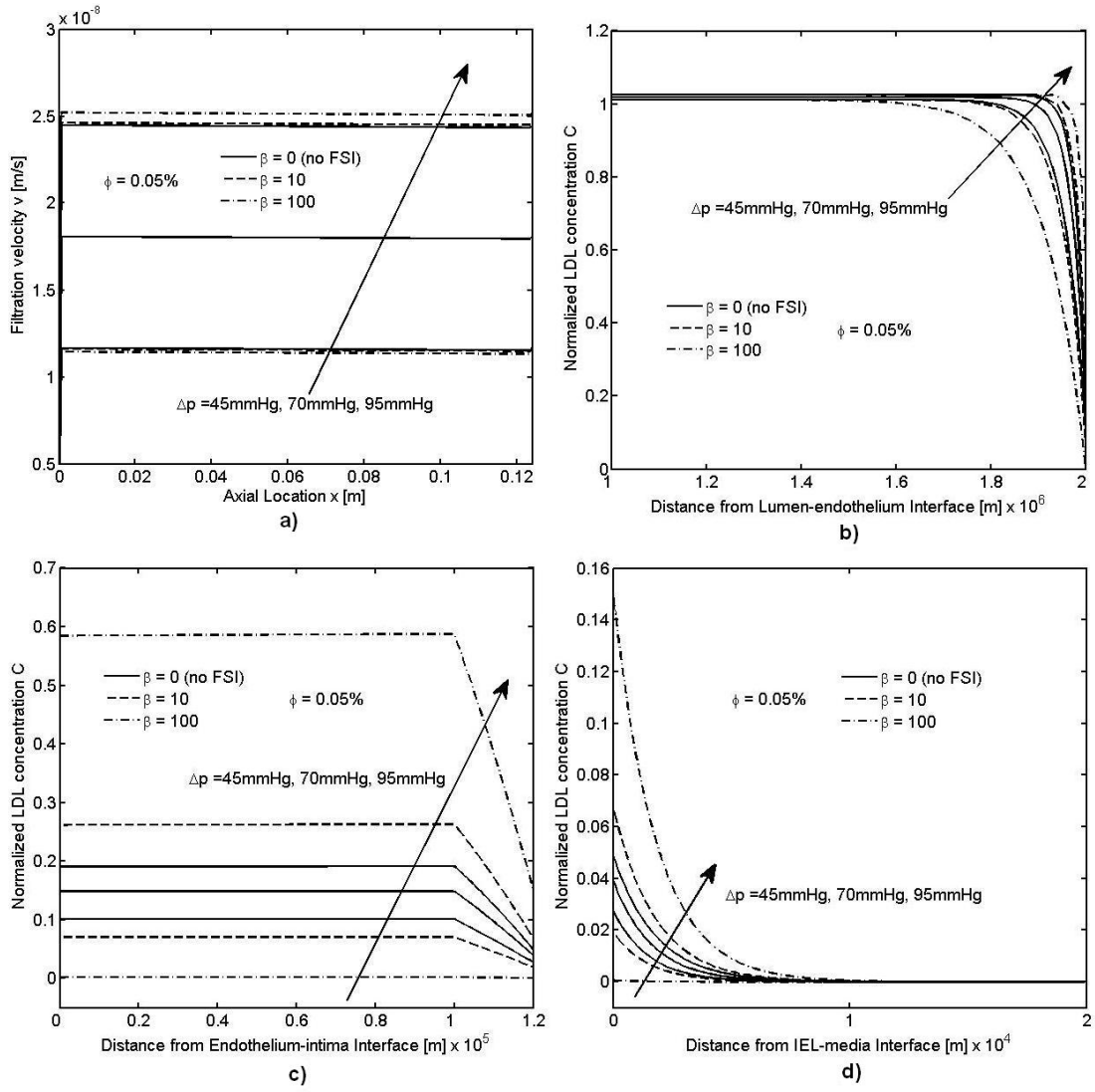

Figure 19 a) Filtration velocity variations at the lumen-endothelium interface, and Normalized LDL concentration across b) endothelium, c) intima and IEL, and d) media, for different β and Δp

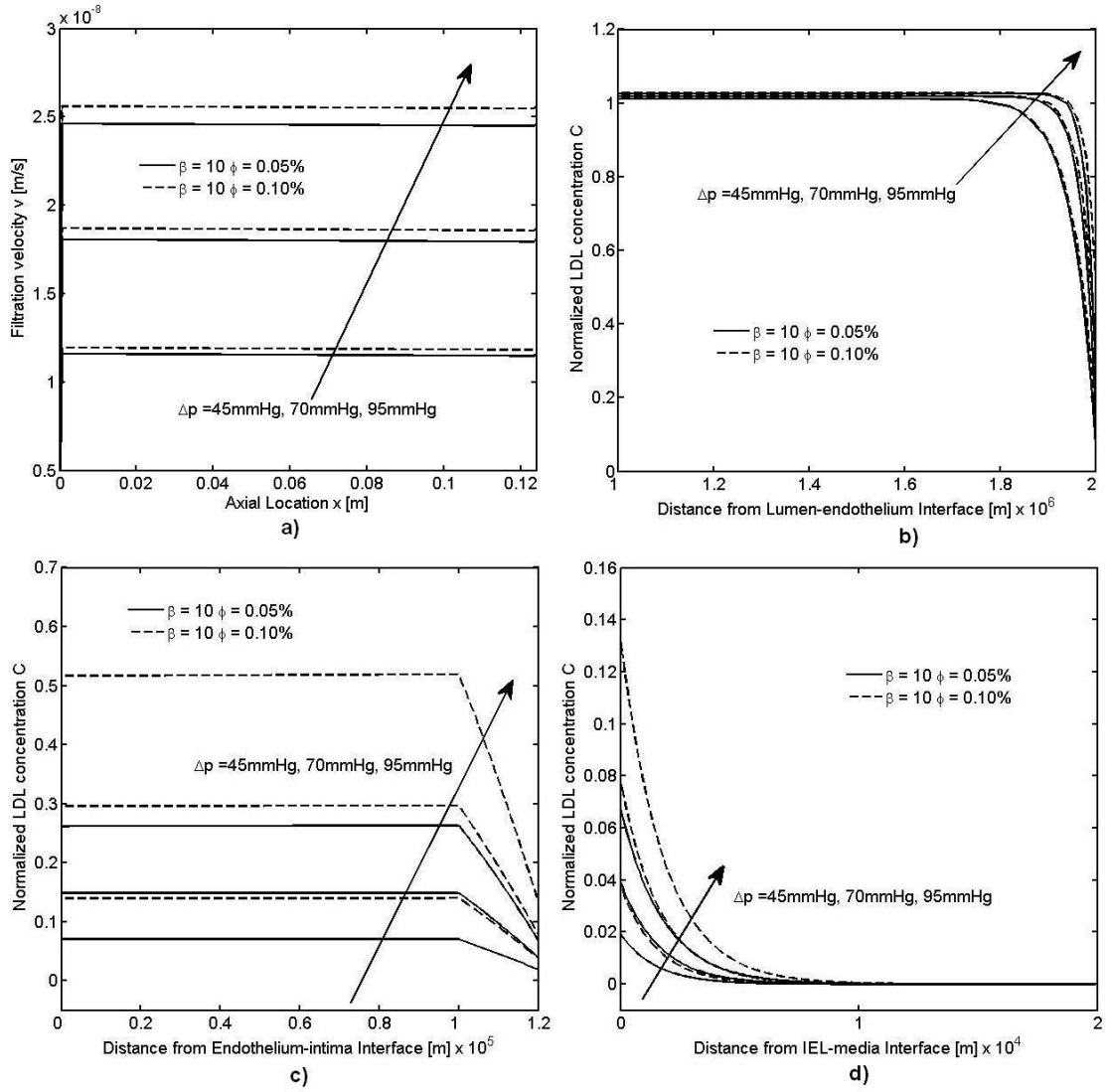

Figure 20 a) Filtration velocity variations at the lumen-endothelium interface, and Normalized LDL concentration across b) endothelium, c) intima and IEL, and d) media, for different ϕ and Δp

5.2 Pulsation effect

Figure 21 shows the impact of pulsation on the entrance velocity and pressure. As can be seen in Fig. 21, the pulsation has a more pronounced effect on the concentration distribution for larger values of pulsation period Γ. Also as can be seen in Fig. 21, incorporating pulsation for the pressure, increases the filtration velocity and concentration, while the velocity pulsation has an insignificant effect on the results. It should be noted that the impact of pulsation on LDL concentration is quite limited, due to the very dominant transient effect on mass transfer caused by the very small pulsation period ($\Gamma = 1s$).

Figure 22 illustrates the FSI effect on filtration velocity when pulsation is taken into account. As was the case for the steady state results (Fig. 19a), FSI does not have a significant effect on the results since the leaky junction plays a minor role on the flow penetration. Figure 23 shows that FSI has a negligible effect on the temporal concentration response in contrast to the FSI's significant effect on the steady state concentration distribution. The reason that FSI has a less pronounced effect on the concentration profile under pulsation, is due to the substantial damping effect of the pulsatile flow in an artery.

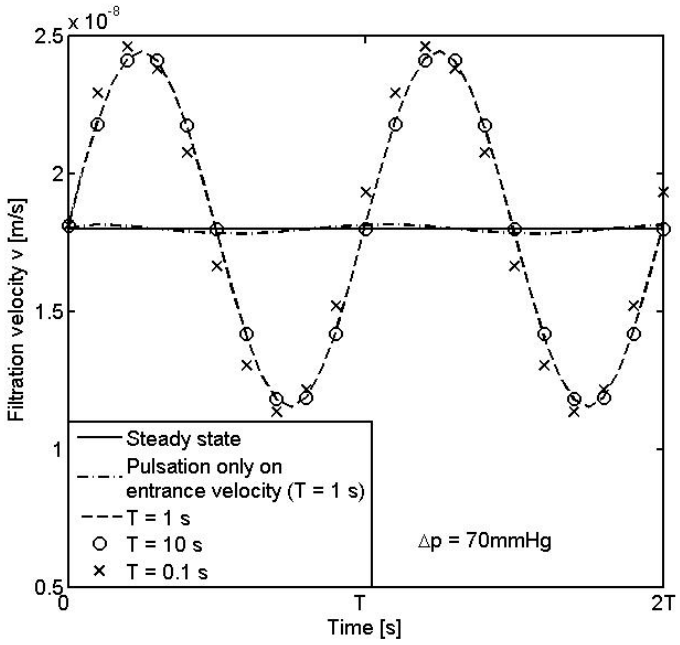

a)

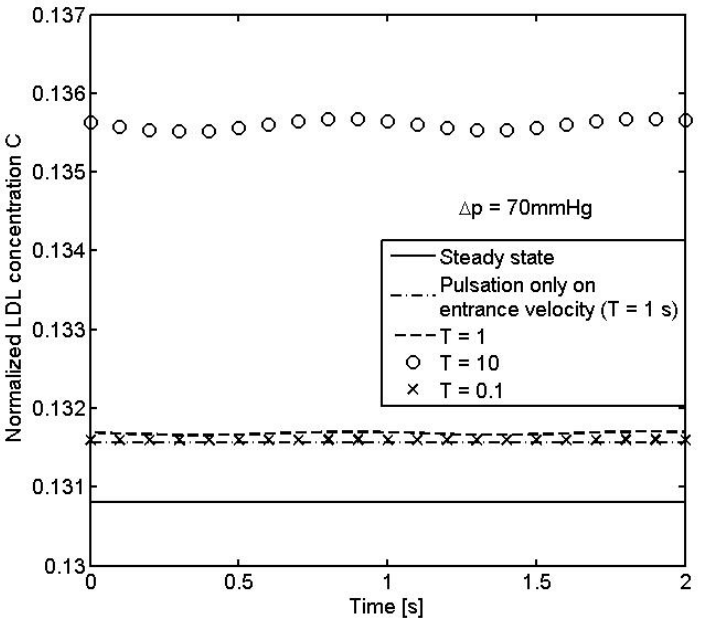

b)

Figure 21 a) Filtration velocity; and b) Normalized LDL concentration; at different pulsation periods

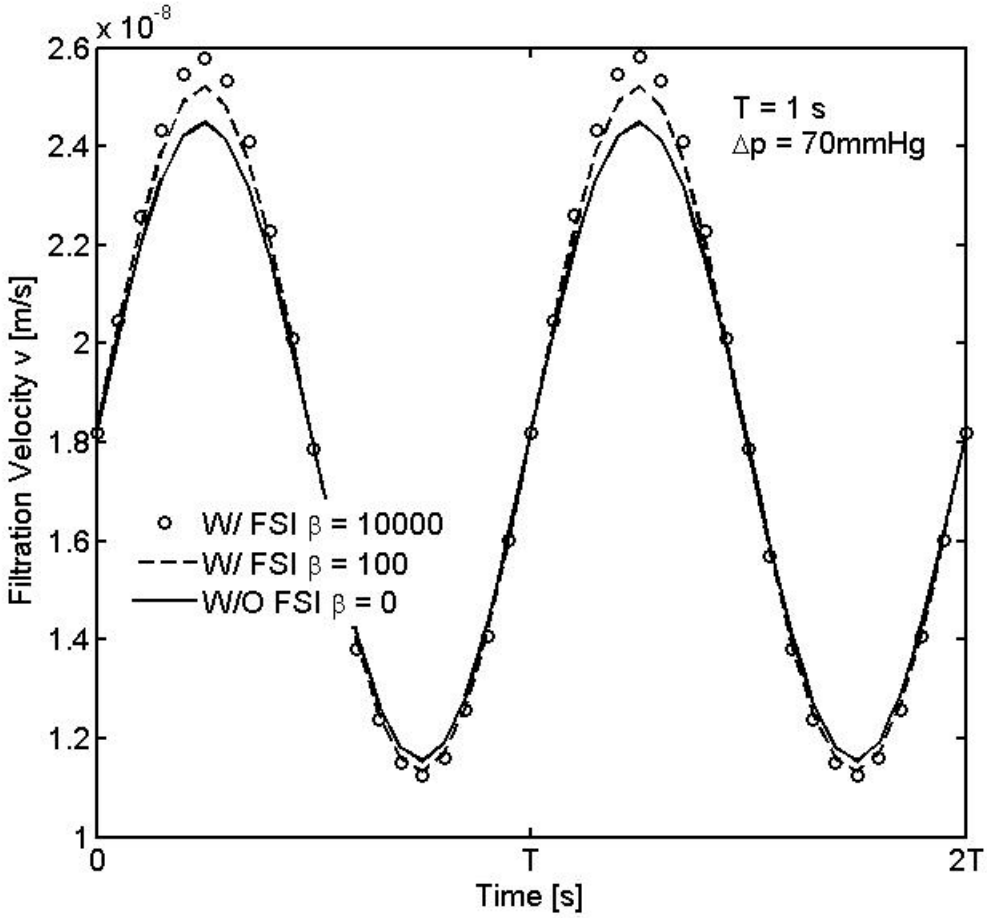

Figure 22 Effect of FSI on filtration velocity incorporating the pulsation at the mid axial position of the endothelium layer

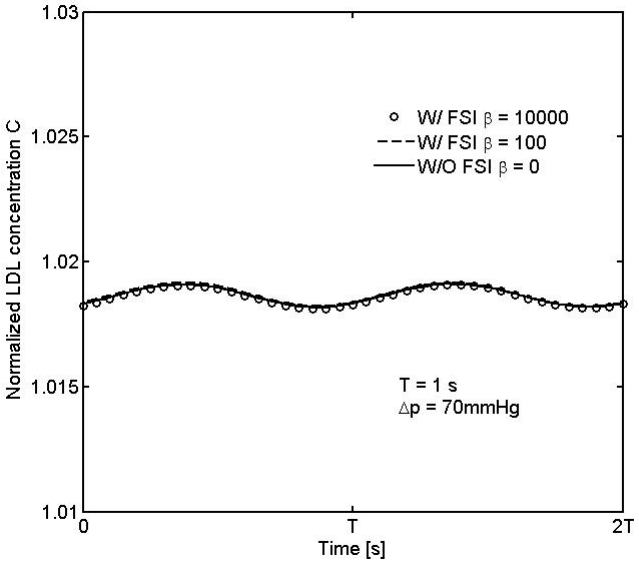

a) mid axial position of the lumen-endothelium interface

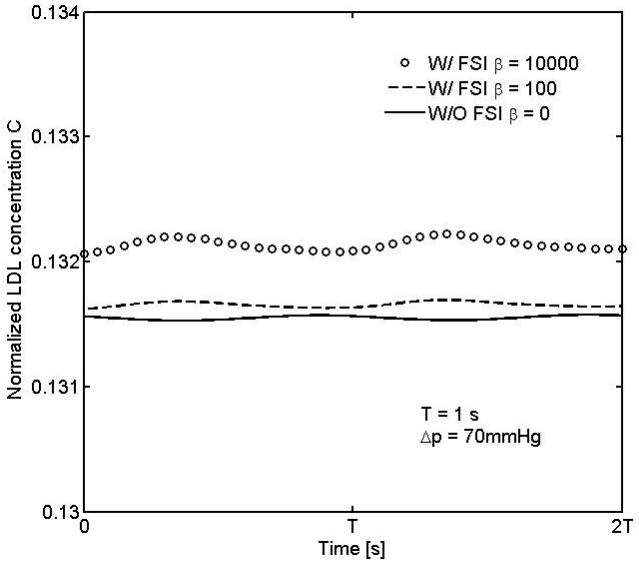

b) mid axial position of the endothelium-intima interface

Figure 23 Effect of FSI on normalized LDL concentration incorporating the pulsation at the a) mid axial position of the lumen-endothelium interface; b) mid axial position of the endothelium-intima interface

5.3 Impact of the Osmotic effect – Osmosis pressure

Osmotic pressure is taken into account in Yang and Vafai (2006) and Ai and Vafai (2006), but not in Chung and Vafai's (2012) work due to its minor influence. Figure 13 not only shows the impact by using different sets of transport properties as discussed earlier, but also validates the assumption invoked by Chung and Vafai (2012) for neglecting the Osmotic effect in an arterial wall. To understand if osmosis has considerable influence, Fig. 13 compares profiles of filtration velocity and LDL concentration in the lumen-wall interface with and without consideration of Osmotic pressure. As can be seen in Fig. 13, the Osmotic pressure has a minor impact on the flow penetration and a negligible effect on the LDL transport, regardless of which set of transport properties is applied. This minor role of the Osmotic pressure is due to a dominant gage pressure of blood across the arterial wall.

To further investigate the effect of Osmotic pressure, its influence is benchmarked against the Darcy resistance in Fig. 24. The ratio of these two effects is expressed as $-\frac{RT\sigma K}{\mu_{eff}}\frac{\nabla c}{\vec{u}}$ and is displayed across the endothelium and IEL layers, where the concentration gradient is most pronounced (Yang and Vafai, 2006; Ai and Vafai, 2006; Chung and Vafai, 2011). Fig. 24a shows that the Osmotic pressure is negligible throughout the endothelium layer by a ratio averaging less than 2% when compared to the

Darcy resistance, regardless of transport properties utilization. Within the IEL layer, the Osmotic pressure has a larger influence of about 10% and 30% depending on which set of properties are used as seen in Fig. 24b. However, since more than 90% of hydraulic pressure drop occurs across the endothelium (Yang and Vafai, 2006; Ai and Vafai, 2006; Chung and Vafai, 2011), a small enhancement within IEL will not significantly affect the plasma filtration flow. Therefore one can state Osmotic pressure has a negligible effect on the LDL transport within an arterial wall.

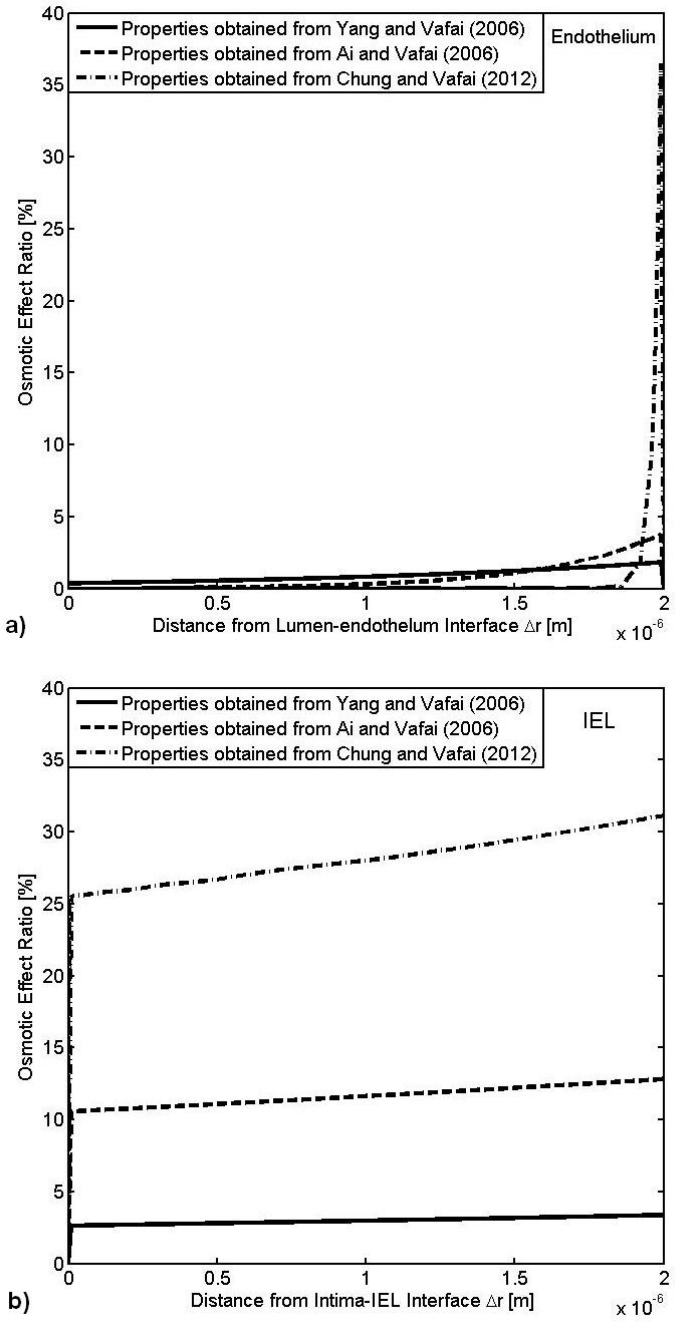

Figure 24 Effects of different sets of properties on the Osmotic effect ratio in a) endothelium, b) IEL where highest concentration gradient appears**.**

5.4 Heat transfer model and thermal impact

A preliminary thermal model is developed in this study based on the assumption of uniform and homogenous thermal properties (Kolios et al., 1995; Kotte et al., 1996) within the arterial wall. As seen in Fig. 25a, the temperature distribution across the arterial wall shows an almost linear profile due to a very small thermal Peclet number ($\sim 3\times10^{-5}$) and a very thin wall thickness ($2\times10^{-4}m$) as compared to the total radius of artery ($3.314\times10^{-3}m$). Fig. 25a illustrates that the Dufour effect has an insignificant effect on the thermal profile within an arterial wall. The ratio of Dufour flux to the ordinary heat flux shown in Fig. 25b further confirms this point.

For thermal modeling, normal human core temperature of 310K is set as the reference temperature, for which effective LDL diffusivity is same as that presented in Chung and Vafais (2011), while 350K is set for the presence of hyperthermia. As can be seen in Fig. 14, the temperature-dependent diffusivity has a relatively mild impact within endothelium and IEL (a & c), and a negligible effect within intima and media (b & d). Influence of variant diffusivity is more significant within the endothelium and IEL layers due to their overall high transport resistance for the LDL molecular transport.

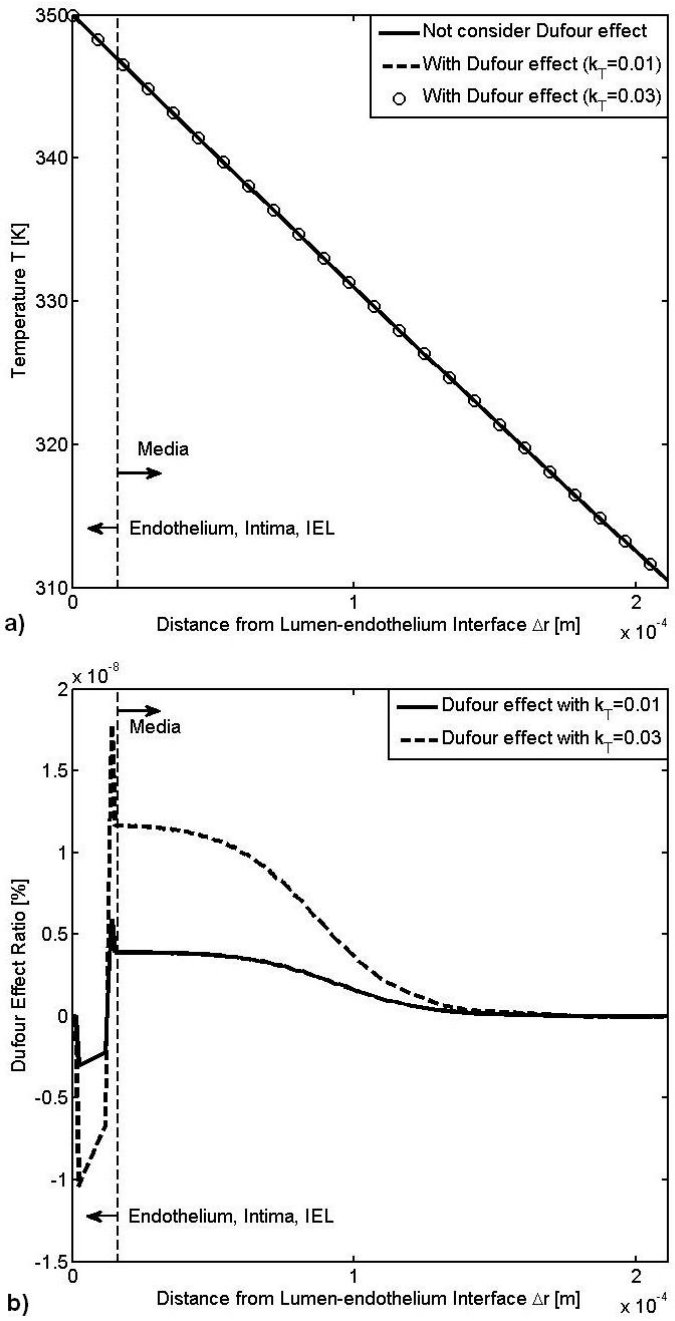

Figure 25 Dufour effect on a) temperature distribution within the arterial wall, b) comparison with ordinary diffusion.

5.5 Effect of Thermo-diffusion

As seen in Fig. 26, Sorret diffusion enhances the LDL transport by increasing overall the LDL concentration within the arterial wall. Also, since Sorret diffusion is driven by temperature gradient, it can be seen that a higher temperature drop across the wall, ΔT, results in a more pronounced LDL enhancement. A typical value of Sorret coefficient k_T is about 0.01 (Chapman and Cowling, 1952; Wakeham et al., 1991) when considering thermo-diffusion. Higher values of k_T increase the LDL enhancement. However, a pronounced Sorret effect normally appears with small particles and a less viscous solvent. As such the Sorret effect on LDL transport in an artery is expected to be lower ($k_T < 0.01$) due to the heavy mass of LDL molecules. Unlike Osmotic and Dufour effect, Sorret effect has a considerable impact on the LDL transport.

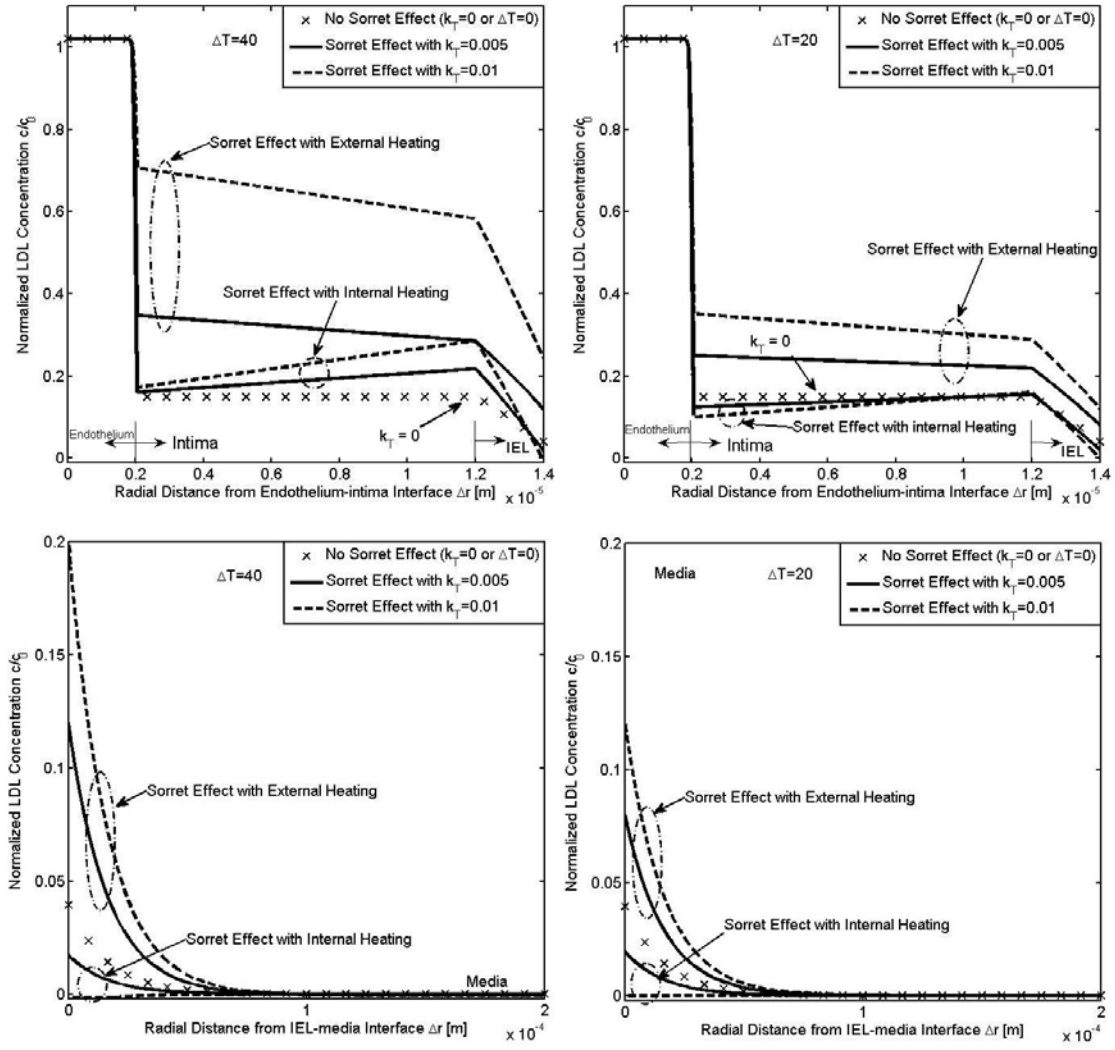

Figure 26 Soret and hyperthermia effects on the LDL concentration distribution across endothelium, intima, IEL, and media.

5.6 The impact by thermal expansion

In this part, the thermal expansion and its impact on LDL transport, incorporating temperature-dependent effective LDL diffusivity and Sorret effect, is investigated. Based on earlier results, Osmosis and Dufour effect are neglected. The results obtained through both full ($\nabla\sigma_s + f_s = 0$ and $\varepsilon_T = \beta_T(T - T_{ref})$) and simplified ($\varepsilon = \varepsilon_T = \beta_T(T - T_{ref})$) models are compared with those without accounting for thermal expansion and are shown in Fig. 8 for filtration velocity, as well as the strain distribution within the endothelium layer.

Fig. 8a shows that the thermal expansion has a minor enhancement on plasma filtration velocity, which is consistent with the study on the flow induced wall expansion given in Chung and Vafai's (2012) work on fluid-structure interaction. The temperature drop has a significant impact on the wall strain which incorporates the elastic effects. A higher temperature drop will result in a lower average temperature through the wall with a fixed value of T_H , which leads to a smaller thermal expansion. On the other hand, the strain which is based on the simplified model is only affected by the local temperature, irrespective of the temperature drop across the whole arterial wall.

The impact of thermal expansion on LDL concentration across each of the arterial layers is shown in Figs. 9 and 10. Applying full thermal elastic model, The effect of temperature distribution described by different ΔT , as well as the variation of β_{lj} ,with

both thermal models of external and internal heating are illustrated in Fig 9. Thermal expansion with both full and simplified elastic models, incorporating Sorret effect with variant k_T. It should be mentioned that variation of thermal-diffusion coefficient, k_T, will have no effect for the case $\Delta T = 0$ because there will be no Sorret effect when there is no applied pressure gradient., as well as an additional enhancement by Sorret effect. As seen in Figs. 9 and 10, Low temperature drop, ΔT, and a high leaky-bulk expansion rate, β_{lj}, will result in a enhancement via thermal expansion.

A higher ΔT causes a larger temperature gradient within the layers which will strengthen Sorret diffusion of LDL, but this also lowers the overall temperature through the arterial wall and reduces the thermal expansion. This competition between the thermo-diffusion and thermal expansion is dominated by parameters k_T and β_{lj} shown in Fig. 10. As seen in Fig. 10, for the full elastic model, as ΔT changes from 0K to 40K, the LDL concentration decreases since the reduction of the thermal expansion is more pronounced compared to the enhancement due to the Sorret effect, especially for small values of k_T. In contrast, the effect of ΔT on thermal expansion diminishes for the simplified model, so that a larger ΔT results in an increase in LDL concentration due to a stronger Sorret diffusion, which is further strengthened for a larger value of k_T.

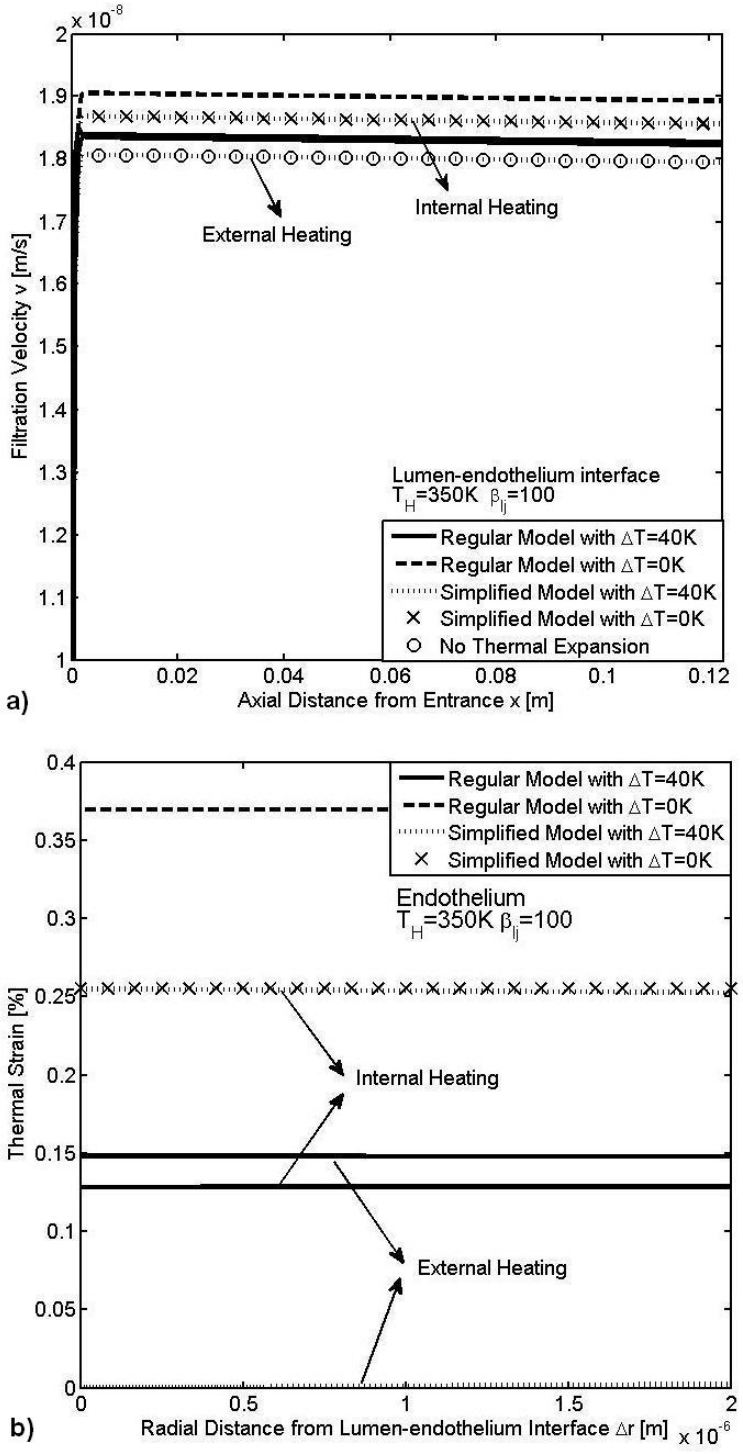

Figure 27 Effect of thermal expansion on a) filtration velocity at the lumen-endothelium interface and b) Thermal strain across endothelium.

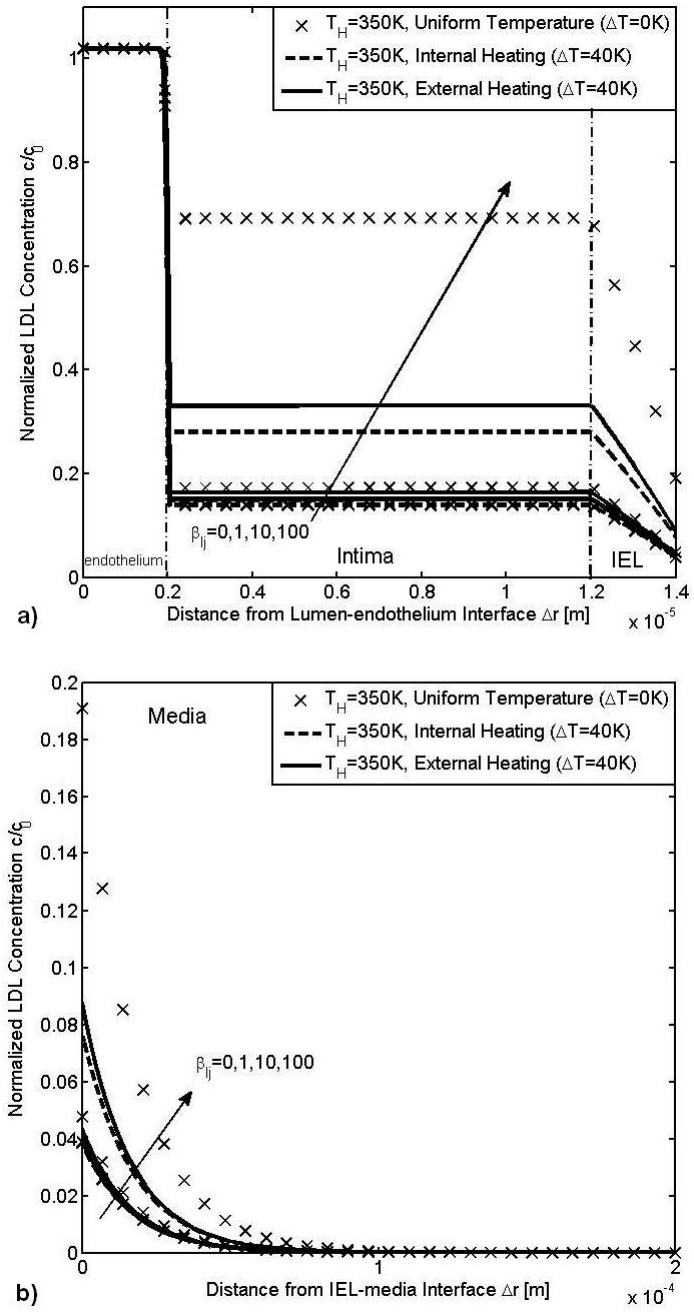

Figure 28 Effect of temperature drop, ΔT, and leaky-bulk expansion rate, β_{lj} on the LDL concentration distributions across a) endothelium, intima, IEL, and b) media ($k_T = 0$).

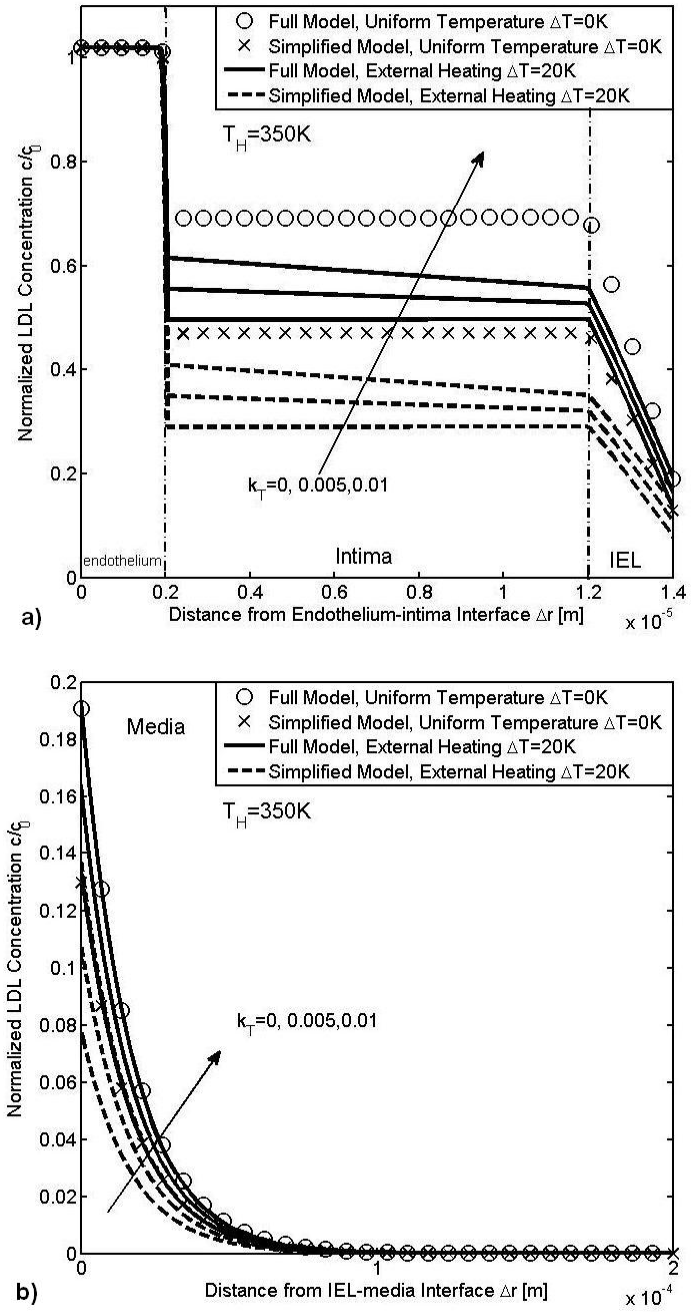

Figure 29 Comparisons between the full and simplified elastic models and their effects on LDL concentration distribution across a) endothelium, intima, IEL, and b) media, incorporating Sorret effect with the variation of Sorret coefficient k_T .

5.7 Impact by effective LDL consumption rate

One factor related to the LDL transport that might vary during the hyperthermia process is the LDL consumption rate k which exists within the media layer. The effect of variations in the effective consumption rate on the LDL concentration profiles across each of the arterial layers is illustrated in Fig. 11. It should be noted that a higher consumption rate leads to a lower LDL concentration.

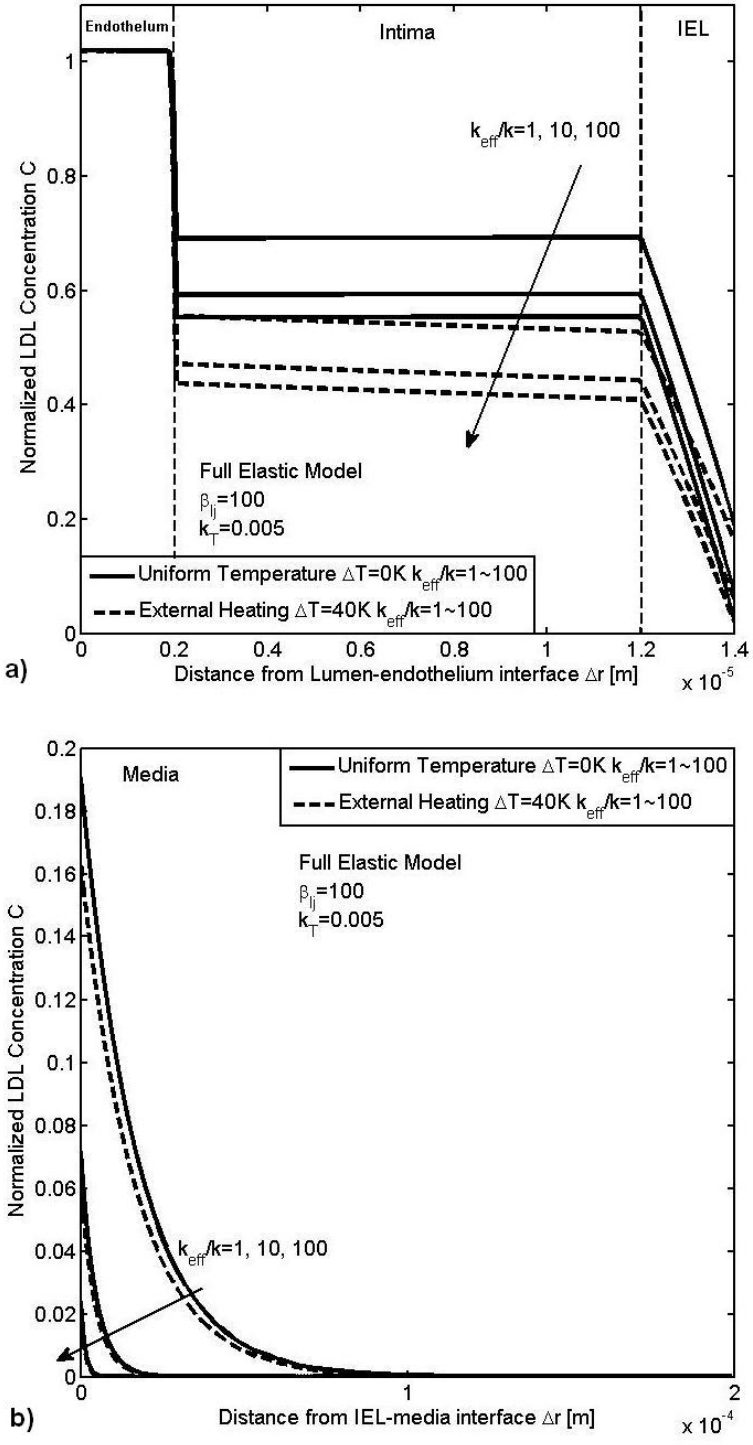

Figure 30 Effect of LDL consumption rate k on its concentration distribution across a) endothelium, intima, IEL, and b) media.

5.8 Impact of atherosclerotic plaque formation – thickening of the wall and the stenosis location

Using the computational domain in Fig. 3a (Ai and Vafai, 2006), Fig. 31 shows an insignificant impact as result of either thickening of the wall or different stenosis locations. This limited effect on LDL molecular transport is caused by the high permeability of the enlarged domain, intima, as compared to the other layers. Varying boundary condition on the outer surface (adventitia side, $r = 3.314mm$), such as zero gradient ($\partial c / \partial r = 0$), zero concentration ($c = 0$), and fixed concentration ($c = 0.012 c_0$), that are commonly applied (Meyer et al., 1996; Yang and Vafai, 2006; Ai and Vafai 2006), also display a negligible effect as seen in Fig. 12. The negligible impact of different outer boundary condition is shown in more detail in Fig. 32.

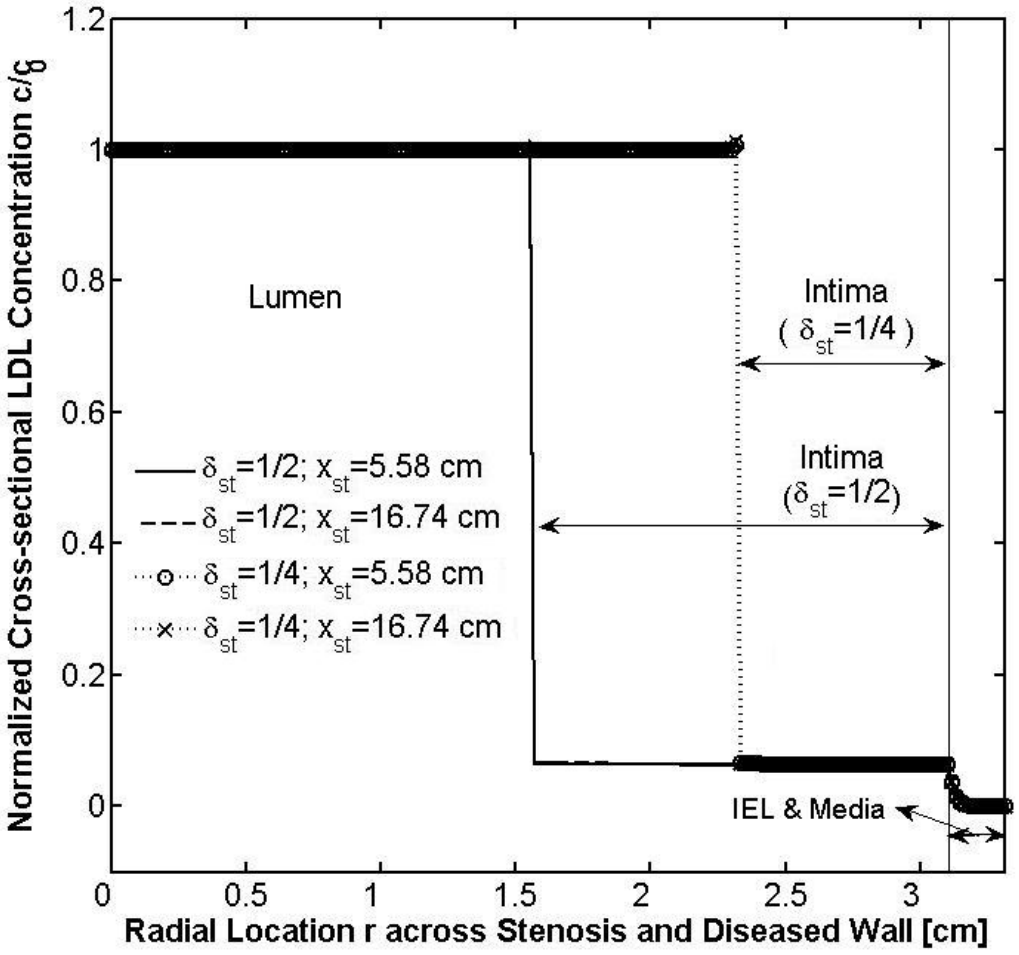

Figure 31 Normalized LDL concentration c/c_0 across diseased artery layers in the presence of stenosis at center of the plaque ($x = x_{st}$; $x_0 = 2R_0$) with different wall thickening δ_{st} and location of stenosis x_{st} .

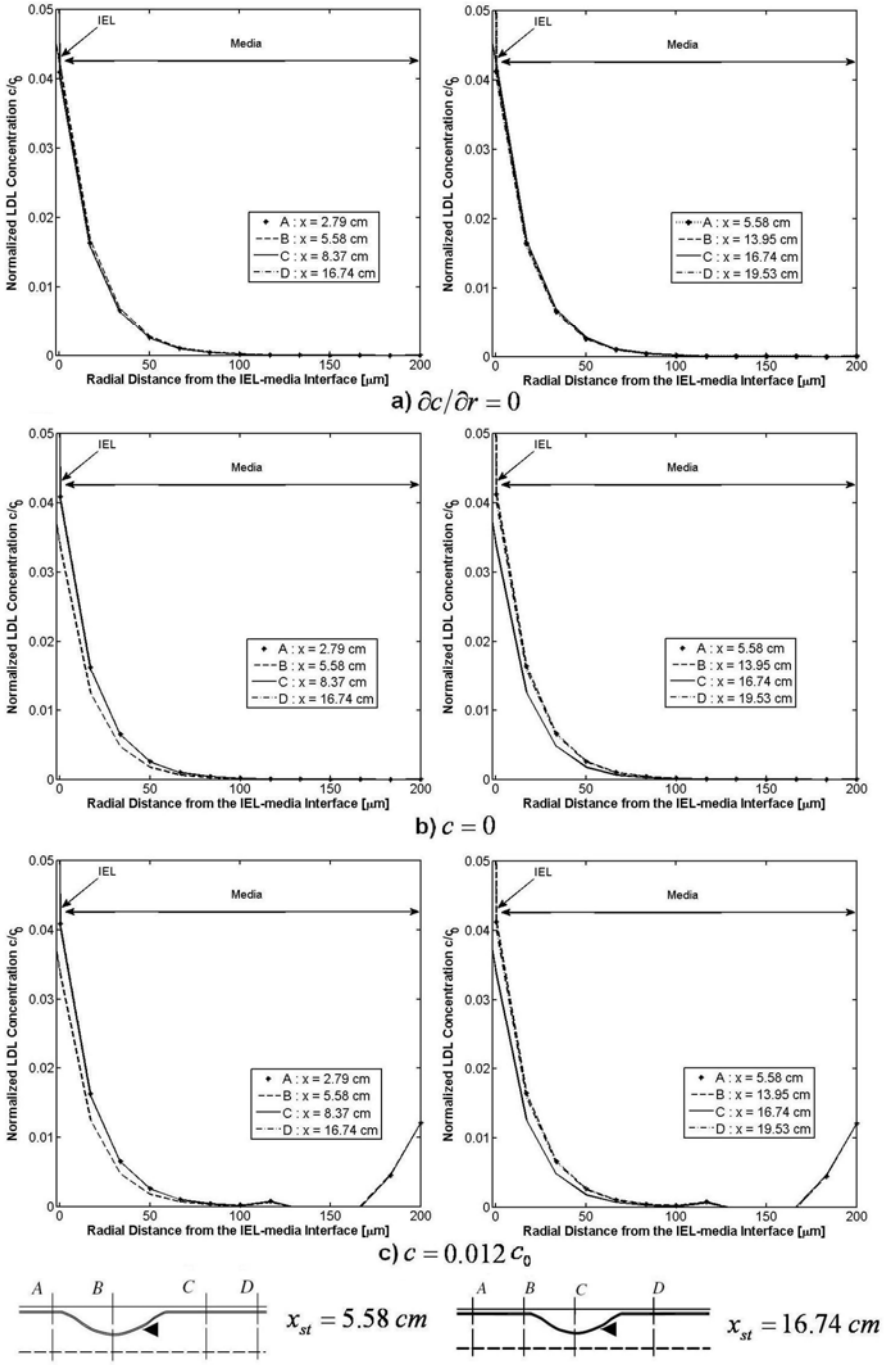

Figure 32 Normalized LDL concentration c/c_0 across IEL and media of a diseased artery at different locations x in the presence of stenosis with $\delta_{st} = 0.5$, $x_{st} = 5.58cm$ and $16.74cm$ for three different boundary conditions at the media-adventitia interface ($r = 3.314\,mm$) as $\partial c/\partial r = 0$, $c = 0$, $c = 0.012c_0$.

5.9 Sensitivity study on plaque geometry and model simplification

Various researchers have modeled the artery both with and without atherosclerosis; however, mostly modeling it as a wall-free or simplified-wall model, which doesn't allow them to look into the highly pertinent transport behavior within the arterial wall. In figure 31, the impact of the macro-structure, i.e., the shape of stenosis due to atherosclerosis is shown to be negligible. Figure 33 & 34, which zooms into the lumen-wall interface for pressure, filtration velocity, and LDL concentration, still shows that this effect is negligible. Figure 33 shows the hydraulic and mass concentration characteristics along the endothelium-intima interface where stenosis effect is more significant due to exposure to the flow in the lumen. As can be seen in Fig. 33, overall the impact of axial location on pressure, filtration velocity and concentration is relatively small. The impact of variations in the plaque width ($x_0 = R_0$ to $6R_0$)is also found to be relatively small as shown in Fig. 34. Therefore, one can conclude that the axial location has a negligible effect on the results.

On the other hand, the impact of the atherosclerosis is shown to be present within the intima as shown in Fig. 35 & 36 due to a smaller exposed surface area of the wall to lumen caused by the radial wall thickening. Along the intima-IEL interface, the pressure, filtration velocity and LDL concentration display a significant drop as seen in Fig. 35.

Furthermore, this drop becomes more pronounced as the plaque builds up. Figure 36 shows that using the reverse boundary conditions at the inlet (specifying pressure instead of velocity) and outlet (specifying velocity instead of pressure), displays the same phenomena seen in Fig. 35, and confirms the fact that the edge effects are insignificant. The effect of boundary condition is also shown to be negligible as can be seen in Fig. 32.

In conclusion, the atherosclerotic impact at the lumen-wall interface is shown to be minor, compared to the concentration distribution within each different layer of the wall. The present results show that the thickening of the arterial wall impacts plasma and LDL transport in the radial direction substantially more than in the axial direction. As such, a simplified computational domain shown in Fig. 3d can be applied. On the other hand, the microstructure and the transport properties of the arterial layers are impacted by atherosclerosis either by cholesterol lipid accumulation and tissue hyperplasia, or the dysfunction of endothelial layer, which is discussed in detail in the present work.

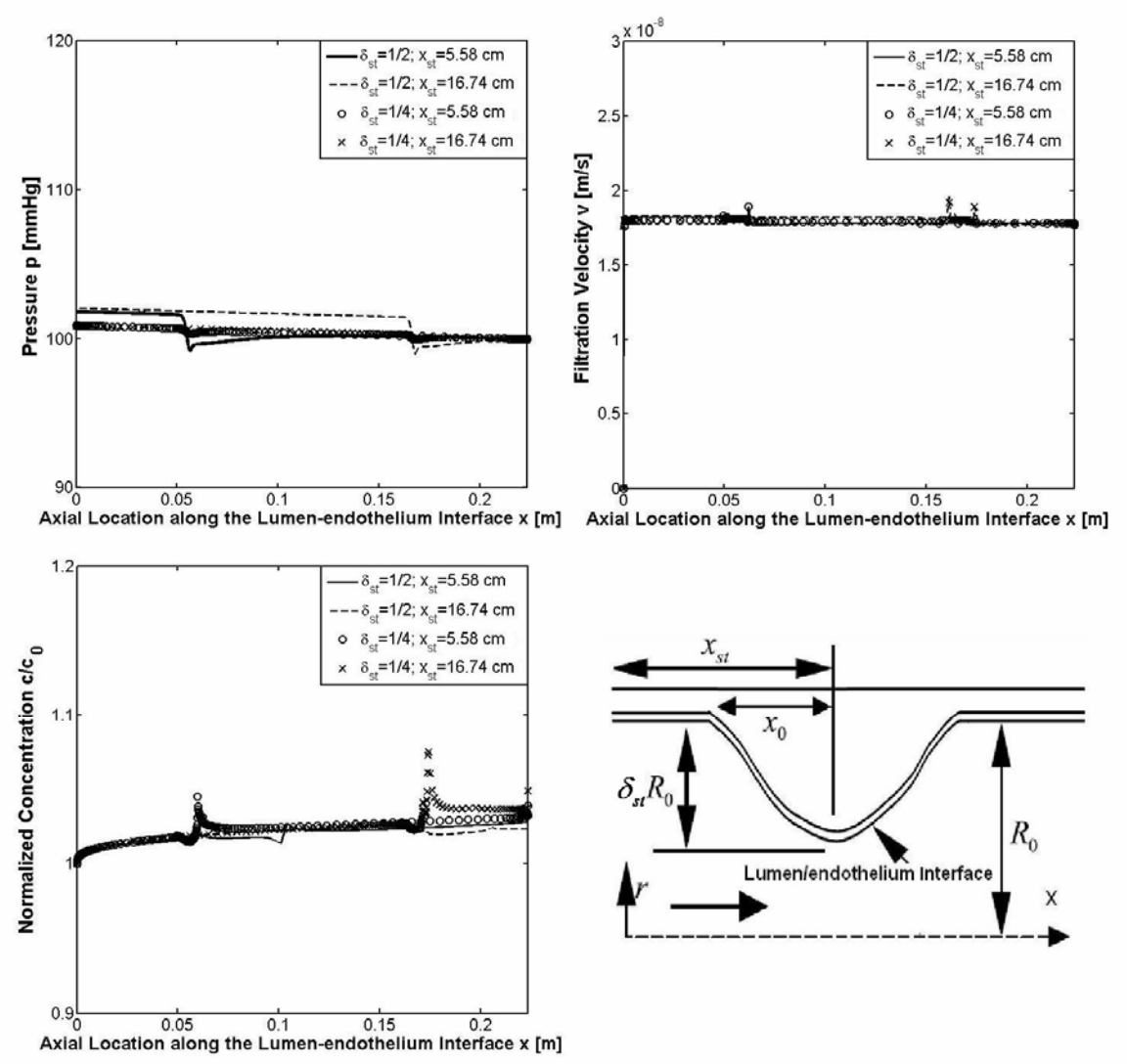

Figure 33 Blood pressure, filtration velocity, and LDL concentration along the lumen-endothelium interface for different wall thickening ratio δ_{st} and stenosis locations x_{st}.

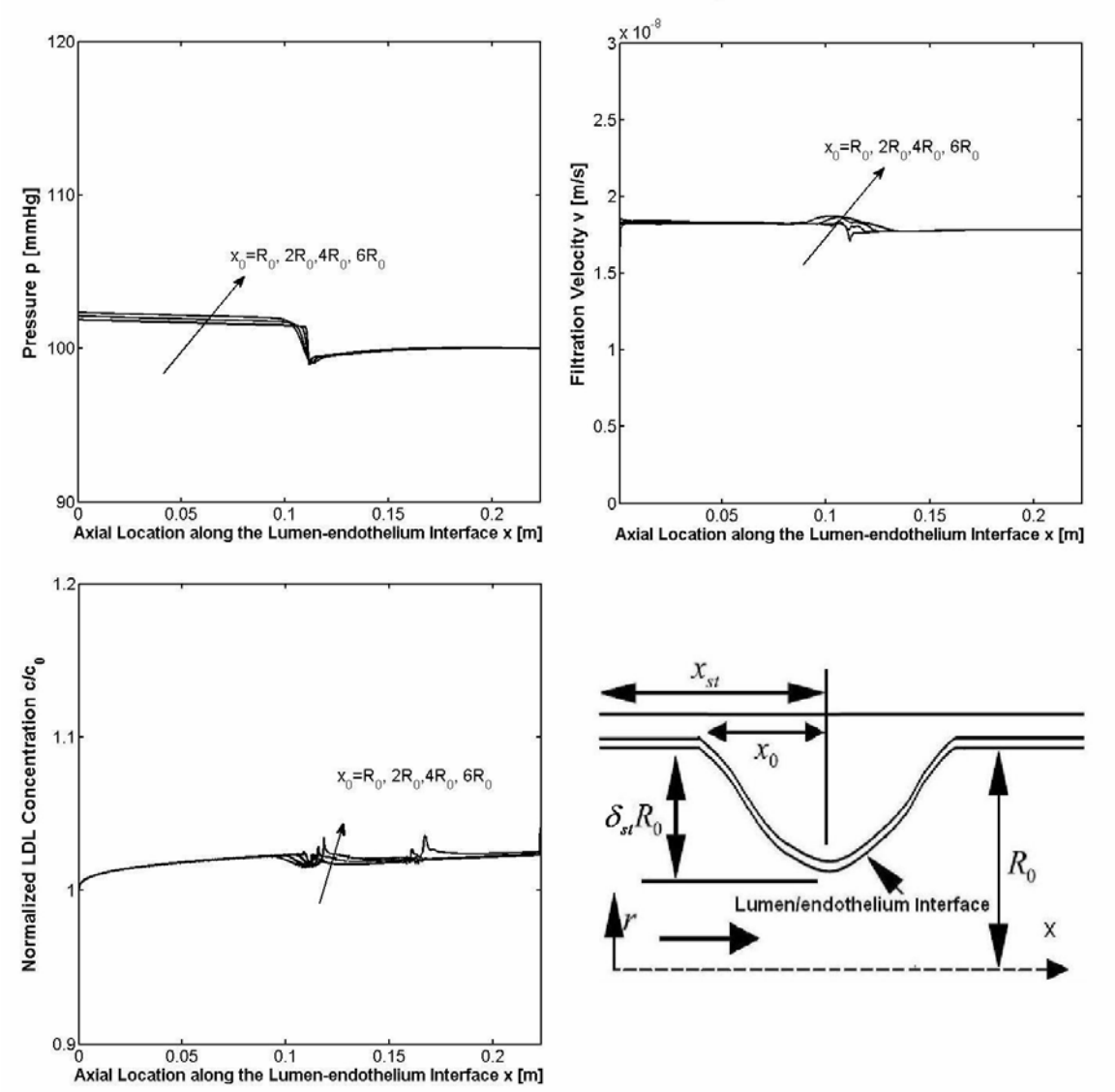

Figure 34 Blood pressure, filtration velocity, and LDL concentration along the lumen-endothelium interface for different values of the plaque half widths x_0.

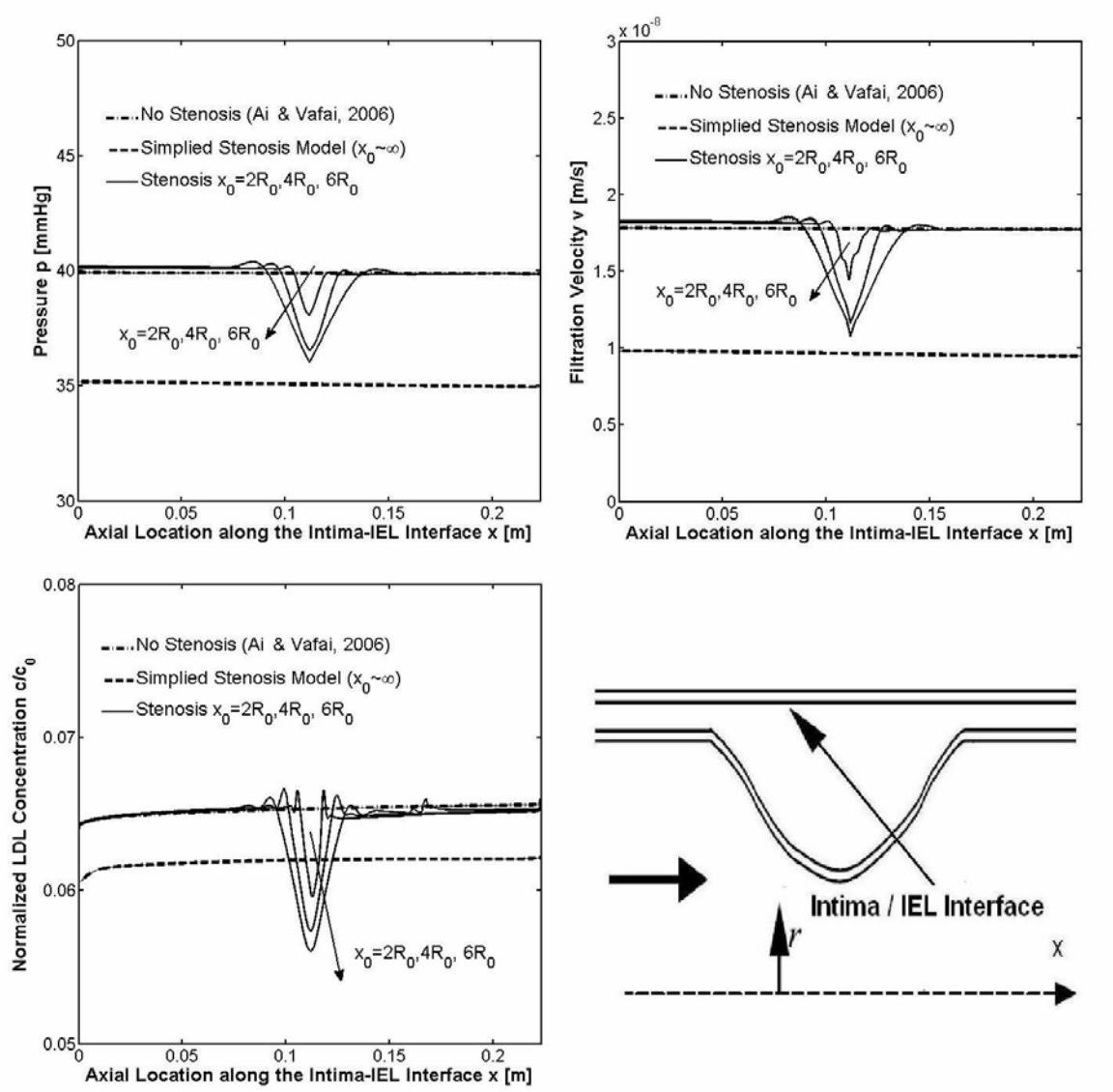

Figure 35 Blood pressure, filtration velocity, and LDL concentration profile along the intima-IEL interface for different plaque half widths x_0.

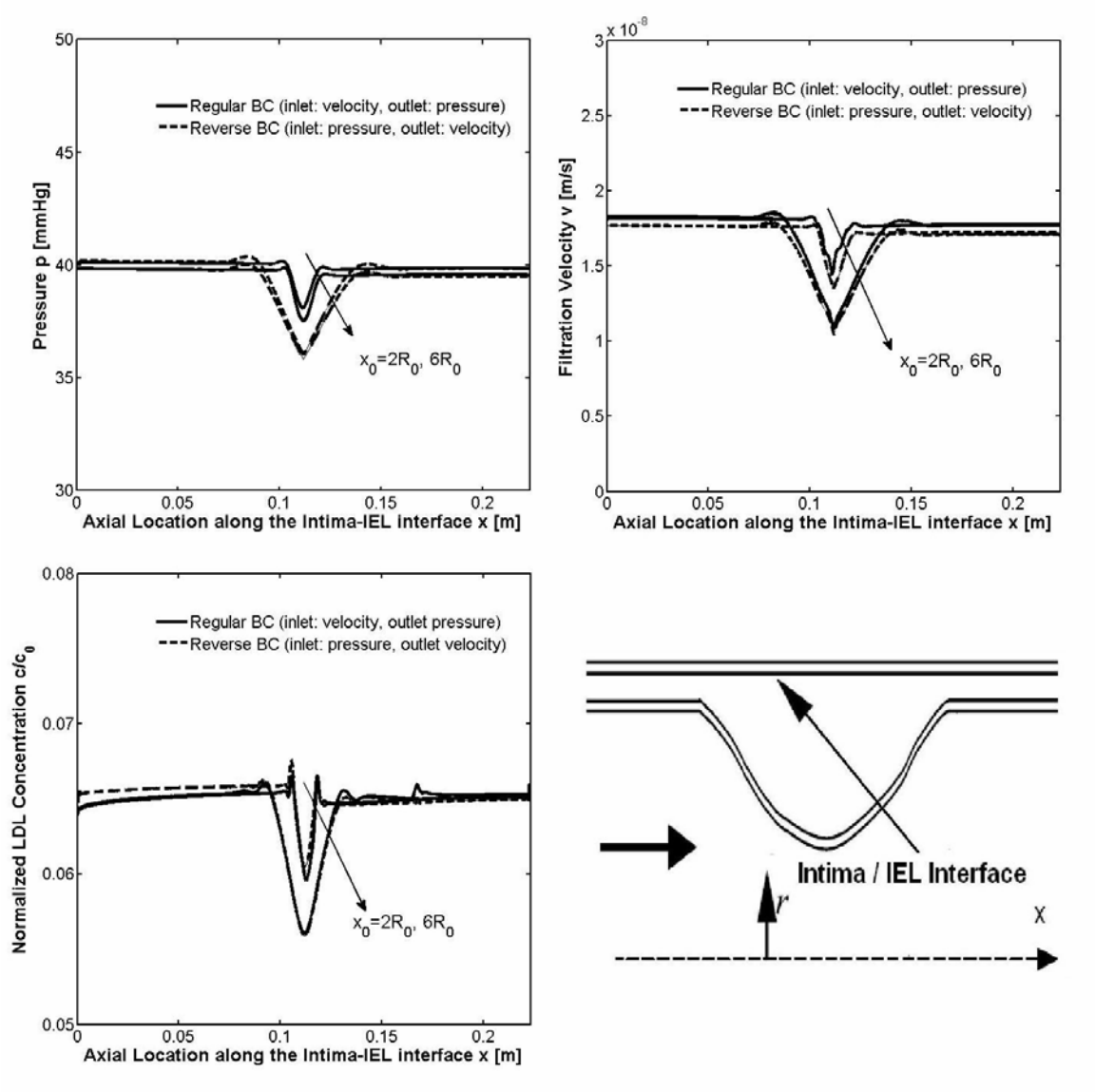

Figure 36 Effect of reversed boundary conditions (inlet: pressure, outlet: velocity) on blood pressure, filtration velocity, and LDL concentration along the intima-IEL interface for different plaque half widths x_0.

5.10 Dysfunctional endothelium and fibrous cap

Dysfunctional endothelium and fibrous cap forms as LDL cholesterol deposits accumulate within intima (Hossain et al., 2011). The transport properties of normal junction (Ai and Vafai, 2006) and leaky junction endothelium (Curry, 1984a; Chung and Vafai, 2012), as well as effective diffusivity of fibrous cap (Hossain et al., 2011) are listed in Table 3. Fig. 37 shows comparison between different considerations for dysfunctional endothelium and fibrous cap on penetration of blood and LDL. The comparison shows that dysfunctional endothelium results a deduction on the resistance from lumen into wall, while fibrous cap results an increasing resistance. The models that were considered on the condition of endothelium and fibrous cap for a diseased artery in this work are: case 1) $65\mu m$ fibrous cap covered by $2\mu m$ normal junction endothelium on the inner surface with all the properties being the same as those given in Table 2b and the effective diffusivity taken from Table 3; case 2) case 1 with the normal endothelium replaced by a leaky endothelium; case 3) case 2 with no endothelium; case 4) case 3 with fibrous cap permeability and reflection coefficient corresponding to a leaky junction. The effect of different physical attributes of endothelium and fibrous cap given in Table 3, on filtration velocity and LDL concentration is shown in Fig. 37. It can be seen that a dysfunctional endothelium leads to a higher infiltration velocity and a higher LDL concentration across endothelium, fibrous cap and intima.

	Normal endothelium	**Leaky endothelium**	**Fibrous cap**
Thickness	$2\mu m$		$65\mu m$
Hydraulic Permeability	$3.21\times10^{-21}m^2$	$2.62\times10^{-19}m^2$	-
Effective Diffusivity	$8.15\times10^{-17}\,m^2/s$	$1.142\times10^{-14}\,m^2/s$	$4.5\times10^{-13}\,m^2/s$
Reflection Coefficient	0.9886	0.7240	-
Reference	Ai and Vafai (2006)	Curry (1984a,b) Chung and Vafai (2012)	Hossain et al. (2011)

Table 3 Properties obtained in previous works for dysfunctional endothelium and fibrous cap.

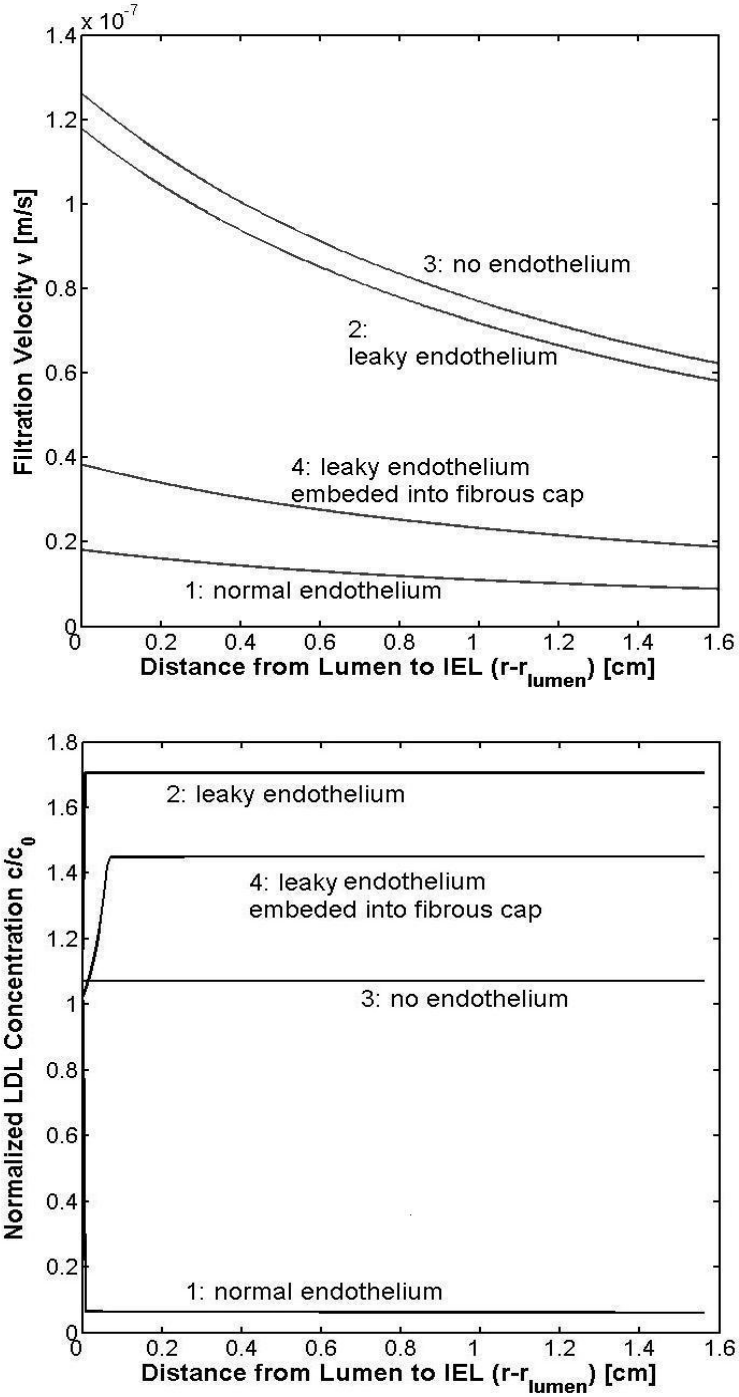

Figure 37 Filtration velocity and LDL concentration across endothelium, fibrous cap, and intima for different physical attributes of endothelium and fibrous cap given in Table 3.

5.11 Calculation of intima properties through fiber matrix model

Table 4a illustrates the intima properties that were used in previous works and were obtained by either experimental, analytical or the fiber matrix method which was introduced in equations 15 and 16, or Eq. 17. However, as seen in Table 4a, not all of the property values were based on the micro-structure information in any of the prior works. It is more reasonable to obtain property values based on the microstructure information through the fiber matrix method. The healthy intima (no cholesterol/lipid accumulation) microstructure characteristics, effective fiber radius r_f and porosity δ are used as a reference point.

Table 4b lists intima properties obtained from Eq. 15 and 16 (considering only the proteoglycan fiber), or Eq. 17 (considering both proteoglycan and collagen fibers) with effective fiber radius r_f obtained from Eq. 14 as 2.31 nm, and the porosity taken from the following prior works: 1) $\delta = 0.983$ (Karner et al., 2001; Yang and Vafai, 2006); 2) $\delta_{PG} = 0.9568$ and $\delta_{CG} = 0.8387$ (Dabagh et al., 2009; Liu et al., 2011); 3) $\delta_{PG} = 0.9866$ and $\varepsilon_{CG} = 0.95$ (Dabagh et al. 2009); 4) $\delta = \delta_{PG}\delta_{CG} = 0.9373$ (Dabagh et al. 2009). These results are shown in Table 4b.

Tables 4a and b show a significant variation with respect to intima's transport properties, especially with respect to the reflection coefficient. This is due to the subdued influence of the intima's resistance compared to the other layers. Figures 38a illustrate the filtration velocity and LDL concentration along the endothelium-intima interface utilizing the data given in Table 4b. These results are compared with the works of Ai and Vafai (2006) and Liu et al. (2011) given in Table 4a. As can be seen in Figs. 38a, even though the intima property values are quite different, as seen in Table 4b, the impact on plasma and LDL molecular transport is limited.

Ai and Vafai (2006) pointed out that, within the intima layer, the transport is mostly dominated by convection flux, and their analytical work resulted a reflection coefficient σ of 0.8292. As such, from the results given in Table 4b, case 2 ($\delta = \delta_{PG}\delta_{CG} = 0.8025$) and case 4 ($\delta = 0.9397$) are selected for comparison with the results of Ai and Vafai (2006). Utilizing Eqs. 16b and c, with the intima reflection coefficient of 0.8292 and porosities δ of 0.9373 and 0.8025, results in an effective radius of intima protein fiber r_f as 2.08 and 4.17 respectively [nm]. These are represented in Table 4c based on Eqs. 15 and 16.

Figures 38b show the comparisons for both filtration velocity and LDL concentration at the endothelium-intima interface using the data given in Table 4c. A perfect agreement is seen with the results of Ai and Vafai (2006) and Liu et al. (2011). It should be noted that since a fiber radius of 2.08 nm is closer to the value which is

obtained through Eq. 14, which is also utilized in Yang and Vafai's work (2006), it is more reasonable to assign the porosity δ and effective fiber radius r_f for a healthy intima as 0.9373 and 2.08 nm.

#	**Porosity** δ or (δ_{PG}, δ_{CG})	**Effective fiber radius [nm]**	**Permeability** $K\ [m^2]$	**Diffusivity** $D_{eff}\ [m^2/s]$	**Reflection coefficient** σ
a)					
1	**0.983**	**2.31**	1.66×10^{-16}	1.35×10^{-11}	**0.1771**
2	**(0.9568, 0.8387)**	**2.31**	3.93×10^{-17}	3.7×10^{-12}	**0.7983**
3	**(0.9866, 0.95)**	**2.31**	2.1×10^{-16}	9.7×10^{-12}	**0.3247**
4	**0.9373**	**2.31**	2.5×10^{-17}	6.78×10^{-12}	**0.7512**
b)					
1	**0.9373**	**2.08**	2.02×10^{-17}	5.94×10^{-12}	**0.8292**
2	**0.8025**	**4.17**	9.59×10^{-18}	5.7×10^{-12}	**0.8292**
c)					
Ai & Vafai (2006)	**0.96**	**-**	2.2×10^{-16}	5×10^{-12}	**0.8292**
Liu et al. (2011)	**(0.9568, 0.8387)**	-	4.2×10^{-17}	3.7×10^{-12} *****	**0.7983***

Table 4 Intima properties a) obtained using fiber matrix method with protein fiber radius r_f of 2.31 nm (Eq. 14) and variation of intima porosity, δ or (δ_{PG}, δ_{CG}) given in previous work (Yang and Vafai, 2006; Dabagh et al., 2009); b) obtained using fiber matrix method variations in both intima porosity ε (Dabagh et al., 2009, $\delta = \delta_{PG}\delta_{CG}$) and protein fiber radius r_f; c) obtained in the prior works (Ai and Vafai, 2006; Liu et al., 2011).

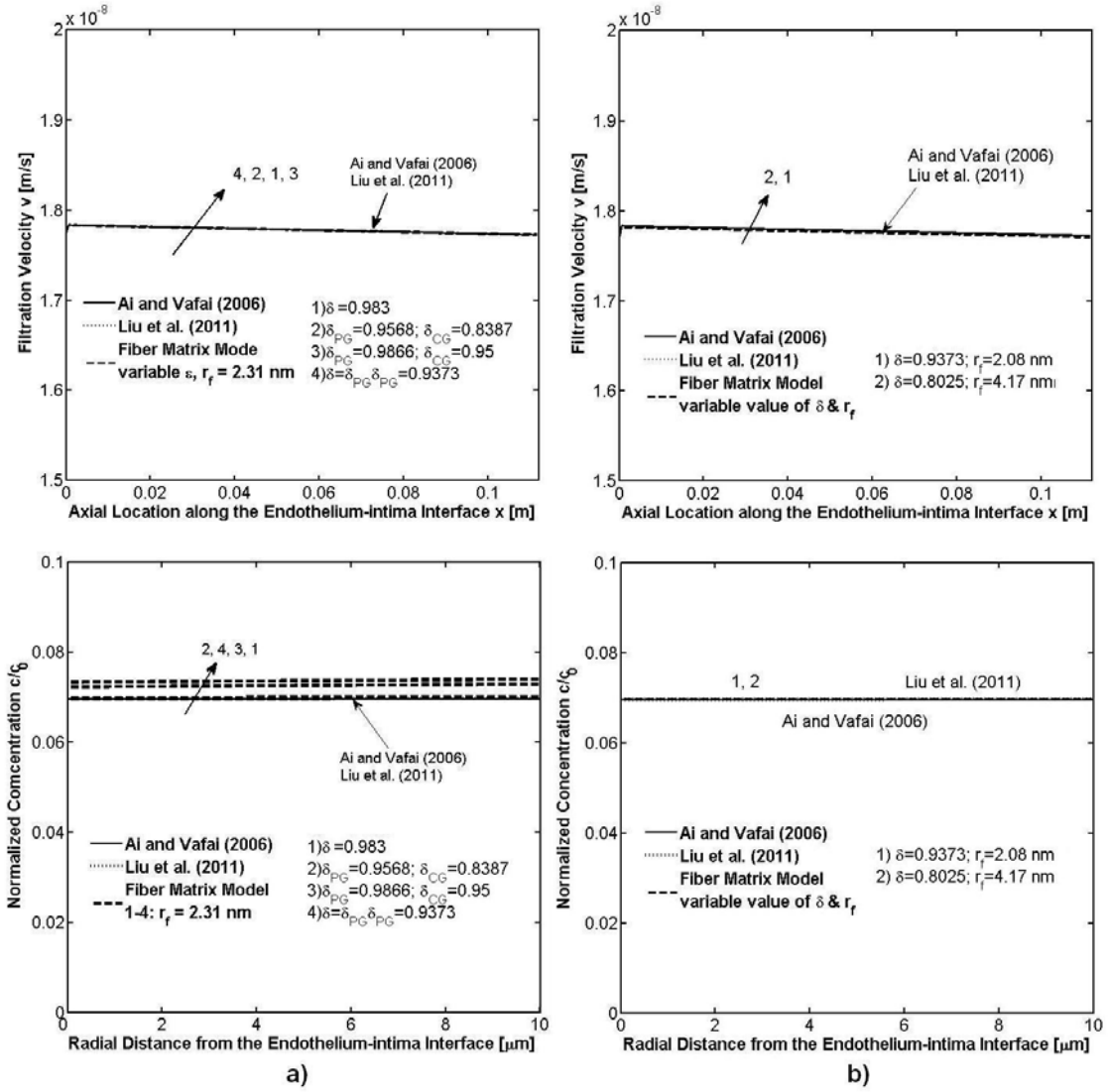

Figure 38 Filtration velocity and LDL concentration along the intima-IEL interface. Intima properties were obtained through fiber matrix model with a) protein fiber radius r_f of 2.31 nm and variations of intima porosity, δ or (δ_{PG} , δ_{CG}) based on data given in Table 4a; and b) variations of intima porosity δ and effective protein fiber radius r_f based on data given in Table 4b, and compared with those based on the properties obtained by Ai and Vafai (2006) and Liu et al (2011) given in Table 4c.

5.12 Impact of variations in intima properties by lipid accumulation

The structure of intima for a normal artery is shown in Fig 1c, while during LDL molecule accumulation, the structure resembles the schematic shown in Fig. 3c displaying a thicker fiber radius $r_{f,Lip}$ and a lower porosity δ_{Lip} due to the lipid deposits as compared to a healthy intima (δ and r_f). As discussed earlier, the normal intima porosity δ and the effective fiber radius r_f are set as 0.9397 and 2.08 nm. The maximum fiber thickening ratio ($r_{f,Lip}/r_f$) is set as 150 which is the same as the ratio of the thickness of atherosclerotic plaque with $\delta_{st}=0.5$ to the thickness of a normal intima layer. With the effective intima porosity δ_{Lip} and protein fiber thickening rate $r_{f,Lip}/r_f$ varying between 20-93.97 % and 1-150 respectively, the variable properties for the hydraulic permeability K, effective diffusivity D_{eff}, and reflection coefficient σ are obtained through fiber matrix model using Eqs. 15 and 16 and represented in Table 5.

To describe LDL transport within a diseased artery (Fig. 3d), a fibrous cap with dysfunctional endothelium embedded (model 4 in Fig. 37) is selected to represent the transport properties. Figure 39 illustrates the impact of variable properties due to lipid accumulation on filtration velocity subject to different effective intima porosity δ_{Lip} and

protein fiber thickening ratio $r_{f,Lip}/r_f$. As can be seen in Fig. 39, a lower porosity leads to a lower permeability, while a thicker effective fiber radius reduces this impact by providing a larger space between the fibers.

Figure 40 displays the effect of variable properties on the LDL transport. As expected, a higher porosity results in more LDL molecule deposits inside the arterial wall. As the thickening ratio $r_{f,Lip}/r_f$ increases, a larger space between the fibers is created resulting in a reduction in the selective behavior for LDL particles inside the intima due to formation of stenosis. As such, LDL particles are deposited more near the intima-IEL interface, instead of the inner wall surface, because the IEL layer with its higher rate of the particle selection takes over the role of blocking LDL particle migration from the lumen side.

Hydraulic Permeability K [m^2]		Porosity δ_{Lip}				
		0.2	0.4	0.6	0.8	0.9373
Intima's fiber thickening ratio $r_{f,Lip}/r_f$	1	3.42×10^{-21}	4.72×10^{-20}	3.24×10^{-19}	3.32×10^{-18}	2.02×10^{-17}
	10	3.42×10^{-19}	4.72×10^{-18}	3.23×10^{-17}	2.32×10^{-16}	2.02×10^{-15}
	50	8.55×10^{-18}	1.18×10^{-16}	8.09×10^{-16}	5.80×10^{-15}	5.06×10^{-14}
	150	7.70×10^{-17}	1.06×10^{-15}	7.28×10^{-15}	5.22×10^{-14}	4.55×10^{-13}

Effective Diffusivity D_{eff} [m^2/s]		Porosity δ_{Lip}				
		0.2	0.4	0.6	0.8	0.9373
Intima's fiber thickening ratio $r_{f,Lip}/r_f$	1	1.04×10^{-13}	2.02×10^{-13}	5.38×10^{-13}	1.72×10^{-12}	5.94×10^{-12}
	10	7.31×10^{-12}	8.77×10^{-12}	1.09×10^{-11}	1.45×10^{-11}	1.96×10^{-11}
	50	1.07×10^{-11}	1.22×10^{-11}	1.42×10^{-11}	1.75×10^{-11}	2.17×10^{-11}
	150	1.14×10^{-11}	1.29×10^{-11}	1.49×10^{-11}	1.80×10^{-11}	2.21×10^{-11}

Reflection Coefficient σ		Porosity δ_{Lip}				
		0.2	0.4	0.6	0.8	0.9373
Intima's fiber thickening ratio $r_{f,Lip}/r_f$	1	1	1	1	0.9991	0.8292
	10	0.4313	0.3042	0.1715	0.055	0.0065
	50	0.0266	0.0156	0.0073	0.0019	0.0002
	150	0.0031	0.0018	0.0008	0.0002	0

Table 5 List of intima property variations with porosity ε and protein fiber radius r_f based on fiber matrix model (Eq. 15 and 16).

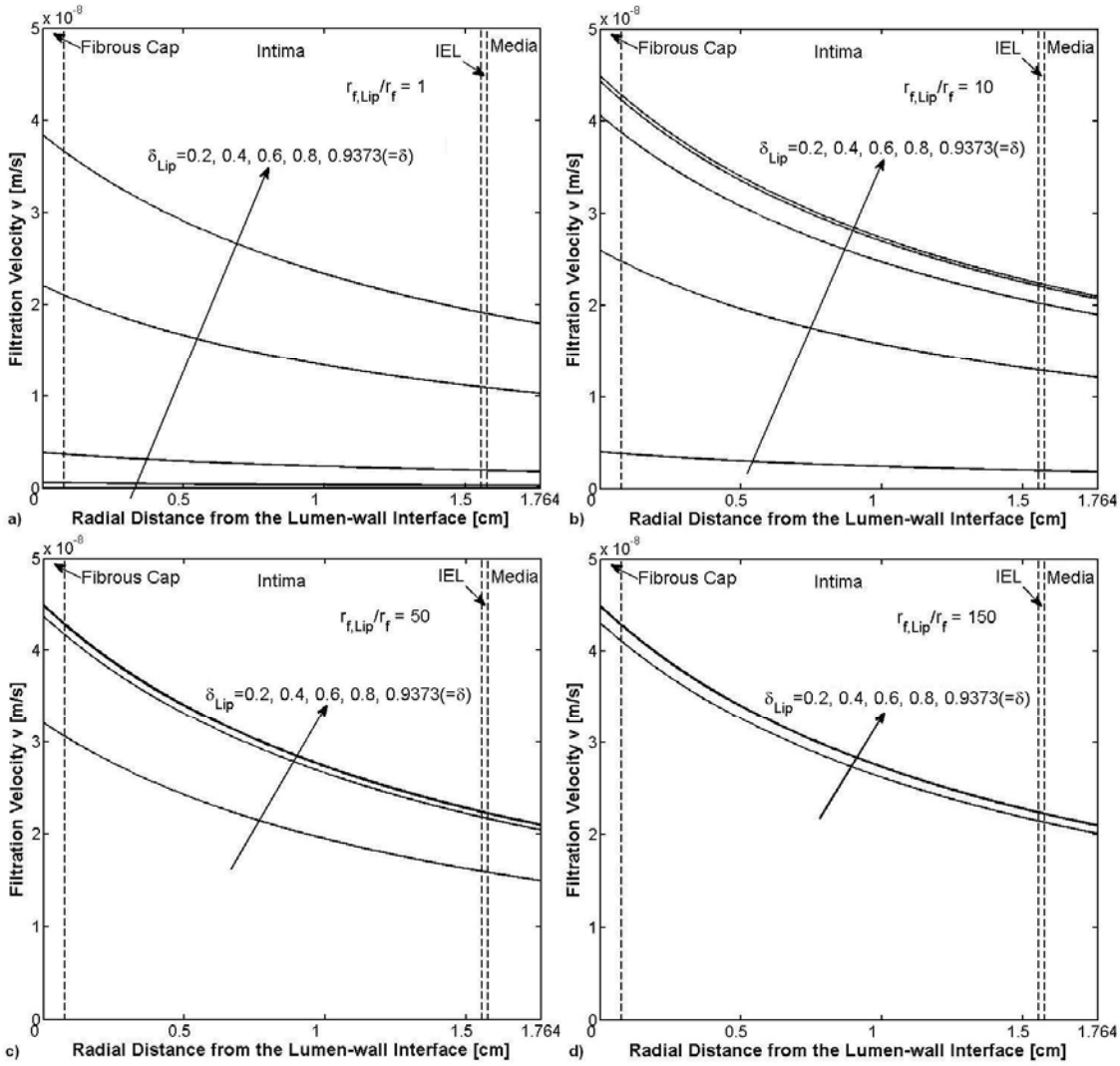

Figure 39 Effect of variations in the effective porosity δ_{Lip} and protein fiber thickening ratio $r_{f,Lip}/r_f$ on the filtration velocity across a diseased arterial wall.

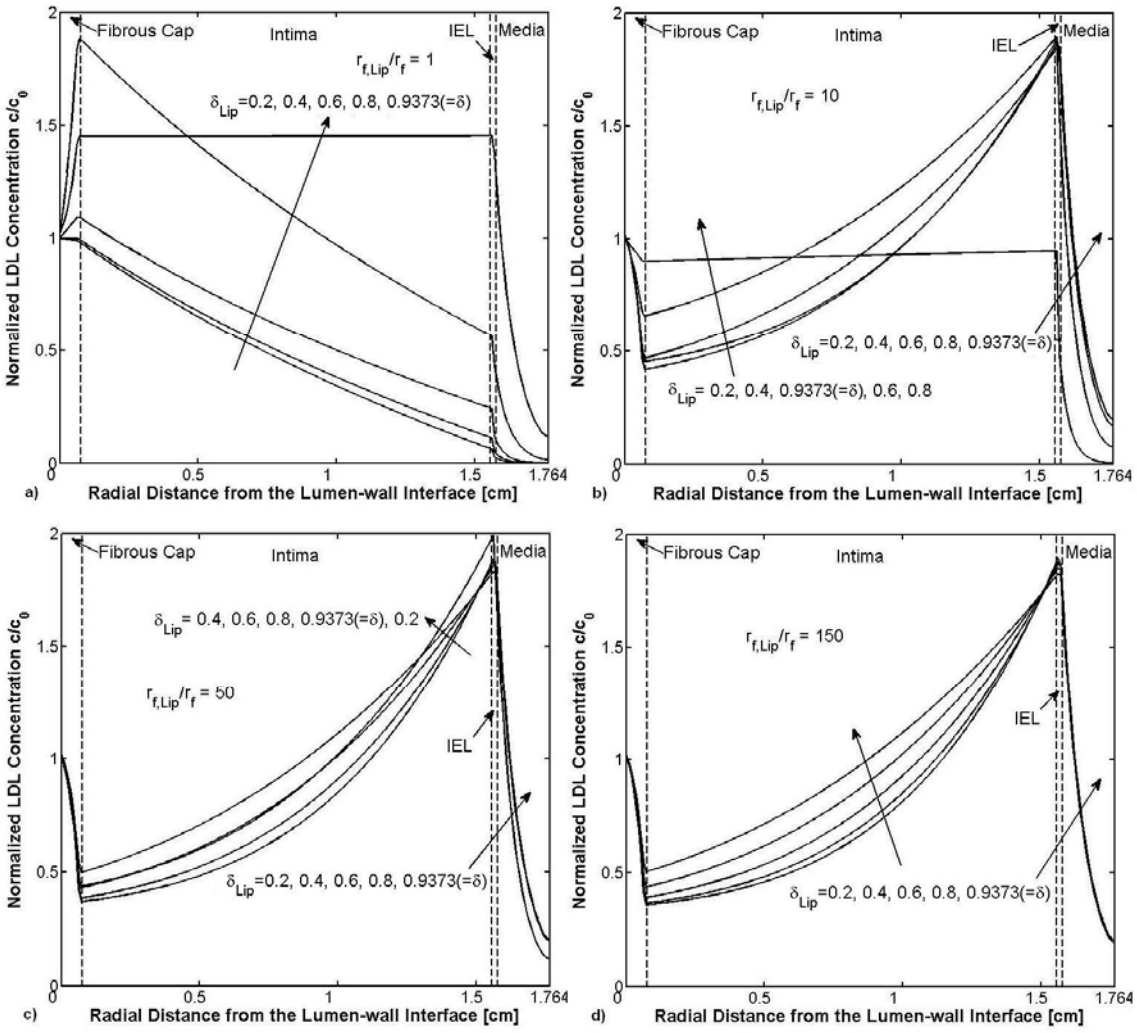

Figure 40 Effect of variations in the effective porosity ε_{Lip} and protein fiber thickening ratio $r_{f,Lip}/r_f$ on the LDL molecule concentration across a diseased arterial wall.

Chapter 6

Conclusion

A comprehensive model which incorporates the multi-layer features as well as Fluid Solid Interactions (FSI), hyperthermia, as well as Atherosclerotic plaque, for investigating LDL transport is analyzed and presented here. The presented model and the computational results are in excellent agreement with prior results.

6.1 FSI and Hyperthermia – Elastic and Thermo induced coupling phenomena

The presented model incorporates coupling of LDL transport and FSI and accounts for the elastic deformation of endothelium. Pore theorem is utilized to relate pore structure with hydraulic and mass-transfer parameters. Under steady state conditions, there is a significant impact from FSI on LDL concentration but a minor effect on filtration velocity. When pulsation effects are taken into account, the impact of FSI is quite minor due to the time period for the blood pulsation.

The effect of hyperthermia and coupling attributes on the Low-density lipoprotein (LDL) transport is studied in this work. Osmotic, Sorret and Dufour effects in an artery for LDL transport are introduced and examined.It is shown that the Osmotic and Dufour effects are negligible while the Sorret diffusion is shown to have a significant effect in enhancing the LDL transport. The increase in the effective LDL diffusivity and consumption rate due to hyperthermia is shown to have a small effect in decreasing the LDL concentration inside the arterial wall. It is shown that the thermal expansion enhances LDL transport by causing a larger cross-section area of leaky junction. The competition between Sorret effect and thermal expansion is discussed and quantified. It is established that overall hyperthermia increase the LDL concentration.

6.2 Atherosclerosis – Plaque/stenosis formation and endothelium dysfunction

The effects of atherosclerotic plaque/stenosis and cholesterol lipid accumulation have been analyzed in detail in this work. A multi-layered model is utilized while incorporating the fiber matrix model to calculate variable properties taking into account the lipid deposits. The present results are compared with pertinent prior works for both normal and stenosed arteries and are found to be in very good agreement. It is established that the geometrical effects of a stenosed artery in the axial direction is not substantial while the geometrical impact in the radial direction is quite significant.

The microstructure details and characteristics of the endothelium and intima due to the formation of plaque/stenosis are incorporated into the present analysis. Pertinent scenarios for transport through a dysfunctional endothelium and fibrous cap within intima have been examined, and it is shown that the dysfunction in the endothelium results in a reduction in the resistance between lumen and intima. The variable intima properties affected by LDL molecule accumulation are analyzed, and its impact on the hydraulic and molecular transport in a thickened arterial wall is examined. Lower porosity by lipid blockage results in a lower permeability, which is diminished by thickening of effective fiber due to more space between the fibers as a result of stenosis.

References

Ai, L., Vafai, K., 2006. A coupling model for macromolecule transport in a stenosed arterial wall. J. Int. Heat Mass Transfer 49, 1568–1591.

American Heart Association, 2005. Heart disease and stroke statistics – 2005 update. American Heart Association. Dallas.

American Heart Association, 2006. Heart disease and stroke statistics – 2006 update. American Heart Association. Dallas.

American Heart Association, 2007. Heart disease and stroke statistics – 2007 update. American Heart Association. Dallas.

American Heart Association, 2008. Heart disease and stroke statistics – 2008 update. American Heart Association. Dallas.

Baer, G. M., Small IV, W., Wilson, T. S., Benett, W. J., Matthews, D. L., Hartman, J., Maitland, D. J., 2007. Fabrication and in vitro deployment of a laser-activated shape memory polymer vascular stent. Biomedical engineering online, 6(1), 43.

Brinkman, H. C., 1947. A calculation of the viscous force exerted by a flowing fluid on a dense swarm of particles, Applied Science Research A1, 24-37.

Buchanan, Jr., J. R., Kleinstreuer, C., 1997. Computational analysis of particle-hemodynamics in a stenosed artery segment. American Society of Mechanical

Engineers, Fluids Engineering Division (Publication) FED, Bio-Medical Fluids Engineering 21, 8.

Buckwalter, J. A., Rosenberg, L. C., 1982. Electron microscopic studies of cartilage proteoglycans. The Journal of Biological Chemistry 257 (16), 9830-9839.

Chapman, S., Cowling, T. G., 1952. The mathematical theory of non-uniform gases: An account of the kinetic theory of viscosity, thermal conduction, and diffusion in gases.

Chung, S., Vafai, K., 2010. Vibration induced mixed convection in an open-ended obstructed cavity. International Journal of Heat and Mass Transfer, 53, 2703-2714.

Chung, S., Vafai, K., 2012. Effect of the Fluid-Structure Interactions on Low-Density Lipoprotein within a Multi-Layered Arterial Wall. Journal of Biomechanics 45, 371-381.

Chung, S., Vafai, K., 2013. Low-density lipoprotein transport within a multi-layered arterial wall - effect of the atherosclerotic plaque/stenosis. Journal of Biomechanics, 46, 574-585.

Curry, F. E., 1984a. Mechanics and thermodynamics of transcapillary exchange. Handbook of Physiology, section 2, The Cardiovascular System, American Physiological Society, Bethesda, MD, 4 309-374.

Curry, F. E., 1984b. Determinants of capillary permeability: a review of mechanism based on capillary studiesy in the frog. Circulation Research 59 (4), 367-380.

Curry, F. E., Michel C. C., 1980. A fiber matrix model of capillary permeability. Microvascular Research 20, 96-99.

Dabagh, M., Jalali, P., Tarbell, J. M., 2009. The transport of LDL across the deformable arterial wall: the effect of endothelial cell turnover and intimal deformation under hypertension. Am. J. Physiol - Heart Circ Physiol 297 983-996.

Frank, J. S., Fogelman, A. M., 1989. Ultrastructure of the intima in WHHL and cholesterol-fed rabbit aorta prepared by ultra-rapid freezing and freeze-etching. Journal of Lipid Research 30, 967-978.

Fry, D. L., 1985. Mathematical models of arterial transmural transport. Am. J. Physiol. 248, H240–H263.

Denekamp, J, 1984. Vascular endothelium as the vulnerable element in tumours. Acta Oncologica, 23(4), 217-225.

Gao, F., Watanabe, M., Matsuzawa, T., 2006a. Stress analysis in a layered aortic arch model under pulsatile blood flow. Biomed. Eng. Online 5, 25.

Gao, F., Guo, Z.H., Sakamoto, M., 2006b. Fluid–structure interaction within a layered aortic arch model. J. Biol. Phys. 32, 435–454.

Gillum, R. F., 1995. Epidemiology of aortic aneurysm in the United States. Journal of Clinical Epidemiology 48, 1289-1298.

Hadim, H. and Vafai, K., 2000. Overview of current computational studies of heat transfer in porous media and their applications-forced convection and multiphase transport. Advances in Numerical Heat Transfer, Vol. 2, Taylor & Francis, New York, (9), 291-330.

Happel, J., Brenner, H, 1965. Low Reynolds number hydrodynamics: with special applications to particulate media. Englewood Cliffs N. J. Prentice-Hall.

Hossain, S. S., Hossainy, S. F. A., Bazilevs, Y., Calo, V. M., Hughes, T. J. R., 2011. Mathematical modeling of coupled drug and drug-encapsulated nanoparticle transport in patient-specific coronary artery walls. Computational Mechanics 49 (2), 213-242.

Huang, Y., Weinbaum, S., Rumschitzki, D., Chien, S. ,1992. A fiber matrix model for the growth of macromolecular leakage spots in the arterial intima. Advanced in Biological Heat and Mass Transfer HTD 231, 81–92.

Huang, Y., Rumschitzki, D., Chien, S., Weinbaum, S., 1994. A fiber matrix model for the growth of macromolecular leakage spots in the arterial intima. J. Biomech. Eng. 116, 430–445

Hunag, Y., Rumschizki, D., Chien, S., Weinbaum, S., 1997. A fiber matrix model for the filtration through fenestral pores in a compressible arterial intima. Am. J. Physiol. 272, 2023–2039

Huang, Z.J., Tarbell, J.M., 1997. Numerical simulation of mass transfer in porous media of blood vessel walls. Am. J. Physiol. 273, H464–H477.

Jain, R. K., 1987. Transport of molecules across tumor vasculature. Cancer and Metastasis Reviews, 6(4), 559-593.

Karner, G., Perktold, K., Zehentner, H.P., 2001. Computational modeling of macro-molecule transport in the arterial wall. Comput. Methods Biomech. Biomed. Eng. 4, 491–504.

Katz, M.A., 1985. New formulation of water and macromolecular fluxwhich corrects for non-ideality: theory and derivation, predictions, and experimental results. J. Theor. Biol. 112, 369–401.

Kedem, O., Katchalsky, A., 1958. Thermodynamic analysis of the permeability of biological membranes to non-electrolytes. Biochem. Biophys. Acta 27, 229–246

Khakpour, M. and Vafai, K., 2008. A comprehensive analytical solution of macromolecular transport within an artery. International Journal of Heat and Mass Transfer, 51, 2905-2913.

Khanafer, K., Berguer, R., 2009. Fluid–structure interaction analysis of turbulent pulsatileflow within a layered aortic wall as related to aortic dissection. J. Biomech. 42, 2642–2648.

Khanafer, K., Bull, J.L., Berguer, R., 2009. Fluid–structure interaction of turbulent pulsatileflow within a flexible wall axisymmetric aortic aneurysm model. Eur. J. Mech. B-Fluids 28, 88–102.

Kolios, M. C., Sherar, M. D., Hunt, J. W., 1995. Large blood vessel cooling in heated tissues: a numerical study. Physics in Medicine and Biology, 40(4), 477-494.

Kotte, A., van Leeuwen, G., de Bree, J., van der Koijk, J., Crezee, H., Lagendijk, J., 1996. A description of discrete vessel segments in thermal modelling of tissues. Physics in Medicine and Biology, 41(5), 865-884.

Lark, M. W., Yeo, T., Mar, H., Lara, S., Hellstrom, I., Hellstrom, K., wight, T. N., 1988. Arterial chondroitin sulfate proteoglycan: localization with a monoclonal antibody. The Journal of Histochemistry and Cytochemistry 36, 1211-1221.

Li, J., Stoliarov. S.I., 2013. Measurement of kinetics and thermodynamics of the thermal degradation for non-charring polymers. Combustion and Flame 160 1287–1297.

Liu, X., Fan, Y., Deng, X., 2011.Effect of the endothelial glycocalyx layer on arterial LDL transport under normal and high pressure. Journal of Theoretical Biology 283 (1, 21), 71-81.

Meyer, G., Merval, R., Tedgui, A., 1996. Effects of pressure-induced stretch and convection on low-density lipoprotein and albumin uptake in the rabbit aortic wall. Circulation Research 79 (3), 532-540.

Michel, C.C., Curry, F.E., 1999. Microvascular permeability. Physiol. Rev. 79, 703–761.

Moore, J.A., Ethier, C.R., 1997. Oxygen mass transfer calculations in large arteries. J. Biomech. Eng. 119, 469–475.

Morris, E.D., Saidel, G.M., Chisolm III, G.M., 1991. Optimal design of experiments to estimate LDL transport parameters in arterial wall. Am J Physiol. 261, 929-949.

Prosi, M., Zunino, P., Perktold, K., Quarteroni, A., 2005. Mathematical and numerical models for transfer of low-density lipoproteins through the arterial walls: a new methodology for the model set up with applications to the study of disturbed luminal flow. J. Biomech. 38, 903–917

Rappitsch, G., Perktold, K., 1996. Pulsatile albumin transport in large arteries: a numerical simulation study. J. Biomech. Eng. 118, 511–519.

Razi, Y.P., Maliwan, K., Carrier-Mojtabi, M.C., Mojtabi, A., 2005. The Influence of

Mechanical Vibrations on Buoyancy Induced Convection in Porous Media, in: Handbook of Porous Media, 321–370.

Jimenez Rios, J. L., Rabin, Y., 2006. Thermal expansion of blood vessels in low cryogenic temperatures Part I: A new experimental device. Cryobiology, 52(2), 269-283.

Rabin, Y., Plitz, J., 2005. Thermal expansion of blood vessels and muscle specimens permeated with DMSO, DP6, and VS55 at cryogenic temperatures. Annals of biomedical engineering, 33(9), 1213-1228.

Shi, W., Vafai, K., 2010. Mixed convection in an obstructed open-ended cavity. Numerical Heat Transfer, Part A, 57, 709-729.

Stangeby, D.K., Ethier, C.R., 2002a. Coupled computational analysis of arterial LDL transport—effects of hypertension. Comput. Meth. Biomech. Biomed. Eng. 5, 233–241

Stangeby, D.K., Ethier, C.R., 2002b. Computational analysis of coupled blood-wall arterial LDL transport. J. Biomech. Eng. 124, 1–8.

Stoeckel, D., Pelton, A., Duerig, T, 2004. Self-expanding nitinol stents: material and design considerations. European radiology, 14(2), 292-301.

Tarbell, J.M., 1993. Bioengineering studies of the endothelial transport barrier. BMES Bull. 17, 35–39.

Tarbell, J.M., 2003. Mass transport in arteries and the localization atherosclerosis. Ann. Rev. Biomed. Eng. 5, 79–118.

Tada, S., Tarbell, J.M., 2004. Internal elastic lamina affects the distribution of macromolecules in the arterial wall: a computational study. Am. J. Physiol. 287, H905–H913

Vafai, K., Tien, C. L., 1981. Boundary and inertia effects on flow and heat transfer in porous media, Int. J. Heat Mass Transfer 24, 195-203.

Vafai, K., Hadim, H., 2000. Overview of current computational studies of heat transfer in porous media and their applications – natural convection and mixed convection. Advances in Numerical Heat Transfer, Vol. 2, Taylor & Francis, New York (10), 331–371.

Wada, S., Karino, T., 2000. Computational study on LDL transfer from flowing blood to arterial walls, in: T. Yamaguchi (Ed.), Clinical Applications of Computational Mechanics to the Cardiovascular System. Springer, Berlin, 157–173.

Wakeham, W. A., Nagashima, A. Sengers, J. V., 1991. Experimental Thermodynamics, Blackwell Scientific Publications, Oxford, Vol. III (10).

Weinbaum, S., Tsay, R., Curry, F.E., 1992. A Three-Dimensional Junction-Pore-Matrix Model forCapillary Permeability. Microvasc Res. 44, 85-111.

Wen, G.B., Weibaum, S., Ganatos, P., Pfeffer R., Chien, S., 1988. On the time dependent diffusion of macromolecules through transient open junctions and their subendothelial spread. 2. Long time model for interaction. J. Theor. Bio. 135, 219-253.

Xu, Y., Hua, T. C., Sun, D. W., Zhou, G. Y., Xu, F., 2007. Effects of freezing rates and dimethyl sulfoxide concentrations on thermal expansion of rabbit aorta during freezing phase change as measured by thermo mechanical analysis. Journal of biomechanics, 40(14), 3201-3206.

Yang, N., Vafai, K., 2006. Modeling of low-density lipoprotein (LDL) transport in the artery – effects of hypertension. J. Int. Heat Mass Transfer 49, 850–867.

Yang, N., Vafai, K., 2008. Low-density lipoprotein (LDL) transport in an artery – A simplified analytical solution. J. Int. Heat Mass Transfer 51, 497–505.

Yuan, F., Chien, S., Weinbaum, S., 1991. A new view of convective–diffusive transport processes in the arterial intima. J. Biomech. Eng. 133, 314–329.